Hydrological Modelling of Mountainous and Glacierised regions under Changing Climate

Hong Li

Dissertation submitted for the degree of Philosophiae Doctor (PhD)

Department of Geosciences
Faculty of Mathematics and Natural Sciences

University of Oslo

Oslo, Norway

July 30, 2015

Series of dissertations submitted to the
Faculty of Mathematics and Natural Sciences, University of Oslo
No. 1656

ISSN 1501-7710

Cover: Hanne Baadsgaard Utigard.
Printed in Norway: AIT Oslo AS.

Produced in co-operation with Akademika Publishing.
The thesis is produced by Akademika Publishing merely in connection with the thesis defence. Kindly direct all inquiries regarding the thesis to the copyright holder or the unit which grants the doctorate.

Abstract

Climate change is one of the most serious environmental threats that humanity has ever been confronted to. Hydrological models are vital tools to asses its impacts on the water cycle and water resources. The goal of this project is to evaluate and improve the capacity of the HBV model (Hydrologiska Byråns Vattenbalansavdelning) in simulating hydrological processes in mountainous and glacierised regions under both the present and future climate. This goal is achieved in two steps: (1) implement routing and glacier retreating modules in a grid-based HBV model for mountainous and glacierised areas in Norway and the Himalayan region (i.e. Bhutan and India); (2) calculate available water resource scenarios for two Himalayan basins with considerable glacier coverage and growing water demand. The thesis is composed of four peer-reviewed articles which focus on the two steps.

Articles I and II examine model setting effects on their performance in reproducing major hydrological processes. Articles I implemented routing algorithms in the grid-based HBV model and tested them at various spatial resolutions in the Glomma basin (Norway). The routing procedures improved the model performance in daily runoff simulation to varying extents. A hillslope routing method and its combination with the channel routing returned a Nash-Sutcliffe coefficient 0.05 higher than the initial grid-based model. Articles II evaluated five variants of the HBV model in runoff simulation of interior points and internal variables in the Norsfoss basin (Norway). The five variants were a lumped (LWhole), a semi-distributed (SBand) and three grid-based models, GRZero (without routing), GROne (hillslope routing) and GRTwo (hillslope and channel routing). For runoff simulations, GRTwo and GROne were superior over other model variants in model efficiency, particularly in simulating low flow. This superiority deteriorated in reproducing runoff at six interior points. Compared with measurements of snow water equivalent at snow pillows and groundwater depth in piezometers, all grid-based models had a similar efficiency.

Articles IIII and IV include an integration of a mass conserving glacier model into the HBV model and its application in water resource projections. Article III combined the glacier retreat model with the HBV model. The coupled model was tested in three basins (the Nigardsbreen basin in Norway, the Chamkhar Chhu basin in Bhutan and the Beas

basin in India) with different glacier coverage and hydrologic regime. Results showed that, in addition to runoff simulation, the model gave a high efficiency in reproducing glacier annual mass balance in the Nigardsbreen basin where measurements are available to verify the results. Moreover, the model provided maps of snow distribution and glacier runoff. Article IV projected available water resources per capita (Wp) for the Chamkhar Chhu (eastern Himalaya) and the Beas (western Himalaya) basins for the period 2010–2050. All climate projections indicated significant increases in annual temperature, but not in annual precipitation. All Wp projections revealed pronounced water resources drops jointly induced by continuous climate change and population growth. The latter is responsible for roughly 40% of the water declines. The regional climate models and CO_2 emissions cause approximately 30% unceratainties ranging from 11% to 44%. When considering $\pm$20% inaccuracy in population estimations, the highest uncertainty reaches 87%. The uncertainties are worthy of attention, but there is no doubt that the two basins are facing serious water scarcity and the water conditions will get worse. Water shortage has been and continues to be a major constraint of economic and social development.

Acknowledgements

I take the opportunity to sincerely express my gratitude to everyone who supported me throughout this PhD project. I am thankful for their aspiring guidance, invaluably constructive criticism and friendly advice. They generously shared their truthful and illuminating views on scientific research and activities.

I wish to address a special acknowledgement to my supervisors Chongyu Xu of the Department of Geosciences (GEO), University of Oslo (UiO) and Stein Beldring of the section of Hydrological Modelling (HM), the Norwegian Water Resources and Energy Directorate (NVE) as well as Lena Merete Tallaksen of GEO, UiO. Their excellent guidance and critical supervision are the basis of this thesis. I will continuously benefit from their advice in the future.

My thanks go to my other co-authors of my papers: Sharad Jain in National Institute of Hydrology (India), Matthias Huss in University of Fribourg (Switzerland) and Kjetil Melvold in NVE (Norway). Their kind help in every stage of paper preparation facilitated my work.

I express my sincere thanks to my colleagues in UiO and NVE. They organised many creative social and scientific events, which are very helpful to get people together for scientific exchanges. I also extend my gratefulness to the technical and administrative staff both in UiO and NVE. They are indeed experts in IT stuff and solving problems. I appreciated their professional support.

My dear friends gave me a lot of comfort and help during this period. Their kindness and patience released me from high pressure and anxiety. Their smiles and laugh made the winter time as bright as the lovely summer.

Finally, I thank my parents and my brothers. Without their continuous encouragement, I could not succeed to be what I am now. Because of their love, I face every challenge with confidence.

Articles

Article I

Li, H., Beldring, S., Xu, C.-Y. (2014): Implementation and testing of routing algorithms in the distributed Hydrologiska Byråns Vattenbalansavdelning model for mountainous catchments—*Hydrology Research* **45(3)**: 322–333, doi: 10.2166/nh.2013.009.

Article II

Li, H., Xu, C.-Y., Beldring, S. (2015): How much can we gain with increasing model complexity with the same model concepts?—*Journal of Hydrology* **527**: 858–871, doi: 10.1016/j.jhydrol.2015.05.044.

Article III

Li, H., Beldring, S., Xu, C.-Y., Huss, M., Melvold, K., Jain, S. (2015): Integrating a glacier retreat model into a hydrological model—Case studies of three glacierised catchments in Norway and Himalayan region—*Journal of Hydrology*, **527**: 656–667, doi: 10.1016/j.jhydrol.2015.05.017.

Article IV

Li, H., Xu, C.-Y., Beldring, S., Tallaksen, L., Jain, S. (2015): Water Resources under Climate Change of Himalayan Basins—*Water Resources Management*, submitted.

In these articles, I was responsible for most of the data collection, programming and analysis. I also wrote the original manuscripts of **Article I, II and IV**, revised and collated the final versions of the articles. In **Article III**, I wrote most of the original manuscript and Dr. Huss contributed to a description of the glacier model.

Contents

Part I

Introduction and Synthesis

1 Introduction

1.1 Motivation

Water is one of the key elements of life on the earth. All living organisms need water every day to survive. For the public community, it is easy to take for granted fresh water once they turn on a tap. In addition to drinking water, we need water for hygiene, agriculture, industry, fishing and recreation. Hydrology is the science that supports proper and sustainable use of water and explores more values.

The earth is a closed system in terms of water exchange. This means that total amount of water on the earth does not change. However, its form can be changed and be transformed according to the water cycle shown in Figure 1.1. Hydrology includes scientific studies of the water cycle, distribution and quality of water on the earth, as well as water resources and environmental watershed sustainability. It provides insight for environmental engineering, policy, and planning.

Water is not only a major driving force shaping our earth and limiting energy exchange with the sun, but it also links atmosphere, ecology, hydrology and human activities. Therefore, accurate modelling of water is vitally meaningful not only to hydrologists, but has also relevance of scientists in other fields.

Hydrological models are useful tools and can explain current knowledge and answer new questions. At present, most hydrological models describe the hydrologic state of the art in mathematical equations and computer programs. Among these models, distributed hydrological models became prevalent since a blueprint proposed by Freeze & Harlan (1969). The distributed models are able to reproduce hydrological processes at a fine spatial resolution and have been used in many areas, such as flood forecasting (Hailegeorgis & Alfredsen, 2015), water resources assessment, streamflow prediction (Peel & Blöschl, 2011) and simulating hydrological effects of climate and environmental changes (Hasson et al., 2014). It is currently well accepted that modelling, particularly distributed modelling,

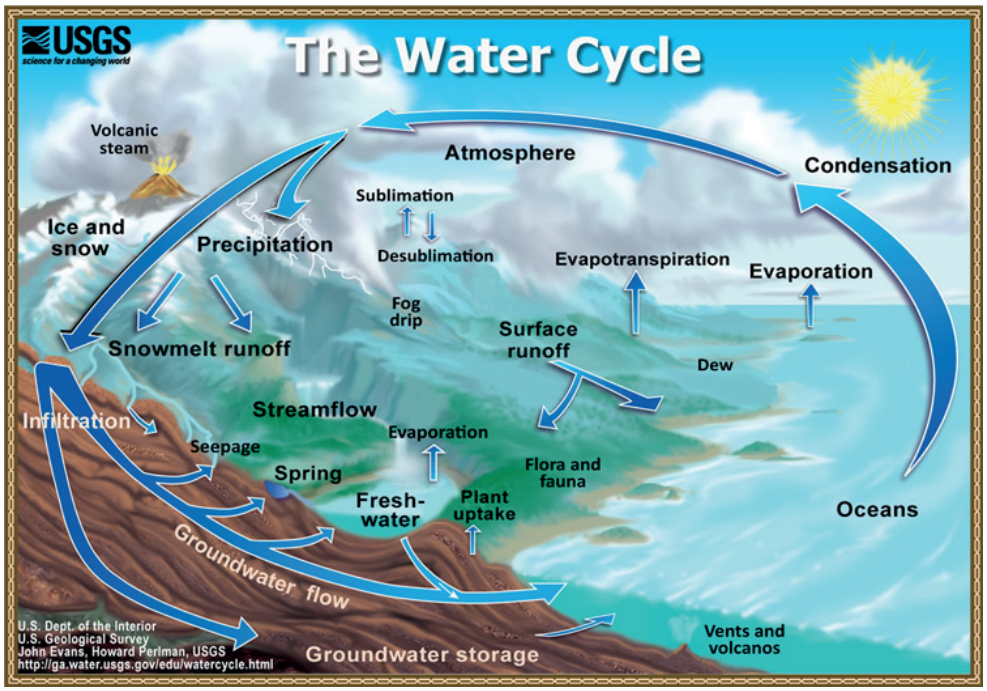

Figure 1.1: The water cycle illustrated by Evans & Periman (2015).

seems to be an irreplaceable resort to address complex environmental and water resources problems.

Caused by greenhouse gas emission, climate change has become a serious environmental threat. Due to global warming and adverse effects of human activities, distributions of precipitation and temperature as well as the resulting runoff will undergo enormous changes throughout the 21^{st} century. These changes have explicit implications for the water cycle and water resources and put forward new requirements for hydrological modelling.

High elevation areas are experiencing more rapid changes than the global average because the warming rate is amplified with elevation (Pepin et al., 2015). In addition, these areas are more sensitive and vulnerable to climate change than other places. All glaciers, except the ice sheets, are located in the high mountains (Khadka et al., 2014). A modification of the prevalent climate can considerably change the glacier existence, the hydrologic regime (Burlando et al., 2002; Radić & Hock, 2014), water resources and the well-being of a large amount of population living in these areas (Beniston, 2003). However, adapting to climate change is difficult in most mountainous areas due to poverty. There are only few similar environments and they are hard to migrate to. Climate change poses difficult and urgent

tasks in mountainous areas.

In spite of the importance, the mountainous areas are not well studied due to complex mechanisms and few available tools. The scopes of this study are hydrological modelling and climate change. This thesis aims at contributing to hydrological modelling by evaluating and improving its capacity under both the present and future climate. The scientific gaps between the current knowledge and the objectives are discussed in the following chapter 2 Scientific Background and Gaps.

1.2 Objectives and Outline

Conceptual models simplify the hydrologic processes according to the purpose which the model was initially developed for. However, some simplifications are not appropriate at present and for the future under a changing climate condition. The goal of this project is to evaluate and improve the capacity of the Hydrologiska Byråns Vattenbalansavdelning (HBV) model to simulate hydrological processes in mountainous and glacierised regions under both the present and future climate.

The HBV model, originally developed for Scandinavia, is selected. The initial version used in this project is a simple grid-based model developed by Beldring et al. (2003) for operational and research purposes used by the Norwegian Water Resources and Energy Directorate (NVE). The water balance calculation is performed in every grid. Runoff at basin outlet is the sum of runoff from all grids. Due to the absence of flow routing, the discharge at the outlet rises at the same time when runoff generation occurs in the basin. For glaciers, the extent is assumed to be constant through one model running. These two limitations are also common for distributed models developed from lumped conceptual hydrological models.

To improve the HBV model taking climate change in mountainous and glacierised areas into account, this project implements routing and glacier retreating modules in the grid-based HBV model. The upgraded model with a glacier retreating module is further used to calculate water resource scenarios. Model improvements and water resource projections are described in four articles, as depicted in Figure 1.2. The routing algorithms including grid-to-grid and source-to-sink methods are described in Article I and Article II. For basins with diminishing glaciers, a mass conserving glacier model, the Δh-parametrisation, is coupled with the HBV model. The hydro-glacial model is tested in three basins (Article III) and used to estimate water resources under changing climate in two Himalayan basins, where glaciers play a vital role in water resources and the ecosystem (Article IV).

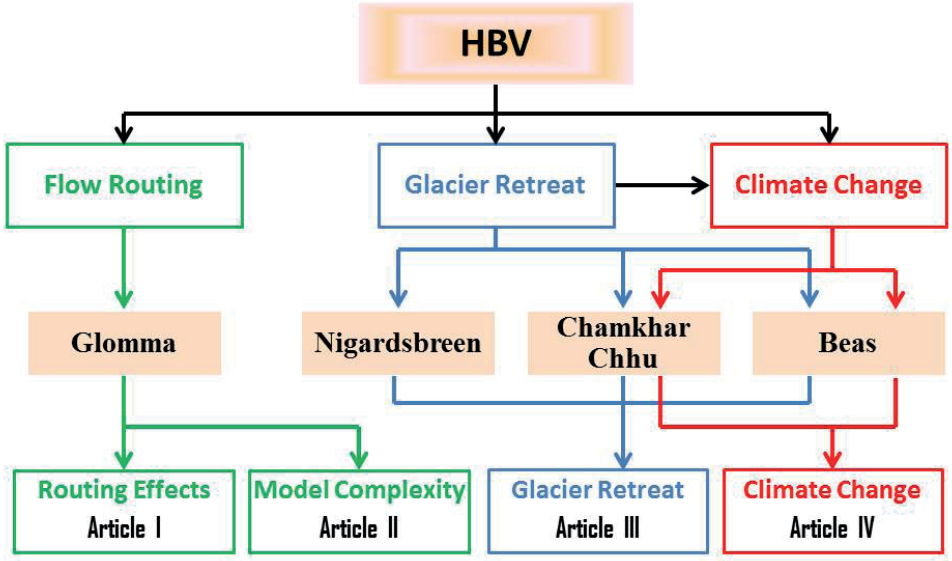

Figure 1.2: Work flow depicting the main methods, study areas and the respective outcomes.

2 Scientific Background and Gaps

2.1 Hydrological Modelling

The first hydrological model was developed to study the relations of rainfall and flood discharge by Mulvaney (1851). Afterwards, numerous hydrological models are sprouting. Particularly after the mid-20^{st} century, hydrological models have prospered due to the advent of computer technology. Among these models, the most frequently and widely used are rainfall-runoff models. They are referred to as hydrological models through this thesis. According to description of processes, hydrological models have undergone three stages. The first were input-output black-box models, the second lumped conceptual models, and eventually physically-based distributed models. There is an evident trend of developing models with a high degree of complexity and this trend reflects growth of hydrological knowledge (Perrin et al., 2001; Mayr et al., 2013).

All three types of models are widely used and each type has its own merits for specific tasks or in capturing certain aspects of real world processes. For example, the Artificial Neutral Network (ANN) method, an example of the black-box models, is applied to forecast river flow for basins with a small number of measurements (Sharmila et al., 2015). The conceptual models originating from the mid-1960s are currently the most extensively used for both research and operation purposes (Zhao, 1992; Perrin et al., 2001). These type of models assume that runoff response is mainly dominated by the dynamics of the saturated area. This can be related to the soil moisture storage using a monotone function (Todini, 2011). Physically-based models (Freeze & Harlan, 1969) are alternatives to conceptual models. They are based on partial differential equations which describe surface and subsurface flow. These watershed models (e.g. the Système Hydrologique Europeén model) usually require a large amount of data and have a large computational demand. These limit their use to small and extensively instrumented basins (Todini, 2011).

The HBV model is a famous conceptual model and it exists in several versions. The first distributed version was achieved by delineating a basin into several sub-basins and the sub-basins were further divided into elevation bands (Lindström et al., 1997). This kind

of modification improved the model performance in many sites (Lindström et al., 1997; Uhlenbrook et al., 1999; Krysanova et al., 1999). However, the grid-based models did not further improve the model (Das et al., 2008; Wrede et al., 2013). A possible explanation is that the input data did not reflect the actual spatial variability.

In the Norwegian hydrological community, a grid-based model is available from NVE (Beldring et al., 2003; Beldring, 2011). This model builds on the Nordic HBV model (Sælthun, 1996) and aims at using the distributed hydrological model for both research and operational purposes, particularly for studies of climate change. However, there is no routing function in the model and the glacier routine is not valid since glaciers are retreating and seasonal snowfalls are diminishing in many regions (Barnett et al., 2005). Therefore, this study implements these two functions to elaborate the HBV model for a wide applicability in hydrology and climate change.

2.2 Glacier Modelling

Glacier mass balance models and hydrological models has been widely used to estimate runoff from glaciers. A large body of literature using these models exists. However, the glacier models surfer from absence or raw presentations of hydrological processes (Kotlarski et al., 2010; Engelhardt et al., 2013) and the hydrological models surfer from static assumptions of glacier extent (Singh & Bengtsson, 2004; Mayr et al., 2013).

An interdisciplinary effort linking glacier dynamics and hydrologic responses represents a realistic presentation of glaciers in hydrological models. A general way is to update the glacier extent according to the mass change by a simple glacial model. For instance, Horton et al. (2006) published a conceptual reservoir-based hydrological model. In this model, the glacier extent was updated by the accumulation area ratio (AAR) method. The basic hypothesis of this AAR method is that the accumulation area is equal to a fixed proportion of the total glacier area. However, this hypothesis is not able to reproduce a transient response of glaciers to a changing climate (Huss et al., 2008). With a specific focus on the transient responses, Stahl et al. (2008) integrated a glacier area evolution model into the HBV model. The evolution model is based on volume-area scaling. This method cannot describe a critical time lag between the area and the volume responses to the climate (Lüthi, 2009; Radić & Hock, 2014).

With access to glacier measurements, some physically-based glacier dynamic models are available. Immerzeel et al. (2012) developed a hydrological and glacial model based on a conceptual rainfall-runoff model and glacier basal sliding. Naz et al. (2014) published

a physically-based distributed model both for runoff and glacier dynamics. A common drawback of these models is a high demand of input data and computational power. Moreover, due to large variability among glaciers, these models can only be used in the same or similar conditions where they were initially developed; therefore their wide applicability is limited.

A glacier model suitable for hydrological purposes should avoid the imperfections mentioned above. It should build on a solid scientific basis and should require low or moderate demand of data and computation resources. In addition, the model should be compatible with hydrological models at temporal and spatial scales. The Δh-parametrisation method proposed by Huss et al. (2008) fits these requirements; therefore this glacier model is selected to simulate glacier extent and surface elevation changes. Details of the algorithms are given in chapter 3.3 Glacier Model.

2.3 Climate Change

The most distinct measure of climate change is an increase of global average temperature (Rogelj et al., 2012). In addition to temperature, precipitation patterns have also changed. Significant changes in heavy precipitation have occurred during the past decades in the Europe, USA, China and western South Africa (Easterling et al., 2000; Iglesias et al., 2011; Ruelland et al., 2012; Yang et al., 2012). The changes of climate and human activities modify the hydrologic regime.

The hydrologic regime can be modified by changes in the mean or variance. High temperature usually leads to a high rate of water loss due to evaporation and more precipitation results in more runoff. High variance of precipitation, even if total amount is less, can result in a high runoff coefficient and finally in an increase in the total runoff (Easterling et al., 2000).

Furthermore, snowfall and glaciers have been significantly altered due to global warming (Barnett et al., 2005; Bolch et al., 2012) and have subsequently affected the regional hydrological regime. Moreover, both are predicted to decrease at accelerating rates (Radić & Hock, 2014). Runoff from retreating glaciers has been generally stated as: it initially increases due to increasing rates of melting and afterwards it stabilises when the glacier is completely removed or obtains a new stable condition (Huss et al., 2008). Hydrologists and glaciologists have made many efforts at more detailed scales (Akhtar et al., 2008; Huss, 2011; Immerzeel et al., 2012; Khadka et al., 2014). Their results suggest a large inhomogeneity among mountain glaciers due to small-scale factors, such as the size, loca-

tion, geometry and climate. This inhomogeneity leads to huge uncertainties when scale-up to the whole glacier population when initially based on few in situ measurements (Vieli, 2015). Plus a large uncertainty inherited from climate models (Huss et al., 2014), a highly accurate assessment remains largely unaccomplished.

Impacts of climate change on water resources is currently drawing strong attention by the research and public community. Generally, annual runoff is used as a measure of the sustainable water resources (Milly et al., 2005; Ruelland et al., 2012). However, in order to keep rivers healthy and avoid harmful environmental consequences, a minimum amount of water is required of fish and other aquatic species and for maintenance of river channel, wetland and riparian vegetation (Smakhtin et al., 2004). This amount of water is defined as the environmental water requirement (EWR), which should not consumed by the humanity. Thereby, EWR should not be considered as the available water resources in sustainable water resources management.

The available water resource per capita is a standard index for measuring the degree to which a country is facing water scarcity and is often used to show a growing global water crisis (Chenoweth, 2008). This water resources indicator depends on both the total amount of available water and population growth. Therefore, assessment of water resources for the future must also consider the population growth, particularly for the developing countries, where population is growing fast.

3 Methodology

3.1 Hydrological Model

The HBV model has three main routines, respectively for snow, soil and groundwater responses. The scientific basis and algorithms have been explicitly described in Bergström (1976) and Lindström et al. (1997). The study builds on the version developed by Beldring et al. (2003) and the important equations to this project are given here.

Precipitation and temperature are the most essential inputs to the HBV model. In the distributed HBV model, station measurements are interpolated to each grid ahead of water balance calculations. However, the interpolation is not necessary for input data in a grid format. The precipitation is first corrected for under catch (Equation 3.1). The corrected precipitation and temperature values are interpolated by the Inverse Distance Weighting (IDW) method with consideration of elevation effects (Equations 3.2 and 3.3).

$$P_{\mathrm{c}} = \begin{cases} K_{\mathrm{r}} \cdot P_{\mathrm{o}} & \text{if rainfall} \\ K_{\mathrm{s}} \cdot K_{\mathrm{r}} \cdot P_{\mathrm{o}} & \text{if snowfall} \end{cases} \tag{3.1}$$

where P_{c} is corrected precipitation (mm/day) and P_{o} is station measured precipitation (mm/day). K_{r} and K_{s} are free parameters respectively for rainfall and snowfall correction.

$$P_{\mathrm{g}} = \sum_{i=1}^{n} W_{\mathrm{i}} \cdot P_{\mathrm{i}} \cdot \gamma_{\mathrm{p}}^{(H_{\mathrm{g}} - H_{\mathrm{i}})/100} \tag{3.2}$$

$$T_{\mathrm{g}} = \sum_{i=1}^{n} W_{\mathrm{i}} \cdot (T_{\mathrm{i}} + \gamma_{\mathrm{t}} \times \frac{H_{\mathrm{g}} - H_{\mathrm{i}}}{100}) \tag{3.3}$$

where P_{g} and T_{g} are precipitation (mm/day) and temperature (°C) of each grid. W_{i} is the weight of station i calculated by the IDW method. H_{g} and H_{i} are the elevations (m amsl) of grid and station i. Further, γ_{t} (°C per 100 m) and γ_{p} are parameters that describe respectively linear and exponentially elevation effects on temperature and precipitation (Beldring et al., 2003).

Snowmelt is calculated by a degree-day method according to Equation 3.4. Ice melting is calculated using the same method but with another higher melting factor.

$$SMelt = SMELTR \times (T - T_{\text{melt}}) \quad T > T_{\text{melt}} \tag{3.4}$$

where $SMelt$ is snowmelt (mm/day); $SMELTR$ is a degree-day factor (mm/°C/day); T is the daily air temperature (°C); T_{melt} is the threshold temperature for snow melting (°C).

The rate of actual evaporation (AE, mm/day) is a function of the potential evaporation rate (PE, mm/day) and available soil moisture (SM, mm).

$$AE = \begin{cases} \frac{PE \times SM}{FC \times FCD} & SM < FC \times FCD \\ PE & SM \geq FC \times FCD \end{cases} \tag{3.5}$$

where FC is the field capacity (mm); FCD is an empirical parameter that takes values between 0 and 1.

Groundwater is conceptualised into two storage reservoirs, the upper zone and lower zone. Runoff components from the two zones have their origins in the fast and slow runoff components of the hydrograph. Total runoff (Q) is formulated as:

$$Q = KUZ \times UZ^{\alpha} + KLZ \times LZ \tag{3.6}$$

where UZ (mm) and LZ (mm) are respectively storage of the upper zone and lower zone, and KUZ (1/day) and KLZ (1/day) are their recession parameters. α describes a fast and non-linear response of runoff to groundwater storage.

3.2 Routing Algorithms

In distributed hydrological models, flow routing is usually dealt with as grid-to-grid or source-to-sink routing (Gong et al., 2009). The grid-to-grid approach, e.g. the Muskingum-Cunge (MC) method, is based on the discharge at the upstream and downstream sections. The source-to-sink approach is a procedure for routing from the grids where runoff is produced to the outlet grid.

The first type is storage based, which means that for each river grid, outflow is a function of inflow and storage. In contrast, the second type is time delay based. The time difference of runoff appearance in every individual grid and at the basin outlet is computable. The two types of routing models cannot replace each other, since the first is only for the channel

routing whereas the second counts the time delay between grids. The delay includes runoff draining from land grid downstream grid, to river grid and eventually arrival the outlet.

For the first type of routing, the MC method is chosen due to its prevalence. The fundamental equation is formulated as:

$$\frac{dS}{dt} = I - O \tag{3.7}$$

$$S = \kappa\varepsilon I + \kappa(1-\varepsilon)O \tag{3.8}$$

where t is time (s); S is the water storage in the channel (m^3); I is the inflow discharge at the upstream section (m^3/s) and O is the outflow discharge at the downstream section (m^3/s). Two parameters, κ and ε respectively describe the required time by a flood wave to travel through the two sections and the relative importance of the inflow on the outflow. Both parameters can be estimated from observations or calibration. A numerical solution proposed by Todini (2007) is adopted due to its advantage in keeping the mass conservative.

For routing between land grids, a simple way is that the runoff from each land grid drains to the next land grid until the runoff discharges into a river grid, which represents the real channel in distribute modelling. The sequence of the grids in a flow path is derived from the flow direction. The reason for this hillslope routing is the absence of overland flow due to large infiltration capacity caused by dense vegetation and glacier deposits in the Nordic countries (Beldring, 2002b).

For the second type of routing, the time delay is calculated as the quotient of the distance and the flow velocity (Gong et al., 2009). The distance is the length of the flow path, which is taken from the land grid where runoff is originally generated to the outlet. The Network Response Function (NRF), originally proposed by Gong et al. (2009), assumes a time-independent flow velocity, which is parametrised as a function of slope. The time delay is formulated as:

$$t = \sum_{i=1}^{i=n} \frac{l_{\mathrm{i}}}{V_{45} \cdot \sqrt{tan(b_{\mathrm{i}})}} \tag{3.9}$$

where i is grid index in a flow path; l_{i} (m) is the length of the flow path in grid i; b_{i} is the slope (^{o}) of grid i; V_{45} (m/s) is a parameter, presenting the flow velocity when the slope is 45^o.

Here, the two types of routing algorithms are implemented in the grid-based HBV model. The updated models are assessed in the Glomma basin in Norway at three spatial resolu-

tions, as presented in Article I.

3.3 Glacier Model

The Δh-parametrisation owes its origin to varying thinning rates across a glacier. For a certain mass change, elevation changes in the high accumulation area are smaller than in other areas. The terminus is usually the place of the largest change. Therefore, the elevation changes can be related to the ice volume change and the relative elevation in the elevation range. The function is parametrised as:

$$\Delta h = (h_{\mathrm{r}} + a)^{\gamma} + b \times (h_{\mathrm{r}} + a) + c \tag{3.10}$$

where Δh is the normalised surface elevation change and h_{r} is the normalised elevation of a glacier. Further, γ, a, b and c are free parameters (Huss et al., 2010) which can be derived from glacier surface maps of different years, or calibrated according to other measurements (e.g. discharge or annual mass balance).

Integration of the dimensionless Δh-function (Equation 3.10) over the whole glacier, taking into account the area A of each grid i and the ice density ρ_{ice} must equal the total annual glacier mass change B_{a} calculated by the HBV model:

$$B_{\mathrm{a}} = f_{\mathrm{s}} \cdot \rho_{\mathrm{ice}} \cdot \sum_{i=0}^{h_{\mathrm{r}}} A_{\mathrm{i}} \cdot \Delta h_{\mathrm{i}} \tag{3.11}$$

where f_{s} is a factor that scales the magnitude of the dimensionless ice thickness change pattern. This factor is chosen for each time interval such that Equation 3.11 is satisfied. The updated surface elevation h_1 is then calculated as Equation 3.12.

$$h_1 = h_0 + f_{\mathrm{s}} \cdot \Delta h_{\mathrm{i}} \tag{3.12}$$

The glacier disappears in a grid when h_1 is equal to the bedrock elevation. The required inputs are the initial ice thickness and surface elevation. The algorithm runs for an individual glacier flow shed constructed from the surface elevation according to the D8 (deterministic eight-node) algorithms (O'Callaghan & Mark, 1984), but all flow sheds in a basin share the same values of the parameters. The glacier area has a slower dynamics than the runoff (Lüthi, 2009). Therefore, the glacier extent is updated at an annual scale, at the end of every hydrological year, i.e. August 31^{st}.

The HBV model with this glacier model is evaluated in three basins (i.e. the Nigardsbreen,

Chamkhar Chhu and Beas basins) with considerable glacier coverage for hydrological and glacial simulations (Article III). The hydro-glacial model is further used to project water resources for the two Himalayan basins forced by two regional climate models (RCMs).

3.4 Calibration Method

Parameter estimation plays an important role in applying complex hydrological and other environmental models. It has been widely recognised that a successful optimisation scheme is not only able to obtain a proper estimation of parameters, but also requires appropriate computation resources (Skahill & Doherty, 2006). A free package called PEST (Parameter ESTimation) fits these requirements. Additionally, PEST is model independent; therefore any arbitrary model can be easily set up (Doherty, 2005).

The algorithms are based on the Gauss—Marquardt—Levenberg algorithm. It combines advantages of the inverse Hessian matrix and the steepest gradient method (Doherty & Johnston, 2003). PEST approaches to the best value of the objective function with with a small number of model runs. The objective function is the square sum of the discrepancies between the simulated and observed series.

PEST has been criticised for poor performance in the face of local optima (Gupta et al., 2003). In contrast, other algorithms such as the Shuffled Complex Evolution algorithm (Duan et al., 1992) are much more likely to find the global optimised objective function with the cost of a much greater number of model runs (Coron et al., 2012). PEST is selected due to its good performance for Norwegian catchments (Lawrence et al., 2009) as well its sophistication after a long term development (Doherty, 2005). Moreover, PEST can achieve an equivalent global optimal parameter set on the basis of different initial values.

To use PEST, users need to determine target outputs and prepare input files in required formats. The series of the target outputs are to calculate the objective function. The input files explicitly describe ranges of parameters that can be tied to each other in models with a large number of parameters. This allows to identify a fixed proportion between the tied and host parameter, facilitating the calibration and reducing the problem of parameter equifinality without losing degree of freedom.

3.5 Statistical Downscaling

Global climate models (GCMs) have demonstrated their applicability to simulate the present climate and they have been used to predict the future climatic changes. However,

they cannot satisfy requirements for hydrological purposes because their spatial scale, typically of 250–600 km, is too sparse to depict hydrological processes. Direct usage of output data from GCMs in hydrological models is not successful due to the inherent simplification of water movements in GCMs and differences in temporal and spatial scales (Xu, 1999). The differences also hinder coupling two types of models.

The idea of downscaling is designed to fill or narrow the gap of different scales. There are two broad classes of downscaling approaches, dynamic models and statistical models (Xu, 1999). The dynamic model approach uses nesting resolution or RCMs. However, the downscaled results still cannot meet the needs of spatially explicit modelling ecosystems or hydrological systems. Results from such models are further downscaled to individual sites by the statistical methods.

The statistical downscaling relates regional-scale atmospheric predictor variables and/or circulation characteristics to the station observed series (Xu, 1999). The statistics involved can be simple or complex, but the final relationships are typically approached by regression analysis. Among the statistical methods, the most popular approaches are statistical transformations that adjust the probability distribution of modelled results to resemble observations.

Seven methods (Table 3.1) are selected to downscale daily precipitation and temperature of the RCMs' data (Gudmundsson et al., 2012). Due to the high variabilitity in daily precipitation, the derived parameter values can vary strongly in different months (Hempel et al., 2013); therefore the methods are performed for each calendar month. To avoid changes of seasons, the previous and the next months are also used for calibration. For example, All series in Janunary, Feburary and March are used to derive the parameter values for January. To conserve trends of climate data for the future scenarios, a trend preserving method (Hempel et al., 2013) is additionally employed for the future climate. A multiplicative correction and an additive correction are respectively used for precipitation and temperature. The correction factors are computed by comparing the mean of the future and of the reference period as shown by Equation 3.13 to 3.14.

$$\widehat{P} = f(\tfrac{P}{\lambda_\mathrm{p}}) \times \lambda_\mathrm{p}, \quad \lambda_\mathrm{p} = \tfrac{\bar{P}}{\bar{P}_0} \tag{3.13}$$

$$\widehat{T} = f(T - \lambda_\mathrm{t}) + \lambda_\mathrm{t}, \quad \lambda_\mathrm{t} = \bar{T} - \bar{T}_0 \tag{3.14}$$

where λ_p and λ_t are correction factors respectively for precipitation and temperature; P and P_0 are modelled precipitation respectively for the future and reference period; $\widehat{P}$

and $\widehat{P}$ are respectively the bias corrected precipitation and temperature. f is the bias correction method in Table 3.1.

Table 3.1: Formulas of seven statistical bias correction methods. $\widehat{P_\mathrm{o}}$ is the calculated value at a observation site. P_m is the RCM modelled value. a, b, c, x and τ are free parameters that are estimated from series of observation period.

Method (short name)	Formula
M1 (empirical)	Empirical quantiles
M2 (splines)	Smoothing splines
M3 (linear)	$\widehat{P_\mathrm{o}} = a + bP_\mathrm{m}$
M4 (power.x)	$\widehat{P_\mathrm{o}} = b(P_\mathrm{m} - x)^c$
M5 (exponential)	$\widehat{P_\mathrm{o}} = (a + bP_\mathrm{m}) \times (1 - e^{-(P_\mathrm{m}-x)/\tau})$
M6 (scale)	$\widehat{P_\mathrm{o}} = bP_\mathrm{m}$
M7 (power)	$\widehat{P_\mathrm{o}} = bP_\mathrm{m}^c$

3.6 Numerical Criteria

Numerical criteria enable to judge simulations in an efficient and reproducible way. However, depending on their formulations, the criteria underscore certain aspects of the set of analysed values. Therefore, the criteria must be deliberately selected with consideration of purpose (Crochemore et al., 2015). Considering complementary criteria is an obvious advantage to obtain a comprehensive assessment. Moreover, standard and common criteria are also included to provide a reference for other researchers.

The criteria are used to quantify similarity of observed and model generated series. In total, eight numerical criteria as formulated in Table 3.2 are used for various purposes and each emphasises on a different aspect. Among them, the *bias* and relative mean error (RME) underline the total volume error. The mean absolute error (MAE) and normalised mean square error ($NMSE$) define the absolute difference between the simulated and observed series. The Nash-Sutcliffe efficiency (NSE) (Nash & Sutcliffe, 1970) and the inverse NSE ($InNSE$) (Pushpalatha et al., 2012) are measures of match of two series, respectively with larger weight on high flow and low flow. The Pearson product-moment correlation coefficient (COR) is for evaluation of the linear relationship between simulated

and observed series. The standard deviation (sd) is used to quantify the amount of variation of a series.

Table 3.2: Formulas of the numerical criteria. O is the observed series; S is the simulated series; n is the length of the series; $\bar{O}$ and $\bar{S}$ are respectively the mean of observed series and simulated series. The series are abbreviated in the column of Series: Precipitation (P, mm/day), Temperature (T, ^{o}C), Discharge (Q, m^3/s), glacier annual Mass change (M, mm/year), Snow water equivalent (S, mm), Groundwater depth (m) or storage (mm), Human population (H). In the column Unit, — indicates dimensionless and the remaining criteria are in the unit of their used series.

Criteria	Formula	Perfect value	Range	Series	Unit
bias	$\frac{\sum_{i=1}^{i=n}(S_\mathrm{i}-O_\mathrm{i})}{n}$	0	$(-\infty, +\infty)$	P, T, H	
RME	$\frac{\sum_{i=1}^{i=n}(S_\mathrm{i}-O_\mathrm{i})}{\sum_{i=1}^{i=n} O_\mathrm{i}} \times 100$	0	$(-\infty, +\infty)$	Q, H	—
MAE	$\frac{\sum_{i=1}^{i=n}\lvert S_\mathrm{i}-O_\mathrm{i}\rvert}{n}$	0	$[0, +\infty)$	P, T	
sd	$\sqrt[2]{\frac{(S_\mathrm{i}-\bar{S})^2}{n}}$	$\sqrt[2]{\frac{(O_\mathrm{i}-\bar{O})^2}{n}}$	$[0, +\infty)$	P, T	
NMSE	$\frac{\sum_{i=1}^{i=n}(S_\mathrm{i}-O_\mathrm{i})^2}{n \times {sd_\mathrm{o}}^2}$	0	$[0, +\infty)$	P, T	—
COR	$\frac{\sum_{i=1}^{i=n}(S_\mathrm{i}-\bar{S})(O_\mathrm{i}-\bar{O})}{\sqrt{\sum_{i=1}^{i=n}(S_\mathrm{i}-\bar{S})^2}\sqrt{\sum_{i=1}^{i=n}(O_\mathrm{i}-\bar{O})^2}}$	1	[-1, +1]	M, S, G	—
NSE	$1-\frac{\sum_{i=1}^{i=n}(S_\mathrm{i}-O_\mathrm{i})^2}{\sum_{i=1}^{i=n}(O_\mathrm{i}-\bar{O})^2}$	1	$(-\infty, 1]$	Q	—
InNSE	$1-\frac{\sum_{i=1}^{i=n}(\frac{1}{S_\mathrm{i}}-\frac{1}{O_\mathrm{i}})^2}{\sum_{i=1}^{i=n}(\frac{1}{O_\mathrm{i}}-\frac{1}{\bar{O}})^2}$	1	$(-\infty, 1]$	Q	—

4 Study Areas and Data

4.1 Study Areas

Glomma Basin

The Glomma or Glåma basin is located in central southern Norway (Figure 4.1). The drainage area is up to 41,963 km^2 and this is almost 15% of the area of Norway. The Glomma river is the longest Norwegian river (618 km) and an important Scandinavian river system. It originates from the northern mountains and flows southward into the Oslofjord at Fredrikstad (L'Abée-Lund et al., 2009).

In general, the land is high in the north and decrease to the southeast. The climate varies considerably with elevation. It can be characterised as summer warm and winter cold. Based on measurements at the meteorological station of Lillehammer (226 m amsl) for the period 1961–1990, the annual temperature is 2.9°C, ranging from -9.3 to 14.7°C, respectively, in January and July. The annual precipitation is 720 mm/year, a large amount of which falls as snow in winter (L'Abée-Lund et al., 2009). Snowmelt is a major reason for severe floods. Streamflow at the snowmelt months, May and June is typically high.

Approximately 600,000 inhabitants are living within the Glomma basin, with a higher population density at the lower basin. Areas below 600 m amsl are cultivated for agriculture. Most of natural lands are covered by forests. They spread widely in the areas under the tree line, i.e. roughly 1,000 m amsl for this area. Above the tree line, bedrock is exposed or covered by glaciers or permanent snow.

For this project, two sub-basins with considerably large sizes are selected. They are located upstream of the western and eastern branches of the river. For the western branch, the area above the Losna gauging station is 11,213 km^2, and has a high and steep terrain. For the eastern branch, the area above the Norsfoss gauging station is 18,932 km^2, and is relative lower and flatter compared with the western branch. The two sub-

basins are regulated and the regulation capacities are 13.66% (Losna) and 8.57% (Norsfoss).

There are six sub-basins in the Norsfoss basin, and their locations are shown in Figure 1: Article II. Their discharge series are used to validate models, but are not involved in the calibration.

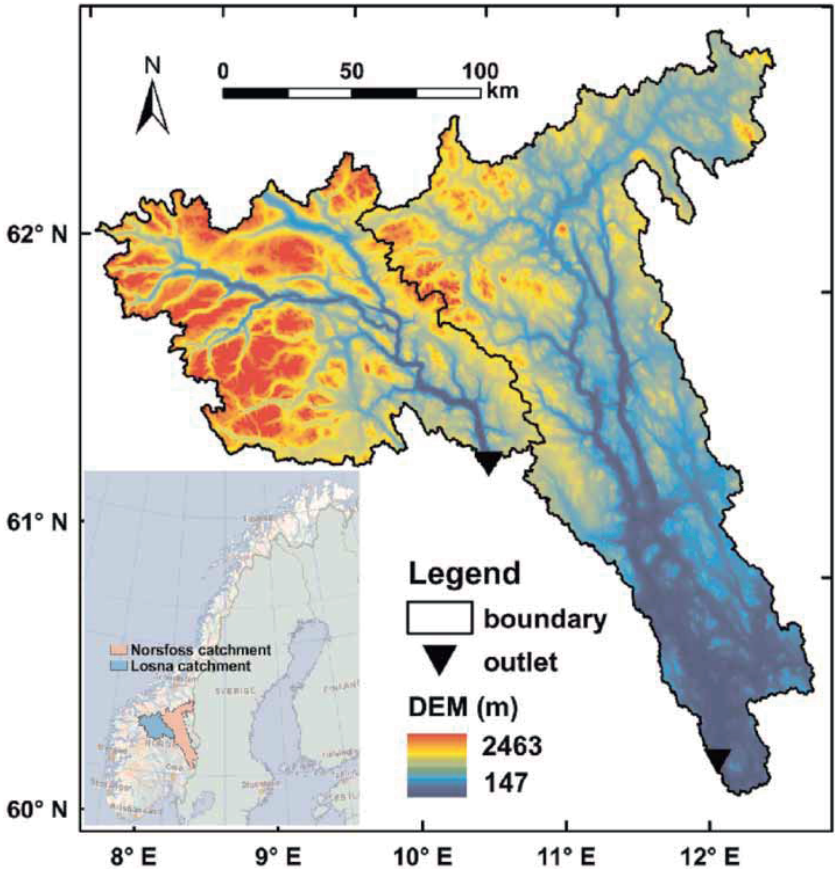

Figure 4.1: Location and Digital Elevation Models (DEMs) of the Glomma basin. The black triangles denote the outlets of the sub-basins. From left to right, they are the Losna and Norsfoss stations.

Nigardsbreen Basin

The Nigardsbreen basin is a mountainous glacierised watershed in western Norway (Figure 4.2). It has an area of 65 km^2 and a large range of elevation. The highest point is at 1,945 m amsl and the lowest is at 285 m amsl. The climate is humid as it is influenced by the moist currents from the ocean. In addition, the climate is locally modified by the presence of the glacier. The annual temperature is -0.47°C and the annual precipitation reaches 3,736 mm/year. A large amount of precipitation is falling in winter as snow. Streamflow is largely from melt of snow and ice in the warm period of the year (Figure 3(a): Article III).

Nigardsbreen is one of the largest outlet glaciers from Jostedalsbreen, which is the largest ice cap in Northern Europe. The glacier ice covers approximately 73% of the basin area. It is orientated towards the southeast and flows along the valley. The glacier extends from 1,957 to 315 m amsl.

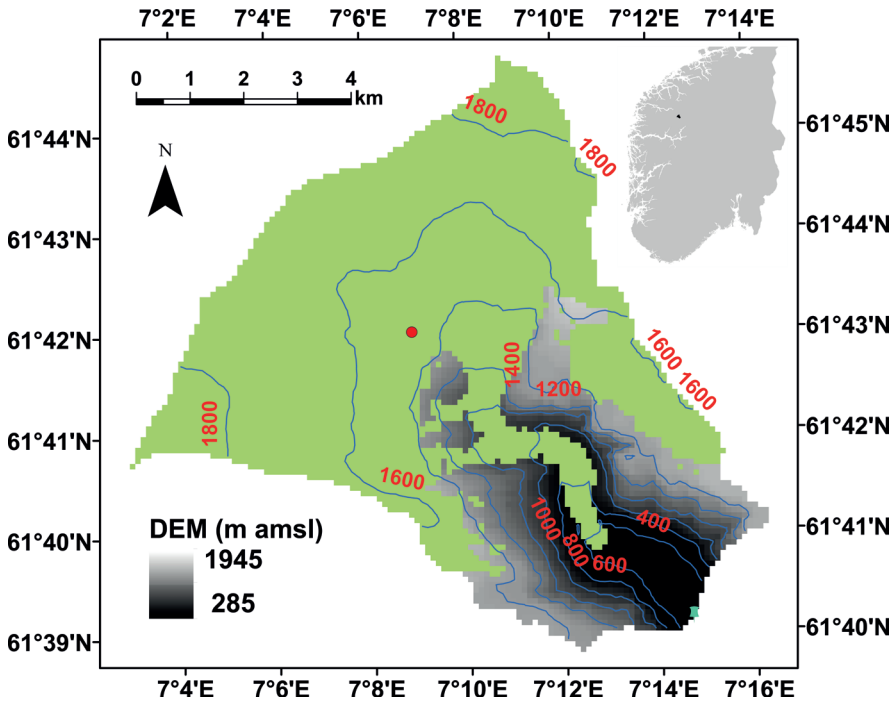

Figure 4.2: Location and DEMs of the Nigardsbreen basin at the Nigardsbreen station. The light green indicates the glacier covered area. The contours are elevations (m amsl). The red dot denotes the location of the virtual meteorological station and the cyan pin marks the location of the discharge gauging station.

Beas Basin

The Beas River is an important branch of the Indus River system in northern India (Figure 4.3(a) and (b)). It originates at the southern side of the Rohtang Pass in the Himalaya. The river is 470 km long and has a drainage area of 12,916 km^2 (Gupta et al., 1982). This area is extremely rich in hydroelectricity resources. In total, there are 11 hydroelectric plants projects and three of them are under constriction or have been finished (SANDRP, 2015).

To avoid the effects of flow regulation and to have a large study area, the Bhuntar gauging station is selected. The area above this station is 3,202 km^2. The station lies downstream of the joint of the eastern branch, the Parbati River. Only the Malana Hydel Scheme, with a capacity of 86 megawatt, was running during the observation period 1997–2005.

The climate is a result of a combined effect of elevation and monsoon. The land decreases from 6,288 m amsl in the northern mountains to 1,055 m amsl. The higher northern part is colder and drier than the lower valleys. Influenced by the monsoon, there are four seasons, winter (January to March), pre-monsoon (April to June), monsoon (July to September) and post-monsoon (October to December). The monsoon strength is a major indicator of the magnitudes of precipitation and temperature. Based on the observations in the period from 1997 to 2005, the annual precipitation is 1,116 mm/year and the annual temperature is -1.04°C. The air currents of the monsoon originate in the Bay of Bengal and they are relatively weak after striking the eastern Himalaya and a long westward travel. Therefore, the precipitation considerably decreases from the low valley areas to the high mountains (Singh & Kumar, 1997).

Glaciers are mainly located along the eastern part of the drainage divide line above 4,500 m amsl. They cover approximately 32.7% of the area. Due to a pleasant view of glaciers and mountains, this area is famous and attractive to tourists. The tourism industry as well as the local inhabits are scattered along the river, particularly along the main Beas branch. The Bhuntar Airport is located further downstream of the Bhuntar station.

Chamkhar Chhu Basin

The Chamkhar Chhu is located in central Bhutan and the river is one of the major national rivers (Figure 4.3(a) and (c)). It has three branches, one western branch and two eastern branches. They respectively originate from the glaciers of the Gangkar Punsum region and the southern glaciers of the Monla Karchung La region. The river flows south-easterly and finally joins the Brahmaputra River in India.

The basin area above the Kurjey gauging station is 1,353 km^2. The elevation ranges from 6,653 m amsl in the upper northern glacial region to 2,643 m amsl in the southern lowland. The northern part above 4,000 m amsl is mainly covered by glaciers. The southern lowland is covered by forests. Inhabitants are dwelling along the river, with a higher population density at the lower elevation. The town of Jakar and the Bathpalathang Airport lie downstream of the Kurjey station and represent popular tourist destinations.

The climate is strongly influenced by elevation and monsoon from the southeast to the northwest. Based on observations in the period from 1998 to 2008, the annual precipitation is 1,786 mm/year and the annual temperature is 1.75°C. The monsoon usually starts in June and lasts until early September. It brings significant amounts of rain and warm weather. Subsequently river flow rises due to the rainfall and melting of snow and ice at the high places. As the monsoon proceeds or retreats, there are four clear seasons, spring (March to May), summer (June to August), autumn (September to November), and winter (December to February).

4.2 Data

The used data can be classified into four types, initialisation values, parametrisation scheme, climate forcing and observations of model variables. The initialisation data are to provide initial values for the models, such as the initial ice thickness maps. The parametrisation scheme is used to derive values of model parameters. The climate data are continuously taken into models to proceed simulation. The observations of model variables are records of simulated variables via utilisation of instruments. The similarity between the observations and modelled results is a measure of model efficiency.

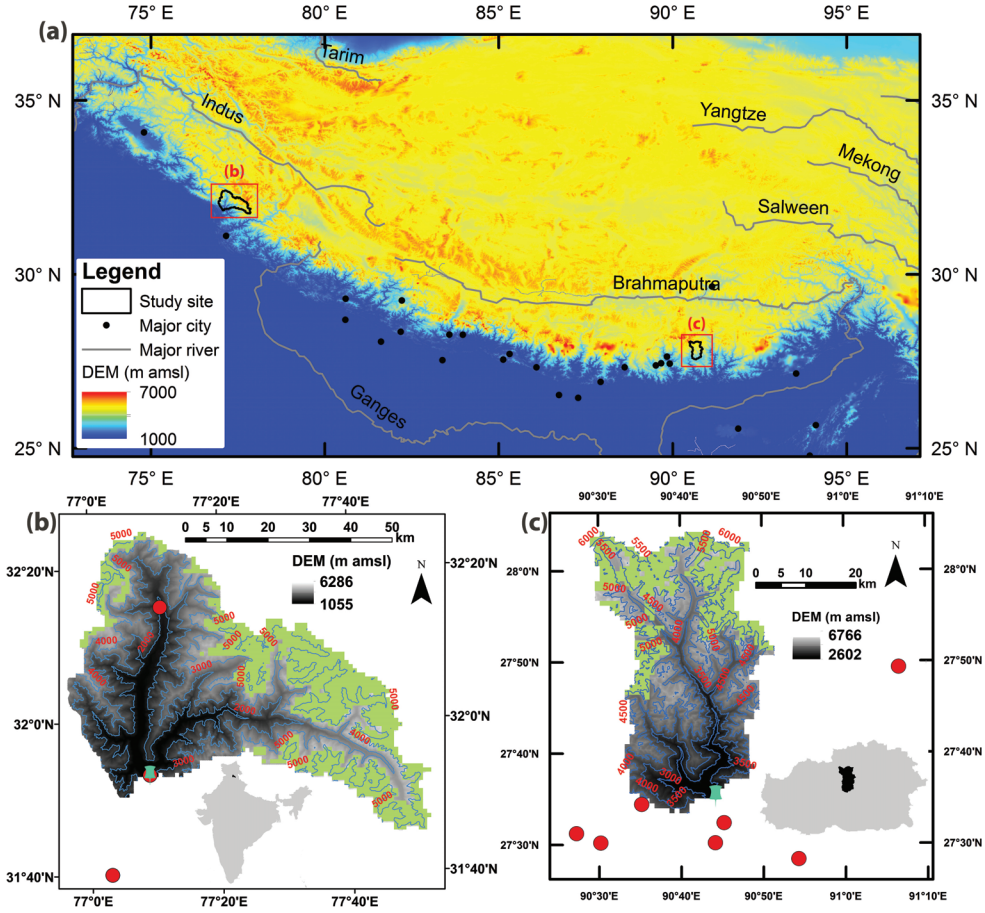

Figure 4.3: (a) Map of the Himalaya showing the elevations (DEMs), major rivers and major cities and the locations of the study sites (Joshi, 2007, 2008, 2011). (b) The Beas basin at the Bhuntar gauging station. (c) The Chamkhar Chhu basin at the Kurjey gauging station. The range of DEM in (a) is assigned to give a better presentation rather than the minimum and maximum for the displaying area. In (b) and (c), the light green indicates glacier covered area. The contours are elevations (m amsl). The red dots denote meteorological stations measuring precipitation and temperature and the cyan pins mark the locations of the discharge gauging stations.

Initialisation

Initial conditions provide a starting point for a model system. In addition, initial values are required for numerical solution by any computer model. Hydrological initial conditions primarily include factors such as soil moisture content, groundwater level and Snow Water Equivalent (SWE), etc. The initial values can be estimated from observations or through model simulations, usually referred to as model "spin-up". The latter is

preferred in most cases due to the high costs of field measurements. Moreover, hydrological models simplify and conceptualise the real processes to certain degrees. Some variables cannot be directly derived from measurements, particularly for conceptual hydrological models.

The sensitivity of the simulation to initial conditions is determined by basin characteristics (Goodrich et al., 1994), predominant mechanisms (Noto et al., 2008), forcing intensity and scale, both in time and space (Bronstert & Bárdossy, 1999; Castillo et al., 2003). Usually, the higher sensitivity requires a longer spin-up period. In addition, in some places, the hydrological system has a reboot function. For example, soil with a large infiltration capacity gets saturated in snow covered areas. In this case, a proper starting date is also important.

The initial conditions of the HBV model are assigned according to experience. They are generally described as low water storage. The starting time of spin-up is the first day of August or September, which is close to the start of a hydrological year. For reproducing runoff of the Norwegian basins, model simulation starts from the first day of the following calendar year.

For glacier simulation, measurements of glacier thickness are required, since glaciers form over many years, often centuries. The glacier volume at present cannot be constructed by usage of the recent climate, particularly the recent warming has induced fast melting globally. Therefore, ice thickness maps are used for initialisation and verification of glacier simulations.

For the Nigardsbreen basin, bedrock and glacier surface elevation maps are available from NVE. They have a spatial resolution of 25 m. The glacier profiles were measured by the Radio-Echo Sounding (RES) method during spring and early summer in the years 1981, 1984 and 1985 (Sætrang & Wold, 1986). The bedrock map is obtained through interpolation of the measured profiles and the open valley. The glacier surface elevation at a spatial resolution of 25 m are derived from complete or partial aerial photos taken within the period 1984–2009. The ice thickness is calculated as the difference between the glacier surface and bedrock for each grid. The thickness map are further aggregated at a resolution of 100 m, which is the spatial resolution of the HBV model for the Nigardsbreen basin. The initial date of the HBV model simulations is September 1^{st}, 1989, which is roughly the middle of the periods when the aerial photos were taken.

For the Chamkhar Chhu and Beas basins, ice thickness is a part of a global dataset generated by Huss & Farinotti (2012) using a method based on glacier mass turnover

and principles of ice-flow mechanics (Farinotti et al., 2009). The map is re-sampled at a spatial resolution of 1 km. Determining the starting date is difficult, since there is no specific date for the ice thickness data. The global dataset is generally thought to represent the state for the year 2000 depending on the date of the utilised glacier inventory data (Pfeffer et al., 2014). For South Asia, five surveys dating from 1995 to 2009 were used by Huss & Farinotti (2012) to generate the dataset. Considering considerable uncertainty (Gärtner-Roer et al., 2014), the starting date is mainly determined by the observation period of the meteorological data. The model starting dates are September 1^{st}, 1993 for the Himalayan basins.

Parametrisation Data

The parametrisation data are used to characterise basins and classify parameter values. These data have more significance for distributed models than for lumped models, since there are considerably more parameters for distributed models than for lumped models. Fortunately, most parameters of hydrological models are highly related to vegetation and soil types. One parameter set for every type of land use or soil type intensely reduces the number of parameters for the distributed models. To parametrise, there are mainly two types, orographic maps and land use data.

The land use data of the Norwegian basins are transformed from two vector maps, one for lakes and glaciers, and another for forest and bogs. Based on the potential tree line, the forests are further divided into forest, heather and subalpine. The remaining areas are open land or bedrock, if below or above the potential tree line (Beldring et al., 2003). Finally, the land use data with eight types have a resolution of 25 m and they are further rescaled at 1, 5 and 10 km.

The orographic maps of the Norwegian basins are from the Norwegian Mapping Authority (NMA). The original DEMs and slope maps have a horizontal resolution of 25 m and they are further rescaled at 1, 5 and 10 km. For drainage networks delineation, the DEMs at 25 m are first aggregated at 100 m to avoid local pour points. Drainage networks are derived from the 100 m DEMs by the method of O'Callaghan & Mark (1984). The drainage networks at 1, 5 and 10 km are up-scaled from the 100 m drainage networks by the river Network Scaling Algorithms (Fekete et al., 2001; Gong et al., 2009). The final drainage networks are visually compared with the National River Network Database (ELVIS) (NVE, 2015b) made in the year 2011 by NVE, and manually modified if necessary.

River channel characteristics are required by the Muskingum-Cunge routing method. They are usually assumed to be rectangular (Todini, 2007) and only the width is needed

to be obtained from measurements. However, field work is very time and money inefficient. Therefore, 111 measurements over the Glomma river are derived from digital maps from NVE. To transform them into a grid format, it is assumed that the width for a river section defined by the Strahler system (Strahler, 1957) does not change. Thereby, the mean of all values for a river section is assigned as the width of this river section.

For the Chamkhar Chhu basin, the DEMs and land use data are obtained from the Department of Hydromet Services, Bhutan. The original data are at a spatial resolution of 25 m and are rescaled at 1 km. The land use data are reclassified into three broad classes, high biomass (including broadleaf forest, coniferous forest and scrub), low biomass (including erosion, pasture, rock) and human affected (agriculture and urban). For the Beas basin, the DEMs data are free to download from a global dataset, the Hydro1k (EROS, 1996).

Climate Data

Climate forcing is the most essential input to hydrological models, particularly precipitation. Temperature is significant in areas with snow. It is fair to acknowledge that qualified precipitation and temperature data are necessary to obtain high model efficiency.

For the Norwegian basins, i.e. the Glomma and the Nigardsbreen basins, the seNorge data are used (NVE, 2015a). The data are daily maps of precipitation and temperature at horizontal resolution of 1 km for entire Norway and are available for free to download (NVE, 2015a). These data are produced by the Norwegian Meteorological Institute (met.no) using daily observations of 24-hour mean temperature and accumulated precipitation measured at meteorological stations.

For precipitation, observations of 630 in situ stations are corrected for systematic under catch due to the station exposure to wind. To interpolate precipitation, a method of triangulation (Mohr, 2008) is used with correction for the altitude of a grid using a vertical precipitation gradient of 10% per 100 m difference below 1,000 m amsl and a vertical precipitation gradient of 5% per 100 m difference above 1,000 m amsl (Mohr, 2008; Vormoor & Skaugen, 2013). For temperature, observations of 150 in situ stations are first projected to sea level by regression coefficients based upon monthly mean temperature data from 1,152 stations in Norway, Sweden, Denmark and Finland. Interpolated temperature values by the residual kriging method are readjusted to terrain elevation using a lapse rate that varies among different seasons (Mohr, 2008).

The seNorge data have been evaluated and used in many studies covering Norway, such as

hydrological modelling (Beldring, 2002a), snow and glaciers (Vormoor & Skaugen, 2013; Engelhardt et al., 2012) and permafrost evolution (Gisnås et al., 2013). They show that the datasets generally are of high quality.

For the Himalayan basins, the meteorological data are measured by in situ meteorological stations. There are seven and three stations respectively for the Chamkhar Chhu and the Beas basins. Their locations are shown in Figure 4.3. The mean of daily maximum and minimum temperatures is taken by the HBV model. All stations, except Manali, are located in the low areas. This distribution leads to a low representativeness of the areal conditions. Therefore, the station observations are corrected and interpolated with consideration of elevation effects.

For climate change impacts, globally available datasets and the most updated scenarios are highly favoured. The Coupled Model Intercomparison Project Phase 5 (CMIP5) global climate projections and the new Representative Concentration Pathways (Rcps) are preferred to previous experiments. With these considerations, the Coordinated Regional Downscaling EXperiment (CORDEX) project is selected for provision of the future climate. For western Asia, there are two RCMs results, by RCA4 (Samuelsson et al., 2011; SMHI, 2015) and REMO (Jacob et al., 2012, 2014). The simulations are at a spatial resolution of 0.44^o, roughly 50 km, and a daily time step under three Rcps.

The simulations for the period 1950–2005 are driven by observed anthropogenic forcings and ERA-Interim reanalysis data. Climate projections for the period 2006–2100 are driven by the projected anthropogenic forcings according to Rcp2.6, Rcp4.5 and Rcp8.5, which respectively prescribe the low, middle, and high concentrations (Teichmann et al., 2013). Other forcings are the same for the reference period, except that volcanic aerosols are set to zero (Jacob et al., 2012).

Hydrological Data

Taking the above inputs, the HBV model can generate series of a large amount of hydrological variables. Some of these variables are of concrete physical meanings. The observed series of such variables can be compared with the modelled results. The similarity of the two series is a measure of model efficiency. Rainfall-runoff models are designed to reproduce observed runoff, which is available and trustworthy in most cases. Therefore, hydrological models are mainly calibrated and validated based on modelling runoff. Model evaluations are additionally extended to other variables if observations are available.

Through this project, discharge measurements of nine Norwegian stations are used. Eight

of them are located in the Glomma basin and the remaining one is the Nigardsbreen station. All are from the national hydrological database, which is collected and managed by NVE. Discharge series are transformed from the in situ measured water depth by the Bayesian Rating Curve Fitting method (Petersen-Øverleir et al., 2009). Missing points or possible errors are checked by the NVE hydrological quality control system.

For the Norsfoss basin, which is a sub-basin of the Glomma basin, model comparison is further accompanied by measurements of snow water equivalent (SWE) and groundwater depth. The SWE series are from three snow pillows (Figure 1: Article II), which are among 31 automatic snow stations for Norway. These snow data are used for flood forecasting and scientific research purposes (Saloranta, 2012; Skaugen et al., 2012). The data in early spring are not as good as other periods due to repeated melting and refreezing. For groundwater depth, there are seven piezometers and their locations are shown in Figure 1: Article II. Three of them are located in the northern part of the Norsfoss basin and the other four are in the southern low areas. Generally, the measurements are of high quality with exceptions at peaks of groundwater depth (Fleig, 2013).

Annual mass balance series of Nigardsbreen have been continuously measured by NVE since the year 1962. The mass changes are derived from the direct glaciological method or stakes-and-pits method, which is traditionally used by glaciologists to measure glacier mass balance (Østrem & Brugman, 1991; Hagg et al., 2004). Stakes are used to measure the changes in thickness and pits are selected sites for measuring the density at different depths. The measurements are interpolated over the glacier to obtain the total amount of glacier mass change. According to the experience of NVE, the measurements are suspected to be subject to a slight positive bias for the Norwegian coastal glaciers and the reason is not clear yet (Andreassen et al., 2011). However, no better dataset is available at present. The mass balance data have been extensively used for glacier modelling purposes (Oerlemans, 1986, 1997, 2007; Engelhardt et al., 2012).

Discharge series of the Himalayan stations are obtained from the national authorities, which are in charge of collecting of the hydrological data. The series are quite short for hydrological modelling purpose. The lengths of the series are only 11 years of the Kurjey gauging station in the Chamkhar Chhu basin and nine years of the Bhuntar gauging station in the Beas basin. The series show a large variance and high peaks, particularly for the Bhuntar discharge. The Kurjey series is qualified for model calibration and validation (Beldring, 2011). The data quality of the Bhuntar series is largely unknown. Therefore, quality control is conducted visually. Points of suspicious errors are not included in model calibration and validation.

Additional Data

Water resources are commonly measured in per capita availability of renewable freshwater. Population projections are as important as hydrological models in calculating water resource scenarios. However, population estimations at a basin scale normally are not available and have to be estimated from national population projections. A linear relationship is assumed between the basin population and the country population.

A national population estimation and projection for the period 1960–2050 can be freely download from the World Bank (2014). This datasets was produced in the year 2012 and there is no error for the following year compared with the estimations from the World Bank (2014). However, the projections for the year 2014 were 2.5% and 4.4% higher than the estimations by CIA (2015), respectively for India and Bhutan. Population distribution maps at a sptial resolution of 1 km (Balk et al., 2006) are available for the years, 1990, 1995 and 2000. The quality of maps are difficult to quantify, particularly in the Himalayan basins. The correlation between the maps and the observations reached 0.6 in Cambodia and Vietnam (Gaughan et al., 2013). The map qualities of two Himalayan basins are suspected to be less due to their remote locations and less development.

5 Results

This chapter shows model performance of the HBV model with the routing algorithms and the glacier retreat model as well as effects of climate change on climate and hydrology in the selected basins.

5.1 Model Performance

Routing Effects

The routing procedures improved the model performance in daily runoff simulation of the Losna and Norsfoss stations to varying extents. A source-to-sink method (NRF) (Gong et al., 2009) and the Muskingum-Cunge (MC) method gave minor improvements over the grid-based model without routing on the spatial resolutions of 1, 5 and 10 km. However, a hillslope routing method and its combination with the MC method produced a 0.05 higher Nash-Sutcliffe coefficient (NSE) than the simple grid-based model (Figure 4: Article I). In addition, the models with hillslope routing (GROne) and its combination (GRTwo) with the MC method were superior over the simple grid-based model at the resolution of 1 km in reproducing low flow series of the Norsfoss station (Figure 5.1 & Figure 3: Article II).

Two models based on the grid-to-grid routing were further compared with the simple model for reproducing discharge series of six interior points of the Norsfoss basin (Figure 5.2). Their discharge series were not included in calibration. The models with routing were still better than the simple model. However, the difference in performance diminished. In addition, there was a clear upward trend of model efficiency with the increasing area of the sub-basins.

For the spatial resolution effects, there were no consistent trends of model efficiency against spatial resolution for the two sub-basins (Figure 4: Article I). For the simple grid-based model and the NRF model, there was a downward trend of NSE with increasing grid size. However, such a trend did not exist for other models.

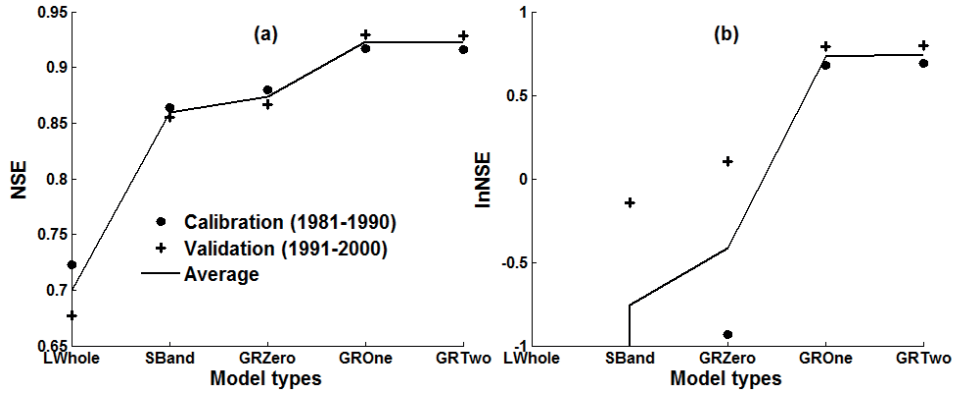

Figure 5.1: Model efficiency in (a) runoff and (b) low flow at the Norsfoss station. In (b), some values are not shown because they are out of the display range. LWhole is a lumped model; SBand is a semi-distributed model with ten elevation bands; GRZero is a grid-based model without any routing. Their details are described in Article II.

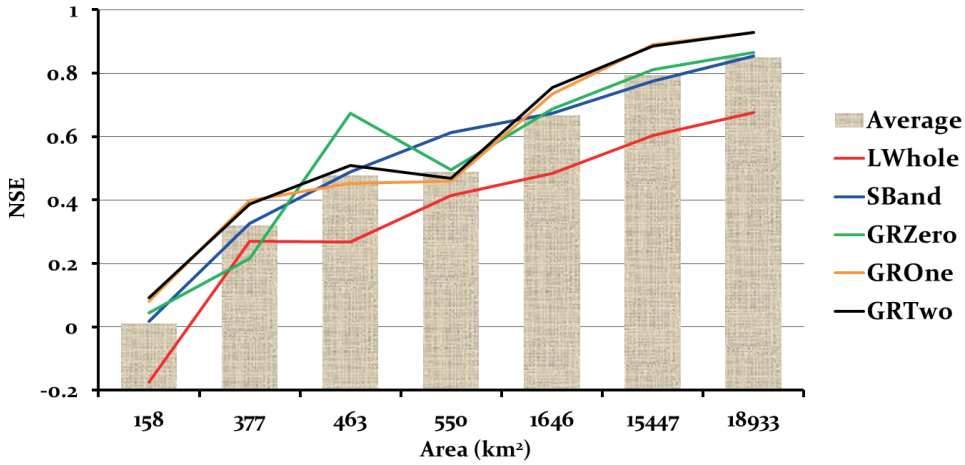

Figure 5.2: Model efficiency at six interior stations and the Norsfoss station. Average is the mean of the NSE values of different model variants. The catchment with the largest area (18,933 km^2) is the entire study area.

Glacier Modelling

The HBV model with glacier retreat model was tested on three basins with considerable glacier coverage, i.e. the Nigardsbreen basin in Norway, the Beas basin in India and the Chamkhar Chhu basin in Bhutan. The glacier retreat model enabled to automatically update the glacier extent according to the mass change calculated by the HBV model.

For the Nigardsbreen basin, the hydro-glacial model at a spatial resolution of 100 m was calibrated based on discharge and annual mass balance series in the period 1991–2002 and validated in the period 2003–2012. The model obtained a very high efficiency. For daily discharge, NSE was up to 0.9 for both calibration and validation (Table 5.1). For glacier annual mass balance, COR was equal or larger than 0.9. The cumulative mass balance change for the period 1991–2012 was +7255 mm water equivalent (w.e.) by observations and +7231 mm w.e. according to the simulation (Figure 5: Article III).

Two Himalayan basins humbled the model performance in terms of reproducing discharge series. For the Beas basin (1 km), the NSE values were 0.65 for the calibration period 1997–2002 and 0.73 for the validation period 2003–2005. For the Chamkhar Chhu basin, the model at 1 km was calibrated based on daily discharge series for the period 1998–2004 and validated for the period 2005–2008. The model predicted daily runoff with a precision of 0.85 in NSE.

Table 5.1: Model performance of the three basins. Q is the daily discharge and M is annual mass balance.

Basin	Variable	Criteria	Calibration	Validation
Nigardsbreen	Q	NSE	0.90	0.90
		RME	4.61	5.38
	M	COR	0.90	0.92
Chamkhar Chhu	Q	NSE	0.87	0.85
		RME	-0.02	10.32
Beas	Q	NSE	0.65	0.73
		RME	2.07	-22.38

The model can estimate runoff components from glaciers, which is investigate glacier effects on runoff. As shown in Figure 5.3, the ranking of glacier contribution to runoff in the descending order is the Nigardsbreen basin (92.5%), the Chamkhar basin (48.1%) and the Beas basin (27.5%). The main reason for the highest contribution in the Nigardsbreen basin is its largest glacierisation. Additionally, the glacier contribution also depends on climate, especially the spatial distribution of precipitation. In the Nigardsbreen and the Chamkhar Chhu basins, the precipitation decreases from upstream to downstream whereas in the Beas basin, more precipitation falls in the valleys compared to the high mountains

(Figure 14: Article III). As a result of these spatial distribution patterns of precipitation, the ratio of the glacier's contribution is higher in the Chamkhar Chhu basin than in the Beas basin, even though the latter has a higher glacierisation.

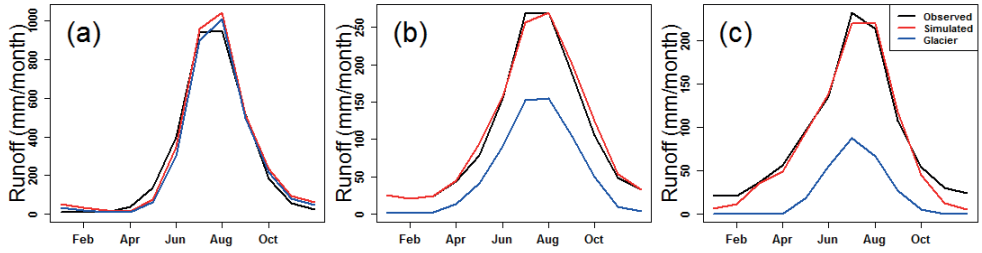

Figure 5.3: Monthly runoff of the three basins, (a) the Nigardsbreen basin, (b) the Chamkhar Chhu basin, and (c) the Beas basin. The glacier runoff is defined, in the most general sense, as the runoff from the glacierised area, including all melt of snow and glacier ice/firn, and rain water (Radić & Hock, 2014; Bliss et al., 2014).

5.2 Climate Change

The future climate for the Beas and Chamkhar Chhu basins was constructed by correcting the CORDEX data (4.2 Data) using the statistical methods (3.5 Statistical Downscaling).

Seven bias correction methods showed similar skills in downscaling precipitation, but not in downscaling temperature (Figure 3: Article IV). For precipitation, the methods were very similar for precipitation in terms of MAE. The mean of MAE was 4.6 mm/day with the lowest by $M6$ (scale, 4.53 mm/day) and the highest by $M3$ (linear, 4.66 mm/day). For temperature, the lowest error was given by $M3$ (linear, 2.29°C) followed by $M1$ (empirical, 2.30°C) and the highest was given by $M7$ (power, 5.73°C). Comparison between the final downscaled series and the original grid series of the RCMs showed that statistical downscaling could significantly reduce the difference between the observed and simulated series by the RCMs (Figure 5.4). The improvements were found in variance shown by sd, total volume shown by *bias* and absolute errors in mean (MAE) and square ($NMSE$).

There were significant warming effects in the future periods than the control period (1981–2005) and the warming effects increased with more CO_2 emissions. The statistics

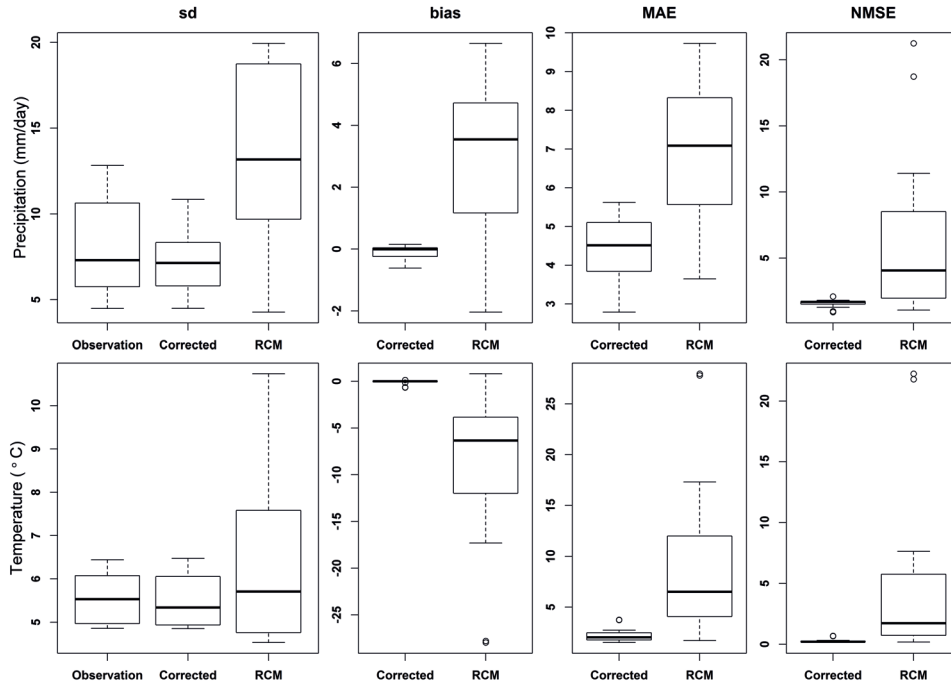

Figure 5.4: Comparison of the original RCM series and the corrected series for precipitation and temperature.

of the Mann-Whitney test suggested that all the changes were significant except at the Torngsa station by RCA4 under Rcp8.5 and Rcp4.5 in the period 2011–2040 (Figure 5: Article IV). The annual temperature of the basins increases approximately 0.05°C/year under Rcp8.5 and 0.02°C/year under Rcp4.5 in the period from 2010 to 2100 (Figure 5.5).

Changes of the annual precipitation were not consistent between the RCMs and no relationships were found associated with CO_2 emissions (Figure 5.5 & Figure 6: Article IV). There were large differences between the two RCMs and it is difficult to say which was more reliable. At the end of the 21^{st} century, the wettest and driest conditions were respectively given by RCA4 and REMO under Rcp8.5. The most notable changes were produced by RCA4 under Rcp8.5 in the Chamkhar Chhu basin. In this projection, the annual mean precipitation increased after the 2030s with fluctuation and reached 2,600 mm/year in the decade 2086–2095. Most of the predictions indicated that the Chamkhar Chhu basin would become wetter and the Beas basin would get drier compared to their respective baseline periods.

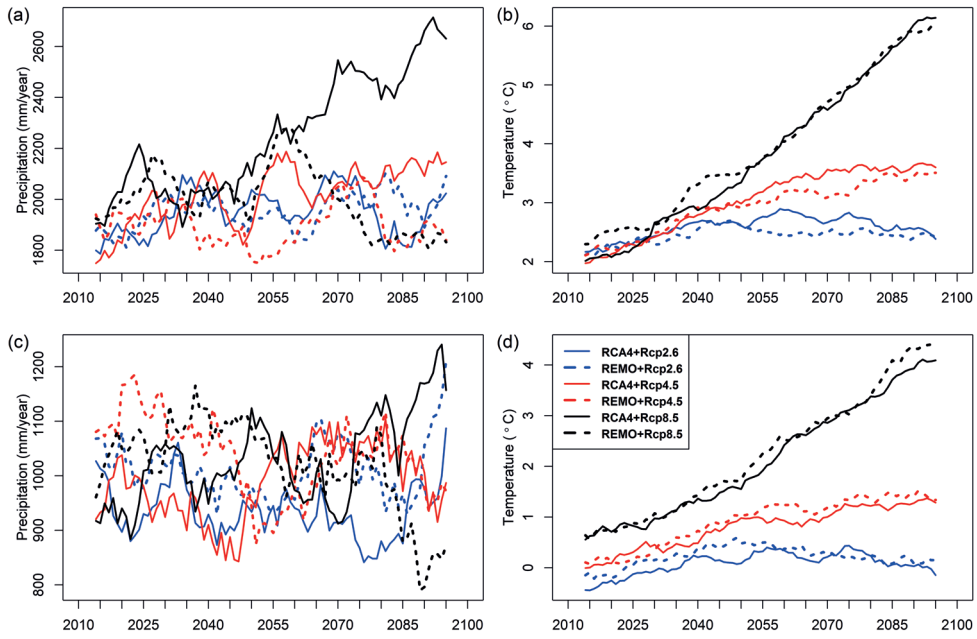

Figure 5.5: Ten-year moving average of annual precipitation and temperature. (a) Precipitation of the Chamkhar Chhu basin; (b) Temperature of the Chamkhar Chhu basin; (c) Precipitation of the Beas basin; (d) Temperature of the Beas basin.

The distance of the two basins is 1,350 km, but the glaciers would respond very differently to climate change (Figure 5.6). The changes of glaciers are simultaneously affected by changes of temperature and precipitation. The annual mean temperature was above the melting point and much warmer than the Beas basin. The glaciers in the Chamkhar Chhu basin were likely to disappear or maintain in a stable condition with a small volume before the 2050s whereas in the Beas basin the glaciers were predicted to experience mass loss with a large range by the two RCMs under the three Rcps before the 2060s. Afterwards the Beas glaciers would grow under Rcp2.6 and Rcp4.5 or speed up mass loss under Rcp8.5.

The simulated runoff after the glacier disappearance or obtaining a new stable condition showed a lower peak and earlier rising compared with the period of glacier melting, even in cases when precipitation increased in the later period (Figures 9: Article IV). As a consequence of changes in precipitation, temperature and glaciers, runoff showed more complex changes than the three factors. Shown by monthly mean runoff, there was a large variety among the periods of the selected two-decade (Figure 10: Article IV). The changes in the summer months were more significant than in the winter months. Additionally, the

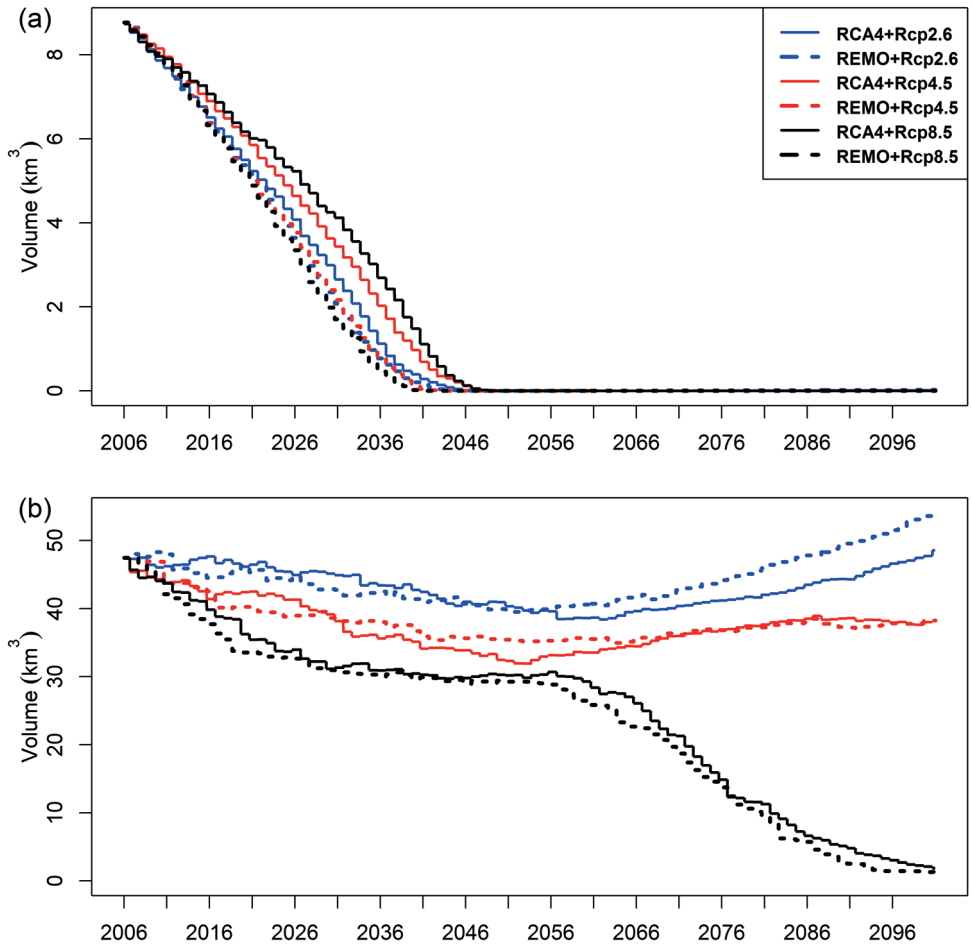

Figure 5.6: Simulated glacier volumes in (a) the Chamkhar Chhu basin and (b) the Beas basin.

differences between the RCMs get larger against time and CO_2 emissions. The largest change ranges were given under Rcp8.5, which also suggested the largest uncertainty under Rcp8.5.

5.3 Water Resources

Calculating the available water resources included estimations of mean Environmental Water Requirements (EWR) and the number of persons living in the basin. As an initial guess, EWR can be assumend as 30% of mean annual runoff of the observed periods.

Assuming EWR would not change significantly in the future, the total available water resources can be calculated for the future.

To estimate basin population for the future, a linear relationship was derived between the basin population and the national population for the years, 1990, 1995 and 2000. The linear function was more accurate for the Beas basin than for the Chamkhar Chhu basin. The maximum RME was 7.9%, (1,439 persons) for the Chamkhar Chhu basin, whereas it was only 0.1% (269 persons) for the Beas basin (Table 5: Article IV). In the period 2000–2050, the numbers of the population were predicted to continuously increase and the number almost doubles in the Chamkhar Chhu basin (Figure 11: Article IV).

There were significant decreases with considerable fluctuations in the available water resources per capita (Wp) by all projections in the two basins (Figure 5.3). In the Chamkhar Chhu basin, Wp would drop from approximately 137 m^3/year in the 2010s to 78 m^3/year in the 2040s, whereas it was predicted to decrease from 21 m^3/year to 14 m^3/year in the Beas basin. Effects of climate change and population growth were split by assuming that the population, conservatively, would not grow after the period 2011–2015 and the remaining was caused by climate change. The water declines were respectively reduced to 34 m^3/year in the Chamkhar Chhu basin and 4 m^3/year in the Beas basin. Therefore, the population growth were approximately responsible for 42% in the Chamkhar Chhu basin and 43% in the Beas basin. The two basins were facing absolute water scarcity, less than 500 m^3/year (Schewe et al., 2014) and the scarcity would intensify in the future.

The ranges of Wp caused by RCMs, Rcps and possible population inaccuracy were given in Table 5.2. The differences among RCMs and Rcps counted less than 30% of Wp ranging from 11% to 44%. However, when considering ±20% inaccuracy in population estimations, the uncertainties mounted up to 68% in the Chamkhar Chhu basin and 73% in the Beas basin. For the period 2016–2020 in the Beas basin, the best water resource scenario was given by REMO under Rcp4.5 and the worst by RCA4 under Rcp4.5. The differences between the best with 80% population estimation and the worst with 120% population estimation reached 18 m^3/year and accounted for 86.6% of the mean of six the estimations. The uncertainties caused by ±20% population inaccuracy were much more than caused by RCMs and Rcps.

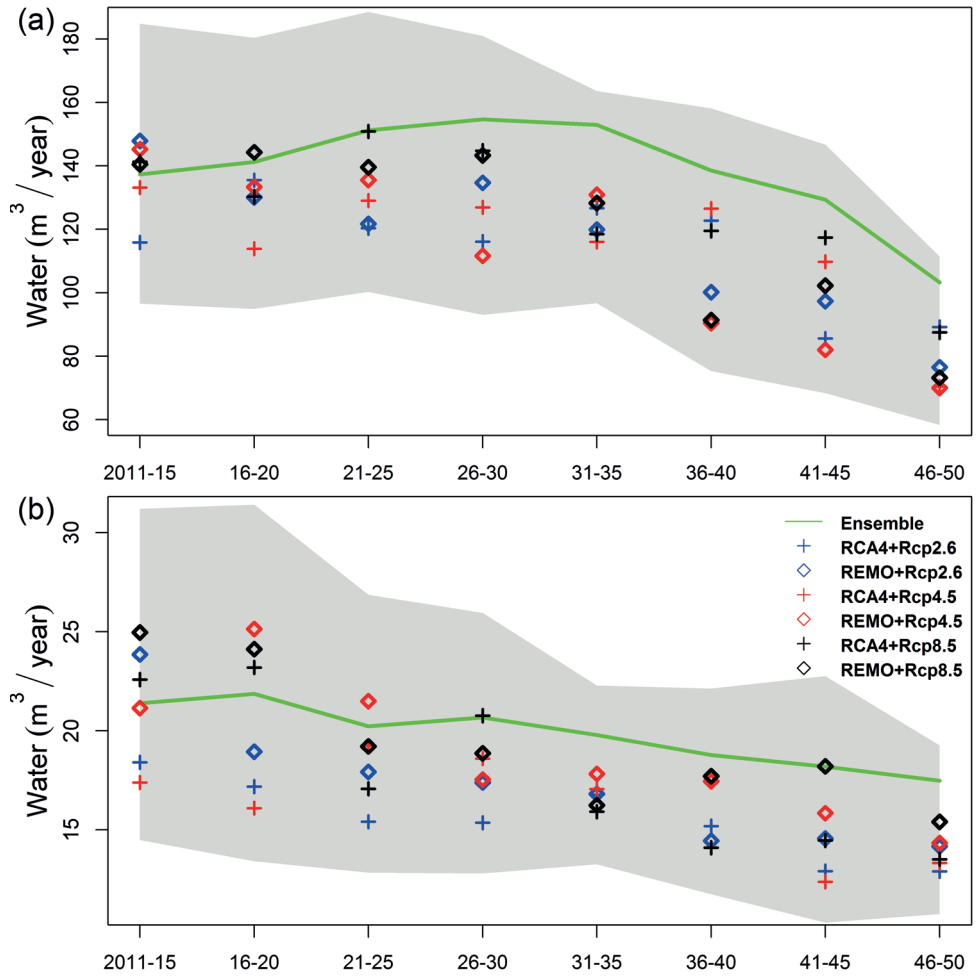

Figure 5.7: Water resources per capita of (a) the Chamkhar Chhu basin and (b) the Beas basin. The shaded area represents the ranges consider ±20% of the population projections. The top boundary is calculated by using the maximum projected available water resources and 80% of the population. The bottom boundary is calculated by using the minimum projected available water resources and 120% of the population. The ensemble is computed by using the mean of six runoff projections and assuming the population does not increase after the period 2011–2015. The ensemble lines aim to show the effects of population on water resources.

Table 5.2: Statics of ranges (R) of Wp caused by RCMs, Rcps and population estimations. For the period i, $Wp_{(\mathrm{i,j})}$ is the available water resources per capita estimated by the projection j ($1 \leq j \leq 6$). In the first row, R_i is $\frac{\max\limits_{1\leq j\leq 6} Wp_{(\mathrm{i,j})} - \min\limits_{1\leq j\leq 6} Wp_{(\mathrm{i,j})}}{\Sigma_{j=1}^{j=6} Wp_{(\mathrm{i,j})}/6} \times 100$ and in the second row, R_i is $\frac{\max\limits_{1\leq j\leq 6} Wp_{(\mathrm{i,j})}/0.8 - \min\limits_{1\leq j\leq 6} Wp_{(\mathrm{i,j})}/1.2}{\Sigma_{j=1}^{j=6} Wp_{(\mathrm{i,j})}/6} \times 100$.

	Chamkhar Chhu			Beas		
	Mean	Minimum	Maximum	Mean	Minimum	Maximum
RCMs;Rcps	25.1	12.0	35.7	29.2	11.4	43.5
RCMs;Rcps;±20%Pop	67.6	54.2	79.1	72.5	53.8	86.6

6 Discussions

6.1 Model Complexity

The trend to develop complex models has been criticised (Beven, 2001) whereas hydrologists are more and more required to predict not only runoff but also other variables for environmental policies and sustainable development (Varado et al., 2006).

Results of the Glomma basin have shown that finer spatial resolution or more detailed description of physical realism could improve the model performance in runoff simulation. The hillslope routing has significantly improved not only the low flow simulation, but also at the interior points of the Norsfoss basin. In Norwegian mountainous basins and other places of high hydraulic conductivity, overland flow is mainly generated due to a rising groundwater table, which can be contributed from interflow and local recharge due to rainfall and snowmelting. Thereby, runoff generation at downstream is an accumulated effects of upstream grids and the local input. Though the method of hillslope routing is simple, it is a proper representation of this process and enhances runoff simulation.

The MC and NRF methods, however, have not increased the model efficiency at current spatial and temporal resolutions. The reasons for the minor improvements are that water flows quick due to a steep terrain and low manning roughness coefficients of sparse vegetation in the Losna and Norsfoss basins. Most runoff drains the basin within two days (Figure 6: Article I), and it is difficult to reflect this in daily models. These two methods probably can add value to runoff simulations at sub-daily or hourly scales and in larger basins than the Norsfoss basin.

For internal variables, such as groundwater or snow water equivalent, however, three grid-based models (no routing, hillslope routing and both hillslope and channel routing) have demonstrated similar model performance. This is likely due to data error in the measurements (more in the following section) and discrepancy in concepts and scale between measurements and simulation (see 6.3 Limitations and Opportunities). In addition, the models were calibrated according to the discharge series, which leads to a higher emphasis

on runoff than other variables. The calibration processes also compensate different parameters and only give good final results (Alley, 1984; Jiang et al., 2007). Therefore, it would be useful to constrain the compensation, for example by reliable estimation of parameters or comparison with other models for individual processes.

These results indicate that a higher degree of model complexity is able to lead to a better model, but the improvements are still limited to runoff simulation. In rainfall-runoff modelling, runoff indeed is the most crucial and traditional output. However, there are emerging demands to predict other variables for environmental assessments and climate change studies. The model capacity in reproducing other variables is likely to become additional criteria for model evaluation and its priority should also be on top in model development.

6.2 Data Uncertainties

Uncertainties are noteworthy, particularly in assessing water resources for the future. The uncertainties inherit from models (e.g. GCMs, RCMs and hydrological models) and their parameters as well as data sources (e.g. emission scenarios and observed data). The uncertainties can accumulate or cascade through the research activities and potentially lead to large uncertainties in the target outputs (Seiller & Anctil, 2014; Bastola et al., 2011). Due to the fact only two RCMs are used and the uncertainties caused by different models has been widely discussed (Butts et al., 2004; Bastola et al., 2011; Chen et al., 2012; Yang et al., 2012); therefore the section focus on the data associated uncertainties.

The quality of climate data is very important in hydrological modelling. In the studies of the Himalayan basins, the meteorological stations are sparsely distributed and mainly located in low elevation places. This distribution leads to a low representativeness of the spatial precipitation and temperature. Though in the interpolation of the station measurements, elevation effects have been considered, mountain aspect and its exposure to the sun also influence precipitation and temperature significantly. Therefore, more climate data, for example, remote sensing data should be involved in the ongoing research.

The discharge series are essential to calibrate and validate hydrological models; therefore, their accuracy and length should be qualified. However, the available discharge series of the Himalayan basins are only approximately ten-year long. In addition, the accuracy is affected by the measurement methodology and human activities. Take the Norsfoss basin as an example. Its regulation capacity is 8.57%, however the regulation has stronger influence on its sub-basins. It is partly responsible for the lower efficiency of runoff simulation at

the interior points than at the Norsfoss station. Not only the discharge measurements, but also the groundwater level is influenced by human activities, for which the groundwater levels at lower elevation places (200 m amsl) in the Norsfoss basin are more difficult to simulate than at the moderate height (650 m amsl).

Initial ice thickness of glaciers is required by the hydro-glacial model and the ice thickness maps play an important role in the simulations of runoff and glacier mass changes, and even more when using the simulation to estimate glacier runoff. The initial ice thickness of glaciers is from a global dataset generated by glacier models (Farinotti et al., 2009). The quality of the thickness dataset is largely depending on the glacier inventory data. There were no surveys located in the Himalayan basins, but no better dataset is available. In the Chamkhar Chhu basin, the total area of glaciers is around 203 km^2 calculated from this dataset; however, Bajracharya et al. (2014) estimated that the area covered only 85 km^2 in the year 1990. To reduce the impacts of the errors in the ice thickness datasets, two possible approaches can be used. The first is to find a good starting point assisted by the recent satellite images. The second is to remove the systematic errors by using point measurements using information at near sites. These two methods of correction would improve usage of this global dataset in glacier and runoff studies in the Himalayan region and other areas.

6.3 Limitations and Opportunities

The HBV model is a conceptual model and some simulated values are not directly comparable to the observations owing to conceptualisation and scaling issues (Beven, 2001; Vaché & McDonnell, 2006). The measurements of snow pillows are compared with the areal mean of a grid of 1 km. The simulated groundwater storage of the areal mean volume is examined by correlating with groundwater depth measurements in piezometers. The differences in the dimensions and scales hamper effectiveness of the measurements. In spite of these difficulties, using measurements of internal variables is an essential way to make a new breakthrough in developing hydrological models (Lindström et al., 1997; Vaché & McDonnell, 2006). To make better use of the point measurements, the model simulation can be scaled ahead of the comparison, or the measurements are interpolated into the model scale (Blöschl & Sivapalan, 1995).

The Δh-parametrisation method is only designed for retreating glaciers, which is valid for most glacier due to global warming. However, in the Karakoram and western Himalaya, the thinning rates of glaciers are very small and some glaciers are even growing (Kääb et al., 2012). This is also likely to happen in the Beas basin in the further (Article IV). In

this case, it is necessary to consider an approach for the growing glaciers. The scientific basis of the Δh-parametrisation method is description of the varying rates over a glacier, which is also valid for growing glaciers. Under the framework of the Δh-parametrisation method, a threshold value can be set for the ice thickness at the terminus. If the thickness is larger than the threshold, the ice flow advances following the flow direction until the thickness is not larger than the threshold value. It can be determined from the statistics of the thickness distribution or other external methods. Additionally, accurate estimation of the empirical parameters should be derived from surface elevation maps. However, these maps are not available for most glaciers. The parameters of the Δh method are calibrated according to the discharge series and available annual mass balance series. However, there is a need to evaluate the parameter sensitivity to the series and the power of the series to define the parameters. Another way is to adopt the parameter values estimated for Rhonegletscher in the Swiss Alps (Huss et al., 2010). Considering the large variability among the glaciers, the transferability of the parameter values requires in depth investigations.

The Himalayan region is extremely diversified due to the complex topography and the monsoon. The selected Himalayan basins are located respectively in northern India (western Himalaya) and in central Bhutan (eastern Himalaya). Their distance is 1,350 km, but the hydrological regimes and glacier responses to climate change are different. This thesis has been a good attempt in terms of including two basins at the different locations in this region. However, due to difficulties in obtaining measurements, this area is still described as a 'white spot' in scientific understanding. Accurate knowledge and a comprehensive assessment have not been achieved. Therefore, it is important to obtain more measurements as well as have a way to share the data, including in situ measurements and satellite images. This can be achieved either by publishing data along with publications or submitting data to a data portal. There has been several successful examples (Kääb et al., 2012; ICIMOD, 2015), but far from enough.

Impacts of human activities on hydrology are as evident as climate change; however, they are not properly considered in the current hydrological models. During the selected periods, effects of hydropower were not significant at the basin outlet, but it was possible that some sub-basins of the Norsfoss basin were affected. In the Himalaya areas, developing countries have started a widespread exploration of hydropower. Hydrologic alternations induced by human activities are occurring at the local, regional and global scales (Sivapalan et al., 2003), particularly in the recent period. However, there are insufficient published data and proper methods to accounts human activities in hydrological studies. Interactions between the water system and the human society will be an important direction of the

future research.

7 Conclusions

The goal of this project is to evaluate and improve the capacity of the HBV model to simulate hydrological processes in mountainous and glacierised regions under both the present and future climate. To achieve this goal, this project implements the flow routing algorithms and glacier retreat module in a simple grid-based version. The implementations not only improve the model performance, but also contribute to a better representation of physical processes for the present and future conditions.

Implementations of routing algorithms enable a high performing model in daily runoff simulation at the basin outlet. The hillslope routing increases the model efficiency by 0.05 Nash-Sutcliffe efficiency (NSE), whereas improvements by the Network Response Function and the Muskingum-Cunge method are not significant. In addition, the models with hillslope routing show exceptional superiority in simulating the low flow. They are also better than other models at interior points, which are not involved in the calibration. However, the higher efficiency does not exist in simulating internal variables, such as evaporation, snow and groundwater.

Hillslope routing is necessary in places where the hydraulic conductivity is high and runoff generation is not only a local response. In Norwegian basins, channel routing and source-to-sink routing do not add value in daily runoff simulation due to a steep terrain and sparse vegetation as well as small or medium basin areas. Model ability in reproducing the internal variables, such as snow and groundwater are hampered by a lack of qualified data and discrepancy in concepts and scale between measurements and simulation. Improving hydrological models in describing internal processes is the key to the future success in model development.

The HBV model with the Δh-parametrisation is tested in three basins, the Nigardsbreen basin in Norway, the Chamkhar Chhu basin in Bhutan and the Beas basin in India. For the Nigardsbreen basin, the model efficiency is as high as 0.9 of NSE in daily discharge and 0.9 of the Pearson product-moment correlation coefficient for glacier annual balance series both in calibration and validation modes. The model efficiency is lower in the

Himalayan basins mainly due to the low quality of the data used. In addition to evaluation based on observations, the hydro-glacial model can provide maps of snowpack distribution and estimate runoff components from glaciers. The model requires only precipitation, temperature and initial ice thickness and it is suitable for large basins with shrinking glaciers. It can be used for hydrological simulations and examining glacier effects on hydrology, particularly under changing climate.

This hydro-glacial model is further used to estimate water resources in the Himalayan basins. The climate scenarios projected by two RCMs suggest significant warming effects and the effects are more obvious with more emission. However, there are no clear changes in precipitation against emission or time. The glaciers in the two basins show different response to climate change. In the Chamkhar Chhu basin, the glaciers will continuously lose mass before the 2050s whereas in the Beas basin, the glaciers are predicted to experience mass loss with a large range before the 2060s, and afterwards the glaciers are likely to grow under Rcp2.6 and Rcp4.5 or lose mass at high rates under Rcp8.5. The two basins are respectively located in the eastern and western Himalaya and their responses to climate are very different. There is no doubt that with global warming, the melting rates are increased. However, the glacier mass changes are simultaneously determined by temperature and precipitation, particularly if temperature is above the melting point.

In the period 2011–2050, the available water resources are predicted to decrease significantly induced by population growth and climate change. The water resources per capita are predicted to drop from 137 m^3/year in the 2010s down to 78 m^3/year in the 2040s in the Chamkhar Chhu basin and from 21 m^3/year to 14 m^3/year in the Beas basin. The population growth is approximately responsible for 40% of the water declines. The uncertainties caused by regional climate models and emission scenarios are roughly 30% ranging from 11% to 44%. When considering $\pm$20% inaccuracy in population estimations, the highest uncertainty reaches 87%. The uncertainties are worthy of attention, but there is no doubt that the two basins are facing serious water scarcity and the water conditions will get worse in the future. Water shortage has been and continues to be a major constraint of economic and social development.

8 Outlook

This thesis implemented the routing and glacier retreat functions in the HBV model. These changes make a better representation of the physical realism and improve the model capacity in glacierised areas for long-term simulation under warming climate. The improvements are crucial to the selected basins and transferability of the models has to be examined in the ongoing research.

There has been a debate among the hydrological modellers for a long period. Does a high degree of complexity improve model accuracy? It is true that not all complexities lead to improvements, but relevant complexities definitely give better outcomes either higher accuracy or extending the boundaries of validity of hydrological models. Additionally, model accuracy is not only restricted to runoff simulation, but also better simulations of other variables, such as groundwater and glacier changes. However, due to the discrepancies in concepts, dimensions and scales, measurements of the internal variables are not efficiently used. In addition to finding approaches to utilise these measurements, it is also important to understand and apply new type data, such as water storage of Gravity Recovery and Climate Experiment (GRACE). They will be the most widely used measurements in the near future due to the increasing price of workforce.

Effects of human activities are as evident as climate change, but human activities studies are mainly limited in water demand and water quality. In these studies, human activities are typically described as boundary conditions or external alteration to the water system. In other way, the water system inversely influences the society, for example, human attitude towards water consumption, international relations and trade. The interaction between the human society and water system plays a far more important role than before. This is not a new science, but this kind research has recently become necessary and feasible with developments of global trade and the internet. This research direction is obviously not easy. It requires a close cooperated knowledge between hydrology and social science and critical thinking mindset of brave researchers.

Bibliography

Akhtar, M., Ahmad, N., & Booij, M. 2008. The impact of climate change on the water resources of Hindukush—Karakorum—Himalaya region under different glacier coverage scenarios. *Journal of Hydrology*, *355*, 148 – 163. doi:10.1016/j.jhydrol.2008.03.015.

Alley, W. M. 1984. On the Treatment of Evapotranspiration, Soil Moisture Accounting, and Aquifer Recharge in Monthly Water Balance Models. *Water Resources Research*, *20*, 1137 – 1149. doi:10.1029/WR020i008p01137.

Andreassen, L. M., Elvehøy, H., Jackson, M., Kjøllmoen, B., & Giesen, R. H. 2011. *Glaciological investigations in Norway in 2010*. Report 03 Norwegian Water Resources and Energy Directorate. URL: http://webby.nve.no/publikasjoner/report/2011/report2011_03.pdf.

Bajracharya, S. R., Maharjan, S. B., & Shrestha, F. 2014. The status and decadal change of glaciers in Bhutan from the 1980s to 2010 based on satellite data. *Annals of Glaciology*, *55*, 159 – 166. doi:10.3189/2014AoG66A125.

Balk, D., Deichmann, U., Yetman, G., Pozzi, F., Hay, S., & Nelson, A. 2006. Determining Global Population Distribution: Methods, Applications and Data, . *62*, 119 – 156. doi:10.1016/S0065-308X(05)62004-0.

Barnett, T. P., Adam, J. C., & Lettenmaier, D. P. 2005. Potential impacts of a warming climate on water availability in snow-dominated regions. *Nature*, *438*, 303 – 309. doi:10.1038/nature04141.

Bastola, S., Murphy, C., & Sweeney, J. 2011. The role of hydrological modelling uncertainties in climate change impact assessments of Irish river catchments. *Advances in Water Resources*, *34*, 562 – 576. doi:10.1016/j.advwatres.2011.01.008.

Beldring, S. 2002a. Multi-criteria validation of a precipitation runoff model. *Journal of Hydrology*, *257*, 189 – 211. doi:10.1016/S0022-1694(01)00541-8.

Beldring, S. 2002b. Runoff generating processes in boreal forest environments with glacial tills. *Nordic hydrology*, *33*, 347 – 372. doi:10.2166/nh.2002.021.

Beldring, S. 2011. *Climate change impacts on the flow regimes of rivers in Bhutan and possible consequences for hydropower development*. Report 04 Norwegian Water Resources and Energy Directorate. URL: http://www.nve.no/Global/Publikasjoner/Publikasjoner%202011/Report%202011/report4-11.pdf.

Beldring, S., Engeland, K., Roald, L. A., Sælthun, N. R., & Voksø, A. 2003. Estimation of parameters in a distributed precipitation-runoff model for Norway. *Hydrology and Earth System Sciences*, *7*, 304 – 316. doi:10.5194/hess-7-304-2003.

Beniston, M. 2003. Climatic Change in Mountain Regions: A Review of Possible Impacts. *Climatic Change*, *59*, 5 – 31. doi:10.1023/A:1024458411589.

Bergström, S. 1976. *Development and application of a conceptual runoff model for Scandinavian catchments*. Report 07 Swedish Meteorological and Hydrological Institute. URL: http://books.google.no/books?id=vRyeQAAACAAJ.

Beven, K. 2001. How far can we go in distributed hydrological modelling? *Hydrology and Earth System Sciences*, *5*, 1 – 12. doi:10.5194/hess-5-1-2001.

Bliss, A., Hock, R., & Radić, V. 2014. Global response of glacier runoff to twenty-first century climate change. *Journal of Geophysical Research: Earth Surface*, *119*, 717 – 730. doi:10.1002/2013JF002931.

Blöschl, G., & Sivapalan, M. April 1995. Scale issues in hydrological modelling: A review. *Hydrological Processes*, *9*, 251 – 290. doi:10.1002/hyp.3360090305.

Bolch, T., Kulkarni, A., Kääb, A., Huggel, C., Paul, F., Cogley, J. G., Frey, H., Kargel, J. S., Fujita, K., Scheel, M., Bajracharya, S., & Stoffel, M. 2012. The State and Fate of Himalayan Glaciers. *Science*, *336*, 310 – 314. doi:10.1126/science.1215828.

Bronstert, A., & Bárdossy, A. 1999. The role of spatial variability of soil moisture for modelling surface runoff generation at the small catchment scale. *Hydrology and Earth System Sciences*, *3*, 505 – 516. doi:10.5194/hess-3-505-1999.

Burlando, P., Pellicciotti, F., & Strasser, U. 2002. Modelling Mountainous Water Systems Between Learning and Speculating Looking for Challenges. *Nordic Hydrology*, *33*, 47 – 74. doi:10.2166/nh.2002.004.

Butts, M. B., Payne, J. T., Kristensen, M., & Madsen, H. 2004. An evaluation of the impact of model structure on hydrological modelling uncertainty for streamflow simulation. *Journal of Hydrology*, *298*, 242 – 266. doi:10.1016/j.jhydrol.2004.03.042.

Castillo, V., Gómez-Plaza, A., & Martínez-Mena, M. 2003. The role of antecedent soil water content in the runoff response of semiarid catchments: a simulation approach. *Journal of Hydrology*, *284*, 114 – 130. doi:10.1016/S0022-1694(03)00264-6.

Chen, H., Xu, C.-Y., & Guo, S. 2012. Comparison and evaluation of multiple GCMs, statistical downscaling and hydrological models in the study of climate change impacts on runoff. *Journal of Hydrology*, *434-435*, 36 – 45. doi:10.1016/j.jhydrol.2012.02.040.

Chenoweth, J. April 2008. A re-assessment of indicators of national water scarcity. *Water International*, *33*, 5–18. doi:10.1080/02508060801927994.

CIA. The World Factbook. Accessed in May 2015. URL: https://www.cia.gov/library/publications/resources/the-world-factbook/docs/contact.html.

Coron, L., Andréassian, V., Perrin, C., Lerat, J., Vaze, J., Bourqui, M., & Hendrickx, F. 2012. Crash testing hydrological models in contrasted climate conditions: An experiment on 216 Australian catchments. *Water Resources Research*, *48*, W05552. doi:10.1029/2011WR011721.

Crochemore, L., Perrin, C., Andréassian, V., Ehret, U., Seibert, S. P., Grimaldi, S., Gupta, H., & Paturel, J.-E. February 2015. Comparing expert judgement and numerical criteria for hydrograph evaluation. *Hydrological Sciences Journal*, *60*, 402 – 423. doi:10.1080/02626667.2014.903331.

Das, T., Bádossy, A., Zehe, E., & He, Y. 2008. Comparison of conceptual model performance using different representations of spatial variability. *Journal of Hydrology*, *356*, 106 – 118. doi:10.1016/j.jhydrol.2008.04.008.

Doherty, J. 2005. *PEST Model-Independent Parameter Estimation User Manual*. Watermark Numerical Computing (5th ed.). URL: http://www.pesthomepage.org/Downloads.php.

Doherty, J., & Johnston, J. M. 2003. Methodologies for calibration and predective analysis of a watershed model[1]. *Journal of the American Water Resources Association*, *39*, 251 – 265. doi:10.1111/j.1752-1688.2003.tb04381.x.

Duan, Q., Sorooshian, S., & Gupta, V. 1992. Effective and efficient global optimization for conceptual rainfall-runoff models. *Water Resources Research*, *28*, 1015 – 1031. doi:10.1029/91WR02985.

Easterling, D. R., Evans, J., Groisman, P. Y., Karl, T., Kunkel, K. E., & Ambenje, P. 2000. Observed Variability and Trends in Extreme Climate Events: A Brief Review*. *Bulletin*

of the American Meteorological Society, *81*, 417 – 425. doi:10.1175/1520-0477(2000)081<0417:OVATIE>2.3.CO;2.

Engelhardt, M., Schuler, T. V., & Anderson, L. M. 2012. Evaluation of gridded precipitation for Norway using glacier mass-balance measurements. *Geografiska Annaler: Series A, Physical Geography*, *94*, 501 – 509. doi:10.1111/j.1468-0459.2012.00473.x.

Engelhardt, M., Schuler, T. V., & Andreassen, L. M. 2013. Glacier mass balance of Norway 1961–2010 calculated by a temperature-index model. *Annals of Glaciology*, *54*, 32 – 40. doi:10.3189/2013AoG63A245.

EROS 1996. Hydro1k elevation derivative database. URL: https://lta.cr.usgs.gov/HYDRO1K.

Evans, J., & Periman, H. Water-Cycle Diagram (English). Accessed in February 2015. URL: http://upload.wikimedia.org/wikipedia/commons/1/19/Watercyclesummary.jpg.

Farinotti, D., Huss, M., Bauder, A., Funk, M., & Truffer, M. 2009. A method to estimate the ice volume and ice-thickness distribution of alpine glaciers. *Journal of Glaciology*, *55*, 422 – 430. doi:10.3189/002214309788816759.

Fekete, B. M., Vörösmarty, C. J., & Lammers, R. B. 2001. Scaling gridded river networks for macroscale hydrology: Development, analysis, and control of error. *Water Resources Research*, *37*, 1955 – 1967. doi:10.1029/2001WR900024.

Fleig, A. K. 2013. *Norwegian Hydrological Reference Dataset for Climate Change Studies*. Report 02 Norwegian Water Resources and Energy Directorate. URL: http://webby.nve.no/publikasjoner/rapport/2013/rapport2013_02.pdf.

Freeze, R., & Harlan, R. 1969. Blueprint for a physically-based, digitally-simulated hydrologic response model. *Journal of Hydrology*, *9*, 237 – 258. doi:10.1016/0022-1694(69)90020-1.

Gärtner-Roer, I., Naegeli, K., Huss, M., Knecht, T., Machguth, H., & Zemp, M. 2014. A database of worldwide glacier thickness observations. *Global and Planetary Change*, *122*, 330 – 344. doi:10.1016/j.gloplacha.2014.09.003.

Gaughan, A. E., Stevens, F. R., Linard, C., Jia, P., & Tatem, A. J. January 2013. High resolution population distribution maps for Southeast Asia in 2010 and 2015. *PloS one*, *8*, e55882. doi:10.1371/journal.pone.0055882.

Gisnås, K., Etzelmüller, B., Farbrot, H., Schuler, T. V., & Westermann, S. 2013. CryoGRID 1.0: Permafrost Distribution in Norway estimated by a Spatial Numerical Model. *Permafrost and Periglacial Processes*, *24*, 2 – 19. doi:10.1002/ppp.1765.

Gong, L., Widén-Nilsson, E., Halldin, S., & Xu, C.-Y. 2009. Large-scale runoff routing with an aggregated network-response function. *Journal of Hydrology*, *368*, 237 – 250. doi:10.1016/j.jhydrol.2009.02.007.

Goodrich, D. C., Schmugge, T. J., Jackson, T. J., Unkrich, C. L., Keefer, T. O., Parry, R., Bach, L. B., & Amer, S. A. 1994. Runoff simulation sensitivity to remotely sensed initial soil water content. *Water Resources Research*, *30*, 1393 – 1405. doi:10.1029/93WR03083.

Gudmundsson, L., Bremnes, J. B., Haugen, J. E., & Engen-Skaugen, T. 2012. Technical Note: Downscaling RCM precipitation to the station scale using statistical transformations—a comparison of methods. *Hydrology and Earth System Sciences*, *16*, 3383 – 3390. doi:10.5194/hess-16-3383-2012.

Gupta, H. V., Sorooshian, S., Hogue, T. S., & Boyle, D. P. 2003. Advances in automatic calibration of watershed models. In Q. Duan, H. V. Gupta, S. Sorooshian, A. N. Rousseau, & R. Turcotte (Eds.), *Calibration of Watershed Models* (pp. 9 – 28). American Geophysical Union volume 6 of *Water Science and Application*. doi:10.1029/WS006p0009.

Gupta, R., Duggal, A., Rao, S., Sankar, G., & Singhal, B. 1982. Snow-cover area vs. snowmelt runoff relation and its dependence on geomorphology?—A study from the Beas catchment (Himalayas, India). *Journal of Hydrology*, *58*, 325 – 339. doi:10.1016/0022-1694(82)90042-7.

Hagg, W. J., Braun, L. N., Uvarov, V. N., & Makarevich, K. G. 2004. A comparison of three methods of mass-balance determination in the Tuyuksu glacier region, Tien Shan, Central Asia. *Journal of Glaciology*, *50*, 505 – 510. doi:10.3189/172756504781829783.

Hailegeorgis, T. T., & Alfredsen, K. 2015. Comparative evaluation of performances of different conceptualisations of distributed HBV runoff response routines for prediction of hourly streamflow in boreal mountainous catchments. *Hydrology Research*, *in press*. doi:10.2166/nh.2014.051.

Hasson, S., Lucarini, V., Khan, M. R., Petitta, M., Bolch, T., & Gioli, G. 2014. Early 21st century snow cover state over the western river basins of the Indus River system. *Hydrology and Earth System Sciences*, *18*, 4077 – 4100. doi:10.5194/hess-18-4077-2014.

Hempel, S., Frieler, K., Warszawski, L., Schewe, J., & Piontek, F. 2013. A trend-preserving bias correction—the ISI-MIP approach. *Earth System Dynamics*, *4*, 219 – 236. doi:10.5194/esd-4-219-2013.

Horton, P., Schaefli, B., Mezghani, A., Hingray, B., & Musy, A. 2006. Assessment of climate-change impacts on alpine discharge regimes with climate model uncertainty. *Hydrological Processes*, *20*, 2091 – 2109. doi:10.1002/hyp.6197.

Huss, M. 2011. Present and future contribution of glacier storage change to runoff from macroscale drainage basins in Europe. *Water Resources Research*, *47*, W07511. doi:10.1029/2010WR010299.

Huss, M., & Farinotti, D. 2012. Distributed ice thickness and volume of all glaciers around the globe. *Journal of Geophysical Research: Earth Surface*, *117*, F04010. doi:10.1029/2012JF002523.

Huss, M., Farinotti, D., Bauder, A., & Funk, M. 2008. Modelling runoff from highly glacierized alpine drainage basins in a changing climate. *Hydrological processes*, *22*, 3888 – 3902. doi:10.1002/hyp.7055.

Huss, M., Jouvet, G., Farinotti, D., & Bauder, A. 2010. Future high-mountain hydrology: a new parameterization of glacier retreat. *Hydrology and Earth System Sciences*, *14*, 815 – 829. doi:10.5194/hess-14-815-2010.

Huss, M., Zemp, M., Joerg, P. C., & Salzmann, N. 2014. High uncertainty in 21stst century runoff projections from glacierized basins. *Journal of Hydrology*, *510*, 35 – 48. doi:10.1016/j.jhydrol.2013.12.017.

ICIMOD. ICIMOD. Accessed in 2015. URL: http://www.icimod.org/.

Iglesias, A., Garrote, L., Diz, A., Schlickenrieder, J., & Martin-Carrasco, F. 2011. Re-thinking water policy priorities in the Mediterranean region in view of climate change. *Environmental Science & Policy*, *14*, 744 – 757. doi:10.1016/j.envsci.2011.02.007.

Immerzeel, W. W., van Beek, L., Konz, M., Shrestha, A., & Bierkens, M. 2012. Hydrological response to climate change in a glacierized catchment in the Himalayas. *Climatic Change*, *110*, 721 – 736. doi:10.1007/s10584-011-0143-4.

Jacob, D., Elizalde, A., Haensler, A., Hagemann, S., Kumar, P., Podzun, R., Rechid, D., Remedio, A. R., Saeed, F., Sieck, K., Teichmann, C., & Wilhelm, C. 2012. Assessing the Transferability of the Regional Climate Model REMO to Different COordinated Regional Climate Downscaling EXperiment (CORDEX) Regions. *Atmosphere*, *3*, 181 – 199. doi:10.3390/atmos3010181.

Jacob, D., Petersen, J., Eggert, B., Alias, A., Christensen, O. B., Bouwer, L., Braun, A., Colette, A., Deque, M., Georgievski, G., Georgopoulou, E., Gobiet, A., Menut, L., Nikulin, G., Haensler, A., Hempelmann, N., Jones, C., Keuler, K., Kovats, S.,

Kroner, N., Kotlarski, S., Kriegsmann, A., Martin, E., van Meijgaard, E., Moseley, C., Pfeifer, S., Preuschmann, S., Radermacher, C., Radtke, K., Rechid, D., Rounsevell, M., Samuelsson, P., Somot, S., Soussana, J.-F., Teichmann, C., Valentini, R., Vautard, R., Weber, B., & Yiou, P. 2014. EURO-CORDEX: new high-resolution climate change projections for European impact research. *Regional Environmental Change*, *14*, 563 – 578. doi:10.1007/s10113-013-0499-2.

Jiang, T., Chen, Y. D., Xu, C.-Y., Chen, X., Chen, X., & Singh, V. 2007. Comparison of hydrological impacts of climate change simulated by six hydrological models in the Dongjiang Basin, South China. *Journal of Hydrology*, *336*, 316 – 333. doi:10.1016/j.jhydrol.2007.01.010.

Joshi, G. Major Cities of Hindu Kush Himalayan (HKH) Region. Accessed in 2007. URL: http://rds.icimod.org/Home/DataDetail?metadataId=3434&searchlist=True.

Joshi, G. Major River Systems of Hindu Kush Himalayan (HKH) Region. Accessed in 2008. URL: http://rds.icimod.org/Home/DataDetail?metadataId=2956&searchlist=True.

Joshi, G. Digital Elevation Model of Hindu Kush Himalayan (HKH) Region. Accessed in 2011. URL: http://rds.icimod.org/Home/DataDetail?metadataId=8744&searchlist=True.

Kääb, A., Berthier, E., Nuth, C., Gardelle, J., & Arnaud, Y. 2012. Contrasting patterns of early twenty-first-century glacier mass change in the Himalayas. *Nature*, *488*, 495 – 498. doi:10.1038/nature11324.

Khadka, D., Babel, M. S., Shrestha, S., & Tripathi, N. K. 2014. Climate change impact on glacier and snow melt and runoff in Tamakoshi basin in the Hindu Kush Himalayan (HKH) region. *Journal of Hydrology*, *511*, 49 – 60. doi:10.1016/j.jhydrol.2014.01.005.

Kotlarski, S., Jacob, D., Podzun, R., & Paul, F. 2010. Representing glaciers in a regional climate model. *Climate Dynamics*, *34*, 27 – 46. doi:10.1007/s00382-009-0685-6.

Krysanova, V., Bronstert, A., & Müller-Wohlfeil, D.-I. 1999. Modelling river discharge for large drainage basins: from lumped to distributed approach. *Hydrological Sciences Journal*, *44*, 313 – 331. doi:10.1080/02626669909492224.

L'Abée-Lund, J., Eie, J., Faugli, P., Haugland, S., Hvidsten, N., Jensen, A., Melvold, K., Pettersen, V., & Saltveit, S. 2009. Rivers of Europe. chapter Rivers in Boreal Uplands. (pp. 577 – 606). Academic Press. URL: http://www.sciencedirect.com/science/book/9780123694492.

Lawrence, D., Haddeland, I., & Langsholt, E. 2009. *Calibration of HBV hydrological models using PEST parameter estimation*. Report 01 Norwegian Water Resources and Energy Directorate. URL: http://www.nve.no/Global/Publikasjoner/Publikasjoner%202009/Report%202009/report1-09.pdf.

Lindström, G., Johansson, B., Persson, M., Gardelin, M., & Bergström, S. 1997. Development and test of the distributed HBV-96 hydrological model. *Journal of Hydrology*, *201*, 272 – 288. doi:10.1016/S0022-1694(97)00041-3.

Lüthi, M. P. 2009. Transient response of idealized glaciers to climate variations. *Journal of Glaciology*, *55*, 918 – 930. doi:10.3189/002214309790152519.

Mayr, E., Hagg, W., Mayer, C., & Braun, L. 2013. Calibrating a spatially distributed conceptual hydrological model using runoff, annual mass balance and winter mass balance. *Journal of Hydrology*, *478*, 40 – 49. doi:10.1016/j.jhydrol.2012.11.035.

Milly, P. C., Dunne, K. A., & Vecchia, A. V. 2005. Global pattern of trends in streamflow and water availability in a changing climate. *Nature*, *438*, 347 – 350. doi:10.1038/nature04312.

Mohr, M. 2008. *New Routines for Gridding of Temperature and Precipitation Observations for "seNorge. no"*. Report 08 Norwegian Meteorological Institute. URL: http://met.no/Forskning/Publikasjoner/Publikasjoner_2008/filestore/NewRoutinesforGriddingofTemperature.pdf.

Mulvaney, T. 1851. On the use of self-registering rain and flood gauges in making observations of the relations of rainfall and flood discharges in a given catchment. In *Proceedings of the institution of Civil Engineers of Ireland* number 2 in 4 (pp. 18 – 33). URL: http://iahs.info/Publications-News.do?dmsSearch_pubno=BM4.

Nash, J., & Sutcliffe, J. 1970. River flow forecasting through conceptual models part I—A discussion of principles. *Journal of Hydrology*, *10*, 282 – 290. doi:10.1016/0022-1694(70)90255-6.

Naz, B. S., Frans, C. D., Clarke, G. K. C., Burns, P., & Lettenmaier, D. P. 2014. Modeling the effect of glacier recession on streamflow response using a coupled glacio-hydrological model. *Hydrology and Earth System Sciences*, *18*, 787 – 802. doi:10.5194/hess-18-787-2014.

Noto, L. V., Ivanov, V. Y., Bras, R. L., & Vivoni, E. R. 2008. Effects of initialization on response of a fully-distributed hydrologic model. *Journal of Hydrology*, *352*, 107 – 125. doi:10.1016/j.jhydrol.2007.12.031.

NVE. seNorge.no. Accessed in March 2015a. URL: http://www.senorge.no/aboutSeNorge.html?show=on.

NVE. The National River Network Database (ELVIS). Accessed in February 2015b. URL: http://www.nve.no/en/Water/NVEs-geographic-databases/The-National-River-Network-Database-ELVIS/.

O'Callaghan, J. F., & Mark, D. M. 1984. The extraction of drainage networks from digital elevation data. *Computer Vision, Graphics, and Image Processing*, *28*, 323 – 344. doi:10.1016/S0734-189X(84)80011-0.

Oerlemans, J. 1986. An attempt to simulate historic front variations of Nigardsbreen, Norway. *Theoretical and Applied Climatology*, *37*, 126 – 135. doi:10.1007/BF00867846.

Oerlemans, J. 1997. A flowline model for Nigardsbreen, Norway: projection of future glacier length based on dynamic calibration with the historic record. *Journal of glaciology*, *24*, 382 – 389. URL: http://dspace.library.uu.nl/handle/1874/22126.

Oerlemans, J. 2007. Estimating response times of Vadret da Morteratsch, Vadret da Palü, Briksdalsbreen and Nigardsbreen from their length records. *Journal of Glaciology*, *53*, 357 – 362. doi:10.3189/002214307783258387.

Østrem, G., & Brugman, M. 1991. *Glacier mass-balance measurements: a manual for field and office work*. Report 04 National Hydrology Reseacrch Institute. URL: http://www.wgms.ch/downloads/Oestrem_Brugman_GlacierMassBalanceMeasurements_1991.pdf.

Peel, M. C., & Blöschl, G. 2011. Hydrological modelling in a changing world. *Progress in Physical Geography*, *35*, 249 – 261. doi:10.1177/0309133311402550.

Pepin, N., Bradley, R. S., Diaz, H. F., Baraer, M., Caceres, E. B., Forsythe, N., Fowler, H., Greenwood, G., Hashmi, M. Z., Liu, X. D., Miller, J. R., Ning, L., Ohmura, A., Palazzi, E., Rangwala, I., Schöner, W., Severskiy, I., Shahgedanova, M., Wang, M. B., Williamson, S. N., & Yang, D. Q. April 2015. Elevation-dependent warming in mountain regions of the world. *Nature Climate Change*, *5*, 424 – 430. doi:10.1038/nclimate2563.

Perrin, C., Michel, C., & Andréassian, V. 2001. Does a large number of parameters enhance model performance? Comparative assessment of common catchment model structures on 429 catchments. *Journal of Hydrology*, *242*, 275 – 301. doi:10.1016/S0022-1694(00)00393-0.

Petersen-Øverleir, A., Soot, A., & Reitan, T. 2009. Bayesian Rating Curve Inference as a Streamflow Data Quality Assessment Tool. *Water Resources Management*, *23*, 1835 – 1842. doi:10.1007/s11269-008-9354-5.

Pfeffer, W. T., Arendt, A. A., Bliss, A., Bolch, T., Cogley, J. G., Gardner, A. S., Hagen, J.-O., Hock, R., Kaser, G., Kienholz, C., Miles, E. S., Moholdt, G., Mölg, N., Paul, F., Radić, V., Rastner, P., Raup, B. H., Rich, J., & Sharp, M. J. 2014. The Randolph Glacier Inventory: a globally complete inventory of glaciers. *Journal of Glaciology*, *60*, 537. doi:10.3189/2014JoG13J176.

Pushpalatha, R., Perrin, C., Moine, N. L., & Andréassian, V. 2012. A review of efficiency criteria suitable for evaluating low-flow simulations. *Journal of Hydrology*, *420-421*, 171 – 182. doi:10.1016/j.jhydrol.2011.11.055.

Radić, V., & Hock, R. 2014. Glaciers in the Earth's Hydrological Cycle: Assessments of Glacier Mass and Runoff Changes on Global and Regional Scales. *Surveys in Geophysics*, *35*, 813 – 837. doi:10.1007/s10712-013-9262-y.

Rogelj, J., Meinshausen, M., & Knutti, R. 2012. Global warming under old and new scenarios using IPCC climate sensitivity range estimates. *Nature Climate Change*, *2*, 248 – 253. doi:10.1038/nclimate1385.

Ruelland, D., Ardoin-Bardin, S., Collet, L., & Roucou, P. 2012. Simulating future trends in hydrological regime of a large Sudano-Sahelian catchment under climate change. *Journal of Hydrology*, *424-425*, 207 – 216. doi:10.1016/j.jhydrol.2012.01.002.

Sælthun, N. R. 1996. *The Nordic HBV model*. Report 07 Norwegian Water Resources and Energy Directorate. URL: http://folk.uio.no/nilsroar/gf247/hbvmod.pdf.

Sætrang, A. C., & Wold, B. 1986. Results from the radio echo-sounding on parts of the Jostedalsbreen ice cap, Norway. *Annals of glaciology*, *8*, 156 – 158. URL: http://www.igsoc.org:8080/annals/8/igs_annals_vol08_year1985_pg156-158.pdf.

Saloranta, T. M. 2012. Simulating snow maps for Norway: Description and statistical evaluation of the seNorge snow model. *Cryosphere*, *6*, 1323 – 1337. doi:10.5194/tc-6-1323-2012.

Samuelsson, P., Jones, C. G., Willén, U., Ullerstig, A., Gollvik, S., Hansson, U., Jansson, C., Kjellstrom, E., Nikulin, G., & Wyser, K. 2011. The Rossby Centre Regional Climate model RCA3: model description and performance. *Tellus A*, *63*, 4 – 23. doi:10.1111/j.1600-0870.2010.00478.x.

SANDRP. Hydro Electric Projects in Beas River Basin. Accessed in February 2015. URL: http://sandrp.in/basin_maps/Hydropower_Projects_in_Beas_Basin.pdf.

Schewe, J., Heinke, J., Gerten, D., Haddeland, I., Arnell, N. W., Clark, D. B., Dankers, R., Eisner, S., Fekete, B. M., Colón-González, F. J., Gosling, S. N., Kimk, H., Liu, X.,

Masakim, Y., Portmann, F. T., Satoh, Y., Stacke, T., Tang, Q., Wada, Y., Wisser, D., Albrecht, T., Frieler, K., Piontek, F., Warszawski, L., & Kabat, P. 2014. Multimodel assessment of water scarcity under climate change. *Proceedings of the National Academy of Sciences*, *111*, 3245 – 3250. doi:10.1073/pnas.1222460110.

Seiller, G., & Anctil, F. 2014. Climate change impacts on the hydrologic regime of a canadian river: comparing uncertainties arising from climate natural variability and lumped hydrological model structures. *Hydrology and Earth System Sciences*, *18*, 2033 – 2047. doi:10.5194/hess-18-2033-2014.

Sharmila, S., Joseph, S., Sahai, A., Abhilash, S., & Chattopadhyay, R. 2015. Future projection of Indian summer monsoon variability under climate change scenario: An assessment from CMIP5 climate models. *Global and Planetary Change*, *124*, 62 – 78. doi:10.1016/j.gloplacha.2014.11.004.

Singh, P., & Bengtsson, L. 2004. Hydrological sensitivity of a large Himalayan basin to climate change. *Hydrological Processes*, *18*, 2363 – 2385. doi:10.1002/hyp.1468.

Singh, P., & Kumar, N. 1997. Effect of orography on precipitation in the western Himalayan region. *Journal of Hydrology*, *199*, 183 – 206. doi:10.1016/S0022-1694(96)03222-2.

Sivapalan, M., Takeuchi, K., Franks, S. W., Gupta, V. K., Karambiri, H., Lakshmi, V., Liang, X., McDonnell, J. J., Mendiondo, E. M., O'Connell, P. E., Oki, T., Pomeroy, J. W., Schertzer, D., Uhlenbrook, S., & Zehe, E. 2003. IAHS Decade on Predictions in Ungauged Basins (PUB), 2003-2012: Shaping an exciting future for the hydrological sciences. *Hydrological Sciences Journal*, *48*, 857 – 880. doi:10.1623/hysj.48.6.857.51421.

Skahill, B. E., & Doherty, J. 2006. Efficient accommodation of local minima in watershed model calibration. *Journal of Hydrology*, *329*, 122 – 139. doi:10.1016/j.jhydrol.2006.02.005.

Skaugen, T., Stranden, H. B., & Saloranta, T. 2012. Trends in snow water equivalent in Norway (1931–2009). *Hydrology Research*, *43*, 489 – 499. doi:10.2166/nh.2011.109.

Smakhtin, V., Revenga, C., & Döll, P. 2004. A Pilot Global Assessment of Environmental Water Requirements and Scarcity. *Water International*, *29*, 307 – 317. doi:10.1080/02508060408691785.

SMHI. Rossby Centre regional atmospheric model, RCA4. Accessed in February 2015. URL: http://www.smhi.se/en/research/research-departments/climate-research-rossby-centre2-552/rossby-centre-regional-atmospheric-model-rca4-1.16562.

Stahl, K., Moore, R. D., Shea, J. M., Hutchinson, D., & Cannon, A. J. 2008. Coupled modelling of glacier and streamflow response to future climate scenarios. *Water Resources Research*, *44*, W02422. doi:10.1029/2007WR005956.

Strahler, A. N. 1957. Quantitative analysis of watershed geomorphology. *Transactions, American Geophysical Union*, *38*, 913 – 920. doi:10.1029/TR038i006p00913.

Teichmann, C., Eggert, B., Elizalde, A., Haensler, A., Jacob, D., Kumar, P., Moseley, C., Pfeifer, S., Rechid, D., Remedio, A. R., Ries, H., Petersen, J., Preuschmann, S., Raub, T., Saeed, F., Sieck, K., & Weber, T. 2013. How Does a Regional Climate Model Modify the Projected Climate Change Signal of the Driving GCM: A Study over Different CORDEX Regions Using REMO. *Atmosphere*, *4*, 214 – 236. doi:10.3390/atmos4020214.

Todini, E. 2007. A mass conservative and water storage consistent variable parameter Muskingum-Cunge approach. *Hydrology and Earth System Sciences*, *11*, 1645 – 1659. doi:10.5194/hess-11-1645-2007.

Todini, E. 2011. History and perspectives of hydrological catchment modelling. *Hydrology Research*, *42*, 73 – 85. doi:10.2166/nh.2011.096.

Uhlenbrook, S., Seibert, J., Leibundgut, C., & Rodhe, A. 1999. Prediction uncertainty of conceptual rainfall-runoff models caused by problems in identifying model parameters and structure. *Hydrological Sciences Journal*, *44*, 779 – 797. doi:10.1080/02626669909492273.

Vaché, K. B., & McDonnell, J. J. February 2006. A process-based rejectionist framework for evaluating catchment runoff model structure. *Water Resources Research*, *42*, W02409. doi:10.1029/2005WR004247.

Varado, N., Braud, I., Galle, S., Le Lay, M., Seguis, L., Kamagate, B., & Depraetere, C. 2006. Multi-criteria assessment of the Representative Elementary Watershed approach on the Donga catchment (Benin) using a downward approach of model complexity. *Hydrology and Earth System Sciences*, *10*, 427 – 442. doi:10.5194/hess-10-427-2006.

Vieli, A. 2015. Glacier change: Dynamic projections. *Nature Geoscience*, *8*, 332 – 333. doi:10.1038/ngeo2425.

Vormoor, K., & Skaugen, T. 2013. Temporal Disaggregation of Daily Temperature and Precipitation Grid Data for Norway. *Journal of Hydrometeorology*, *14*, 989 – 999. doi:10.1175/JHM-D-12-0139.1.

World Bank. Health Nutrition and Population Statistics: Population estimates and projections. Accessed in September 2014. URL:

http://databank.worldbank.org/data/views/variableselection/selectvariables.aspx?source=health-nutrition-and-population-statistics:-population-estimates-and-projections.

Wrede, S., Seibert, J., & Uhlenbrook, S. 2013. Distributed conceptual modelling in a Swedish lowland catchment: a multi-criteria model assessment. *Hydrology Research*, *44*, 318 – 333. doi:10.2166/nh.2012.056.

Xu, C.-Y. 1999. From GCMs to river flow: a review of downscaling methods and hydrologic modelling approaches. *Progress in Physical Geography*, *23*, 229 – 249. doi:10.1177/030913339902300204.

Yang, T., Hao, X., Shao, Q., Xu, C.-Y., Zhao, C., Chen, X., & Wang, W. 2012. Multi-model ensemble projections in temperature and precipitation extremes of the Tibetan Plateau in the 21st century. *Global and Planetary Change*, *80-81*, 1 – 13. doi:10.1016/j.gloplacha.2011.08.006.

Zhao, R. 1992. The Xinanjiang model applied in China. *Journal of Hydrology*, *135*, 371 – 381. doi:10.1016/0022-1694(92)90096-E.

Part II

Publications

1 Article I

– **Li, H.**, Beldring, S., Xu, C.-Y. (2014): Implementation and testing of routing algorithms in the distributed Hydrologiska Byråns Vattenbalansavdelning model for mountainous catchments.—*Hydrology Research* **45(3)**: 322–333, doi: 10.2166/nh.2013.009.

2 Article II

– **Li, H.**, Xu, C.-Y., Beldring, S. (2015): How much can we gain with increasing model complexity with the same model concepts?—*Journal of Hydrology*, **527**: 858–871, doi:10.1016/j.jhydrol.2015.05.044.

Journal of Hydrology 527 (2015) 858–871

Contents lists available at ScienceDirect

Journal of Hydrology

journal homepage: www.elsevier.com/locate/jhydrol

How much can we gain with increasing model complexity with the same model concepts?

Hong Li [a], C.-Y. Xu [a,*], Stein Beldring [b]

[a] Department of Geosciences, University of Oslo, Norway
[b] Norwegian Water Resources and Energy Directorate, Norway

ARTICLE INFO

Article history:
Received 17 January 2015
Received in revised form 20 May 2015
Accepted 23 May 2015
Available online 28 May 2015
This manuscript was handled by Konstantine P. Georgakakos, Editor-in-Chief, with the assistance of Yu Zhang, Associate Editor

Keywords:
Distributed models
HBV
Internal variables
Lumped model
Model comparison

SUMMARY

The main purpose of this study is to test the hypothesis that, with appropriate structures, increasing model complexity with the same model concepts would lead to an increase in the model efficiency in simulating either runoff or internal variables. Five variants of the Hydrologiska Byråns Vattenbalansavdelning (HBV) model, i.e. a lumped model (LWhole), a semi-distributed model (SBand), a grid-model without routing (GRZero), a grid-model with hillslope routing (GROne), and a grid-model with both hillslope and channel routing (GRTwo) are compared in a cold and mountainous catchment in central southern Norway. The five models are compared with respects to (1) runoff simulation at the catchment outlet and the interior points, and (2) simulations of internal variables, i.e. evapotranspiration, snow water equivalent and groundwater depth. The results show that the models with higher complexity can improve the runoff simulation both at the catchment outlet and the interior points. However, there is no superiority of complex grid-models over simple grid-models in reproducing internal variables in this study.

1. Introduction

The fundamental work of hydrologists is to quantify relationship of precipitation over a catchment area and resulting runoff. In the last three decades, a large amount of hydrological models have been published to describe this relationship (Singh and Woolhiser, 2002). These models are suited to simulate runoff at certain spatial and temporal scales (Praskievicz and Chang, 2009). Basically, the differences among the models come from three aspects (Butts et al., 2004): (1) assumptions about factors influencing hydrology or response functions, (2) numerical solutions, and (3) spatial discretisation, such as sub-catchments or square grids.

There has been an evident trend to develop models with high degree of complexity (Mayr et al., 2013; Perrin et al., 2001). The development of hydrological models has gone through three stages, from input–output black-box models, through lumped conceptual models, to physically-based and/or conceptual distributed models. The physically-based distributed models tend to represent physical processes by partial differential equations at a fine spatial resolution. To develop models with high degree of physical dependence and structural complexity is long-sighted and useful in terms of knowledge gained about hydrological processes from catchment studies. However, it would lead to increasing difficulty in estimating parameters and large parameter uncertainty (Butts et al., 2004).

Hydrologists show high interest in comparing hydrological models of varying complexity. The conclusions are not consistent due to many reasons, for example, the models used in the comparisons, data quality and catchment characteristics, etc. However, if the models differ in the assumptions about factors influencing hydrology or the runoff process, results of comparisons are determined by the basins used.

To focus on the model itself, we assume that the responses of runoff to areal mean precipitation are described by the model concepts, which can be described by a lumped model. The model complexity exists in the way that water balance components are presented. For example, the lumped HBV model formulates all basic concepts of the HBV model. The semi-distributed models with elevation bands or sub-catchments and the grid-distributed models are of a higher degree of model complexity. The routing procedure, such as the Muskingum method also adds an additional degree of complexity, because it links the model elements to each other.

This research examines if increasing degree of model complexity improves the model performance and how much. A review of

* Corresponding author.
E-mail address: chongyu.xu@geo.uio.no (C.-Y. Xu).

http://dx.doi.org/10.1016/j.jhydrol.2015.05.044
0022-1694/

the scientific literature did not provide a clear guidance on this issue. In 2004, the Distributed Model Intercomparison Project (DMIP) compared distributed and lumped versions of twelve models with radar precipitation data at a 4 km spatial resolution and hourly temporal resolution (Smith et al., 2004). Twenty one events in eight catchments with areas ranging from 65 to 2484 km^2 were selected in the comparative studies. This project results showed that overall, lumped models outperformed distributed models in terms of discharge simulation, and some distributed models showed comparable results to lumped models in many basins (Reed et al., 2004). The results depended on the basin's shape, orientation, soil and climatic characteristics (Butts et al., 2004; Reed et al., 2004).

Different results are reported by other studies. Atkinson et al. (2003) demonstrated that the best simulation of runoff was obtained by a fully distributed model in a small catchment at an hourly time step. Han et al. (2014) and Yan and Zhang (2014) respectively examined effects of watershed subdivision on modelling runoff. They found that with a larger number of sub-catchments, the model gave a better performance and there was a threshold level, beyond which no significant improvements could be obtained with increasing number of sub-catchments. This confirms the results by comparing two watershed subdivision schemes by Varado et al. (2006). Michaud and Sorooshian (1994) compared the lumped and distributed Soil Conservation Service (CSC) models on a semi-arid catchment of 150 km^2 and the results showed that neither of the models could accurately simulate the peak flows or runoff volumes from 24 sever thunderstorms at an one-minute time step. Using the same model, Boyle et al. (2001) found improvements were related to spatial distribution of model input and streamflow routing and no additional benefits could be obtained when the number of watersheds were more than three.

A well-known way for a better model comparison is involving internal points and state variables in model evaluation (Lindström et al., 1997; Uhlenbrook et al., 1999; Vaché and McDonnell, 2006). Alley (1984) was probably the first to notice that models were similar in runoff simulation while substantial differences existed in other variables. Furthermore, Jiang et al. (2007) found that models differed least in discharge among simulations of discharge, actual evapotranspiration and soil moisture. Varado et al. (2006) applied a conceptual model on the Donga catchment (Benin), and found that the model was only good at simulating runoff, but not at reproducing groundwater table. Vaché and McDonnell (2006) showed that, among the models they evaluated, only the most complex model successfully reproduced both discharge dynamics and residence time. The results of their research indicate that the best objective function value in discharge are obtained during calibration, but with sacrifice of other hydrological variables, where the error resides. In order to achieve deliberate conclusions, comparisons including other hydrological measurements, such as evapotranspiration and groundwater should be adopted (Bookhagen and Burbank, 2010; Lindström et al., 1997; Wagener et al., 2001). This multi-variable comparison will not only contribute to an improved understanding of hydrology processes, but also provide guidance for developing hydrological models.

The aim of this paper is to test the hypothesis that, with appropriate way of organising, increasing complexity leads to an increase in model efficiency of simulating either runoff or other internal variables. A conceptual rainfall–runoff model, the HBV model is selected and modified to five model variants of different complexities, i.e. a lumped model (LWhole), a semi-distributed model with ten elevation bands (SBand), a simple grid-model (GRZero), a grid-model with hillslope routing (GROne), and a grid-model with both hillslope routing and river channel routing (GRTwo). The selection of the models is threefold. Firstly, LWhole is the most widely used HBV model variant for scientific and operational purposes globally. Secondly, SBand is currently used in the Norwegian Water Resources and Energy Directorate (NVE), which is responsible for flood forecasting and water resources administration in Norway. Thirdly, three distributed models are included in the sense of having a higher level of physical realism. The spatial variability and how the runoff routes to the catchment outlet are described in the three grid distributed models at various degrees of complexity.

Lindström et al. (1997) made the first attempt to make a distributed version of the HBV model. They used a typical resolution of 40 km^2 of sub-catchments and each sub-catchment was further divided into elevation bands. This modification significantly improved model performance. In the late 1990s, Uhlenbrook et al. (1999) and Krysanova et al. (1999) respectively compared the effects of spatial distribution on runoff simulation. Uhlenbrook et al. (1999) compared three model variants with different number of elevation bands and land use zone and various runoff generation conceptualisation, on a small mountainous catchment of 40 km^2 in south western Germany. They concluded that the models considering more spatial variability were better than the lumped models when separately computing of the upper zone storage for each model unit. Krysanova et al. (1999) applied the semi-distributed HBV model of elevation bands to a large German catchment of 96,000 km^2. The model with sub-catchments enabled better runoff simulation than without sub-catchment division. However, Das et al. (2008) compared four versions of the HBV model and found that semi-distributed and semi-lumped (a lumped model for each sub-catchment) outperformed the distributed (1 km regular grid) and lumped model structures. The authors suspected that the input data did not reflect the actual spatial variability. The study by Wrede et al. (2013) in a Swedish lowland catchment of 2000 km^2 using the distributed model (250 m regular grid) also showed that the quality of input data was a limitation factor for model performance. For modelling other variables, Mayr et al. (2013) reported that involving glacier mass balance in calibration gave a better prediction in the glacier mass but a slightly worsened discharge prediction. Moreover, they revealed that incorrect snow and ice simulations did not necessarily affect the quality of the runoff simulation.

2. Study area and data

2.1. Study area

The Norsfoss catchment is located in upstream of the longest Norwegian river, the Glomma River in central southern Norway (Fig. 1). This catchment covers an area of 18,932 km^2. The mean altitude is 732 m above the mean sea level (m amsl) ranging from 147 to 2170 m amsl, and approximately 26% of the area is above the potential tree level. The mean slope is 6.7° with a range from 0.0° to 73.2°. Climate varies along the river from upper mountain regions in north to lowlands in south. Additionally, the north-western part is characterised by lower temperature, lower precipitation and longer snow-cover period than the lowland area. Annual precipitation is 849 mm/year, and yearly mean air temperature is −0.62 °C based on the period from 1961 to 1990 with 10.68 °C in July and −11.48 °C in January. More than 60% of the catchment area is covered by forest and marsh, and approximately 20% is covered by bedrock. Floods are usually associated with snow melt, heavy rainfall or their combination (L'Abée-Lund et al., 2009).

2.2. Geography data and processing

Data of elevation, slope and land covers are provided by the Norwegian Mapping Authority, which bears nationwide

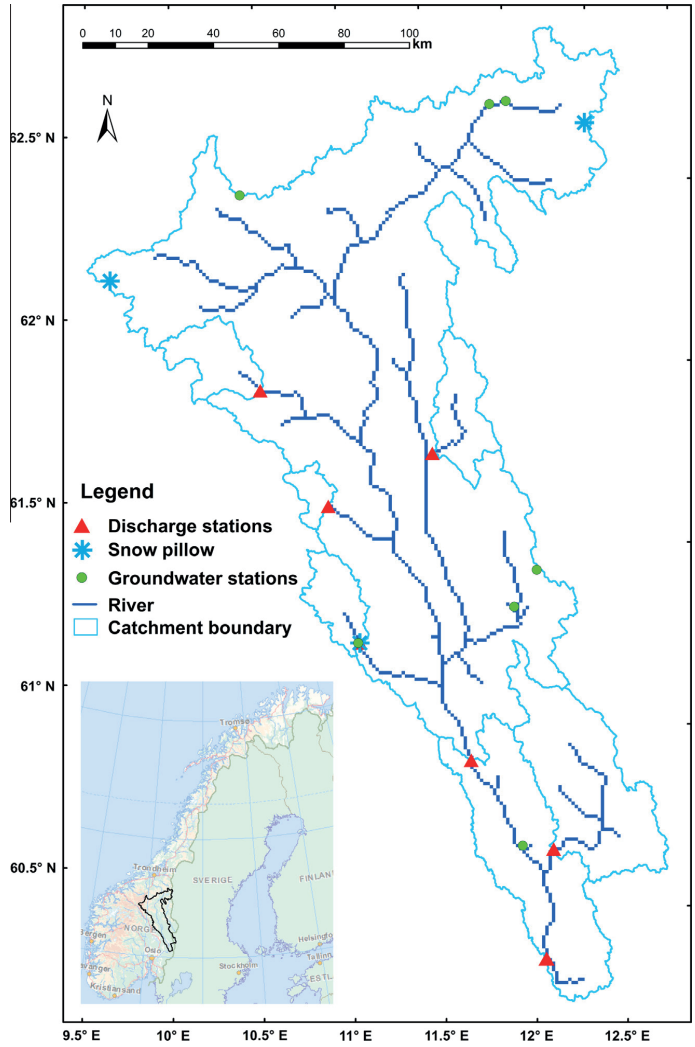

Fig. 1. Location and Digital Elevation Models (DEMs) of the Norsfoss catchment, Norway. The locations of snow pillows, groundwater stations and discharge stations are also shown; more detailed information is given in Table 1. Note that only the discharge at the catchment outlet (the lower right corner discharge station) is used in calibration.

responsibility for geographical information. These datasets are at a spatial resolution of 25 m regular grid.

For elevation and slope, the original datasets are aggregated at 1 km. There are eight land cover types, i.e. lake, bog, forest, bedrock, heather, alpine forest, open land and glacier. Their fractions in each 1 km grid are computed from their respective numbers of small grids at 25 m within 1 km grid.

The drainage networks delineation is constructed in three steps. Firstly, the DEMs at 25 m are aggregated at 100 m. The reason for the aggregation is that there are many small lakes and bogs in the study area. This aggregation removes these local pour points. Secondly, flow direction data are built based on the 100 m DEMs according to the D8 (deterministic eight-node) method. The D8 method developed by O'Callaghan and Mark (1984) assumes that water flows to only one of the eight nearest neighbours based on the steepest slope. Lastly, the drainage networks at a resolution of 1 km are created by using the river Network Scaling Algorithms (Fekete et al., 2001; Gong et al., 2009). The drainage networks are also visually checked according to the National River Network Database (ELVIS) (NVE, 2015) made in the year 2011, and manually modified if necessary. More details can be found in Li et al. (2014).

Estimating the channel cross-sectional size is difficult and essential in channel routing. In this study, 111 cross-sections are measured from digital maps; however, these measurements cannot be utilised without pre-processing by distributed models for three reasons. Firstly, the digital river network sometimes does not really match most natural rivers, which may lead to usage of only a small number of the measured river cross-sections. Secondly, in Norway, some lakes, such as Storsjøen, are very long

and crossed by rivers. The widths of these long lakes are much wider than rivers and should not be counted in the river routing. Thirdly, in some grids, there are more than one measured cross-sections. A simple method assuming that widths along a river section are similar, is developed to get river width of river grids in two steps. Firstly, the digital river network is divided into different sections according to the Strahler system (Strahler, 1957). Secondly the width of one river section is assigned the mean of the widths of all river cross-sections measured in the respective local sub-catchment.

2.3. Climate data

Daily maps of precipitation and temperature at a resolution of 1 km for mainland Norway are used in this study. These datasets are produced by the Norwegian Meteorological Institute (met.no) using daily observations of 24-h mean temperature and accumulated precipitation measured at meteorological stations.

For temperature, daily mean observations of 150 stations are first projected to the mean sea level by regression analysis based upon monthly mean temperature data from 1152 stations in Norway, Sweden, Denmark and Finland. Interpolated temperature by the residual kriging method is readjusted to terrain elevation using a lapse rate that varies among different seasons (Mohr, 2008).

For precipitation, observations of 630 stations are corrected for systematic under-catch due to station's exposure to wind. To interpolate precipitation, a method of triangulation (Mohr, 2008) is used with correction for the altitude of grid point using a vertical precipitation gradient of 10% per 100 m difference below 1000 m amsl and a vertical precipitation gradient of 5% per 100 m difference above 1000 m amsl (Mohr, 2008; Vormoor and Skaugen, 2013). These datasets have been evaluated and used in many studies covering Norway, such as hydrology modelling (Beldring, 2002a; Li et al., 2014), glacier mass estimation (Engelhardt et al., 2012; Engelhardt et al., 2013), permafrost evolution (Gisnås et al., 2013) and snow depth estimation (Mohr, 2008; Vormoor and Skaugen, 2013; Bruland et al., 2015). These studies have shown that the datasets are generally of high quality. In the Norsfoss catchment, there are 64 stations roughly uniformly distributed, which means a station density of 3.4 per 1000 km^2. The high density of stations ensures a good quality of the climate data in this study.

2.4. Observations

Discharge, snow water equivalent (SWE) and groundwater depth are used to calibrate or validate the models.

Discharge is transformed from measured stage using the Bayesian Rating Curve Fitting method (Petersen-Øverleir et al., 2009). Time series of daily discharge in the period from 1981 to 1990 at the Norsfoss gauging station are used in calibration and the period 1991–2000 are used for validation.

SWE is measured by three snow pillows, which are in the national network of Norway. The measurements of the national snow pillows have been re-verified by extensive sampling on a monthly basis during the winter of the two years, 1998 and 1999.

Groundwater depth is measured by seven piezometers. All the piezometers are located in sparse vegetation areas and the measured aquifers are shallow glacier tills. The Gbr Vika and Abrahamsvoll stations are very close to lakes. Generally the measurements are of high quality; however there is a large uncertainty in peak groundwater measurements due to manual measurement at weekly time step (Fleig, 2013). Locations of the piezometers are depicted in Fig. 1 and tabulated in Table 1.

3. Methodology

3.1. Model description

The HBV model concepts were initially developed for usage in the Scandinavia in the 1970s (Bergström, 1976) and the model has been modified into many versions (Sælthun, 1996; Beldring et al., 2003; Ehret et al., 2008; Hailegeorgis and Alfredsen, 2015). The model contains routines for snow accumulation and melting, soil moisture accounting and runoff generation. The HBV model has been applied in more than 80 countries and is currently used as a standard tool for flood forecasting and simulating inflow to hydropower reservoirs in many areas. In NVE, which provides flood forecasting services for the entire Norway, the semi-distributed HBV model with ten elevation bands (SBand) is currently used for flood forecasting.

Bergström (1976) and Lindström et al. (1997) have explicitly described the model algorithms and the scientific bases. Uhlenbrook et al. (1999) further demonstrated the plausibility of the model structure and process conceptualizations by using the GLUE approach. Therefore, only the equations of the studied components, namely runoff, evaporation, snow storage and groundwater are given in this paper.

Snow accumulation and melting are calculated based on temperature according to Eqs. (1) and (2) (Lindström et al., 1997). Snow is a porous media and some rain and melt water can be retained in the pores. In the models, porosity of 8% of the snowpack water equivalent is assumed. Melt water can be released only after pores are filled up. Hence, SWE is the sum of snow and contained liquid water.

$$SF = P \quad T < TACCT \tag{1}$$

$$SMelt = SMELTR \times (T - MELTT) \quad T > TACCT \tag{2}$$

where SF is snow fall; P is precipitation; T is air temperature; $SMelt$ is snow melt rate. $ACCT$, $SMELTR$ and $MELTT$ are parameters. In this study, $ACCT$ is fixed as zero and other parameters are calibrated.

Evaporation is calculated based on the potential evaporation rate (PE) and available water for evaporation. PE is computed based on a parameter for land surface and temperature. Lakes evaporate at PE.

$$PE = EPOT \times T \quad T > 0 \tag{3}$$

Table 1
Types, names and locations of the observing stations. The areas (km^2) of the catchments are shown in the parentheses following the names of the discharge stations. The elevations (in m amsl) of the snow pillows and ground piezometers are in the parentheses following the name.

Type	Name	Longitude (E)	Latitude (N)
Discharge	Søndre Imssjøen (158)	10.6618	61.5479
	Kvarstadseter (377)	10.8933	61.1785
	Atnasjø (463)	10.2221	61.8519
	Mistra Bru (550)	11.2419	61.7111
	Knappom (1,646)	12.0471	60.6412
	Elverum (15,447)	11.5607	60.8742
	Norsfoss (18,933)	12.0355	60.339
Snow pillow	Kvarstadseter (665)	10.8933	61.1785
	Fokstugu (980)	9.2971	62.1188
	Vauldalen (830)	12.0334	62.6411
Groundwater	Haslemoen (169)	11.8738	60.6467
	Kvarstadseter (698)	10.8837	61.1781
	Gbr Vika (436)	11.7595	61.3019
	Stenerseter (625)	11.8782	61.4065
	Settalbekken (994)	10.0159	62.3828
	Glåmos (700)	11.4609	62.6789
	Abrahamsvoll (710)	11.5576	62.6897

where *EPOT* is a parameter for potential evaporation rate.

The rate of actual evaporation (*AE*) is a function of *PE* and available soil moisture (*SM*):

$$AE = \begin{cases} \frac{PE \times SM}{FC \times FCD} & SM < FC \times FCD \\ PE & SM \geqslant FC \times FCD \end{cases} \quad (4)$$

where *FC* is the field capacity; *FCD* is a parameter that takes values between 0 and 1. It is fixed as 1 in this study.

The infiltration is controlled by a infiltration capacity, *INFMAX*. The part of the water input exceeding this parameter goes directly to the upper zone of the groundwater storage (*UZ*) as well as a fraction of the input water.

$$UZ = Inf_e + InSoil \times \left(\frac{SM}{FC}\right)^{BETA} \quad (5)$$

where Inf_e is the input water exceeding *INFMAX*. *InSoil* is the water getting into the soil. *BETA* is a parameter describing shape of soil moisture release curve.

Deep percolation from the upper zone to the lower zone is a product of a soil parameter, *PERC* and *UZ*. Total runoff, *Q*, is sum of the runoff from the upper zone and lower zone (Eq. (6)). This conceptualisation is based on that runoff is mainly generated due to a rising groundwater table and Horton overland flow rarely occurs due to a large hydraulic conductivity of the glacial till deposits (Beldring, 2002b). The runoff from the upper zone represents the quick flow and the runoff from the lower zone represents the base flow.

$$Q = KUZ \times UZ^{ALFA} + KLZ \times LZ \quad (6)$$

where *LZ* is storage of the lower zone; *KUZ* and *KLZ* are recession parameters. *ALFA* is a parameter introduced by Lindström et al. (1997) to handle the over-parametrisation problem. *ALFA* replaces two parameters of the response function of the upper zone and improved the model efficiency (Lindström et al., 1997). This non-linear response reflects the rapidly decreased conductivity of surface deposits in the Nordic countries (Beldring, 2002b). The groundwater storage is the sum of *UZ* and *LZ*.

3.2. Five models

Five models based on the same HBV concepts are compared, namely, LWhole, SBand, GRZero, GROne, and GRTwo. These five models are presenting increasing levels of spatial discretisation and process details. All the models are run at the daily time step with the same input data.

The lumped model, LWhole, is a simple HBV model using the areal mean precipitation and temperature over a catchment with a uniform characteristic. All types of land covers and soil are sharing the common parameter values.

The semi-distributed model with elevation bands, SBand, is the most widely used model setting in Norway. The catchment is divided into ten elevation bands with equal area according to the hypsometry curve. For each zone, time series of mean precipitation and temperature are inputs. Calibrated parameters vary from different type of land cover and soil. The sub-catchments share the same elevation band division and input data but with different weighting of each band.

For the grid-model without routing, GRZero, runoff generation is performed in every grid. Discharge at outlet is sum of runoff from all catchment grids. This model is of high spatial representation in forcing data and in parameter values.

For the grid-model with hillslope routing, GROne, the runoff generation subroutine runs on the most upslope grid, and the generated runoff is added to the groundwater storage of its downslope landscape grid. The downslope grid performs the groundwater routine with input equal to sum of the runoff from its upslope grids and the local net precipitation. This procedure runs from the upstream area to the downstream area until the runoff discharges into the river grids. Then the model runs for next time step.

For the grid-model with both hillslope routing and river flow routing, GRTwo, runoff is summed at respective river grid and routed by the Muskingum-Cunge method between river grids. River channel cross-sections are assumed to be rectangular. When the Courant number is greater than one, output discharge is equal to input discharge, which means no routing. Details of the Muskingum-Cunge method can be seen from, e.g. Todini (2007).

Among the five models, the lumped model, LWhole is the simplest. The semi-distributed model, SBand is suggested to represent the important features of catchment, while at the same time this model does not require high demand of data and computation. The first grid-model, GRZero, is a large assembly of LWhole with high spatial representation. The second grid-model, GROne describes hillslope routing. The third grid-model, GRTwo describes both hillslope routing and channel routing.

3.3. Parameters and calibration

Model parameters are calibrated by a model-independent non-linear parameter estimation and optimization package called PEST (Parameter ESTimation), which is frequently used for model calibration in different research fields. PEST reads files of input parameters and target output, thus calibration with any arbitrary model can be easily set up. The algorithms are based on the implementation of the Gauss–Marquardt–Levenberg algorithm, which combines advantages of the inverse Hessian matrix and the steepest gradient method to allow a fast and efficient convergence towards to the best value of the objective function. It is the minimum of a weighted least square sum of the discrepancies between simulated and observed discharge where similar weights are assumed. Within specified ranges of parameters, PEST approaches to an optimised parameter set (Doherty and Johnston, 2003; Wrede et al., 2013).

The Gauss–Marquardt–Levenberg method can efficiently find local objective function minima (Skahill and Doherty, 2006) with a small number of model runs. In contrast, other algorithms such as the Shuffled Complex Evolution algorithm (Duan et al., 1992) are much more likely to find the global objective function minimum with the cost of a much greater number of model runs (Coron et al., 2012). PEST is selected due to its good performance for Norwegian catchments (Lawrence et al., 2009) as well its sophistication after a long term development (Doherty, 2005). The optimal global parameter set is verified on the basis of different initial parameter sets.

The sensitivity and uncertainty of model parameters of the HBV model have been widely studied in Sweden and Norway. Bergström (1976) mapped the mean square error function of streamflow by the trial and error method. In snow routine, *MELTT* and *SMELTR* in Eq. (2) were sensitive and the sensitivity of *SMELTR* increased with lower *MELTT*. In the soil moisture accounting routine, *BETA* (in Table 2) was sensitive and its sensitivity decreased with increased *FC* in Eq. (4). In the dynamic response, *KUZ* in Eq. (5), *PERC* (in Table 2) and *KLZ* in Eq. (6) were greatly influenced by each other and the parameters in other routines. Using the Monte Carlo method, Harlin and Kung (1992) demonstrated that *SMELTR* and *KUZ* were sensitive, and *BETA* and *KLZ* were moderate. Furthermore, Seibert (1997) found that the sensitivity was hard to be described quantitatively, since the sensitivity changes greatly with different parameter values. *MELTT* and *KUZ* were most sensitive near the optimised value (Seibert, 1997). To achieve good performance in streamflow, only *MELTT* and *SMELTR* were in narrow range (Uhlenbrook et al., 1999). By similar

Table 2
Optimised values of the selected parameters. The parameters for SBand and the grid-based models are land use dependent; therefore the areal mean is given.

Group	Name	Meaning (unit)	LWhole	SBand	GRZero	GROne	GRTwo
Evaporation	*EPOT*	Potential evaporation capacity (m/day/°C)	5.02E−03	1.31E−02	1.31E−02	8.50E−03	7.14E−03
	INT_MAX	Interception storage (m/day)	2.91E−04	2.87E−04	2.86E−04	2.71E−04	2.32E−04
Snow	*MELTT*	Melting temperature of snow (°C)	−1.98	−0.84	−0.84	0.92	0.92
	SMELTR	Temperature index of snow melting rate (m/day/°C)	2.27E−03	3.93E−03	3.89E−03	8.06E−03	7.91E−03
Soil	*FC*	Field capacity (m)	1.293	0.738	0.751	0.318	0.335
	BETA	Shape coefficient of soil moisture	0.396	1.473	1.775	16.009	15.933
Runoff	*KUZ*	Recession coefficient of the upper zone (1/day)	0.133	0.536	0.541	0.567	0.694
	ALFA	Non-linear drainage coefficient of the upper zone	0.976	2.392	2.293	1.379	1.364
	PERC	Percolation from upper zone to the lower zone	0.013	0.019	0.020	0.006	0.005
	KLZ	Recession coefficient of the lower zone (1/day)	0.035	0.074	0.074	0.019	0.014

approach, Seibert (1999) found *MELTT* was the most constrained parameter by the objective function. In addition to studies in Nordic countries, Abebe et al. (2010) concluded that *FC* and *BETA* were sensitive to volume error and *KUZ* and *KLZ* were sensitive to high flow series in semi-humid watershed located in the sub-tropical coastal plain of south-eastern United States.

In the Nordic countries, glacial till deposits over an impermeable bedrock are the main aquifers. The subsurface conditions heavily depend on the land cover (Beldring, 2002b). To simplify, we assume that parameters vary among different land cover (Beldring et al., 2003; Wrede et al., 2013). To reduce the difficulty caused by the larger number of parameters in calibration, some parameters are tied, which means that they are simply maintaining a constant ratio to their parent parameter, which are optimised (Doherty, 2005). The calibrated parameters are the lake parameters, land cover parameters and soil parameters for bog, forest and alpine and *KLZ* for other land covers. Other parameters in the land cover and soil groups are tied to forest.

Initial parameter values were selected on the basis of previous best manual calibration trials. To achieve global optimised parameter values, we did start calibrations with different initial values and different parameter ranges. The meaning and optimised value of every parameter are shown in Appendix A and their areal means are summarised in Table 2.

3.4. Evaluation criteria

The models are evaluated with respect to the comparison between simulated and observed runoff both at the catchment outlet and internal points, and evapotranspiration, SWE and groundwater table are also compared among the models. These variables are selected because they are important components of water balance or can be validated by in situ measurements. The relative mean error (*RME*), the Nash–Sutcliffe efficiency (*NSE*) (Nash and Sutcliffe, 1970), the inverse Nash–Sutcliffe efficiency (*InNSE*) (Pushpalatha et al., 2012) and the correlation coefficient (*R*) were used as criteria for model performance.

$$RME = \frac{\sum_{i=1}^{n}(S_i - O_i)}{\sum_{i=1}^{n} O_i} \times 100 \quad (7)$$

$$NSE = 1 - \frac{\sum_{i=1}^{n}(S_i - O_i)^2}{\sum_{i=1}^{n}(O_i - \overline{O})^2} \quad (8)$$

$$InNSE = 1 - \frac{\sum_{i=1}^{n}\left(\frac{1}{S_i} - \frac{1}{O_i}\right)^2}{\sum_{i=1}^{n}\left(\frac{1}{O_i} - \frac{1}{\overline{O}}\right)^2} \quad (9)$$

$$R = \frac{\sum_{i=1}^{n}(S_i - \overline{S})(O_i - \overline{O})}{\sqrt{\sum_{i=1}^{n}(S_i - \overline{S})^2}\sqrt{\sum_{i=1}^{n}(O_i - \overline{O})^2}} \quad (10)$$

where O_i is the observed series; S_i is the simulated series; n is the length of series; $\overline{O}$ and $\overline{S}$ are the mean of observed series and simulated series. The perfect values (dimensionless) are 1 except *RME* being 0.

RME is for water balance error; *NSE* is for match of simulations and observations with large weight on high flow; *InNSE* is also for closeness of simulations and observations with large weight on the low flow (Pushpalatha et al., 2012). *R* is used in evaluating internal variables. Therefore, combination of these four criteria can give an appropriate evaluation of model performance.

4. Results

In this study, the model comparison is partly done according to runoff simulation either at the catchment outlet or interior points. The better a model is in runoff simulation, the more reliable the model is. Additionally, the differences of model simulations in evapotranspiration, SWE and groundwater storage are also analysed.

4.1. Discharge estimation at the catchment outlet

Results of *NSE* and *InNSE* are shown in Fig. 2. Differences existing in LWhole, SBand and GRZero show effects of finer spatial representation of the input data; differences existing in GRZero, GROne and GRTwo show effects of finer spatial representation of hydrologic processes. The figure shows that (1) The values of *NSE* increase from LWhole to the fully distributed model, GRTwo. (2) The most significant improvement occurs from LWhole to SBand and then from GRZero to GROne. (3) In simulation of the low flow, GROne and GRTwo are still able to give a fair estimation with relatively high *InNSE* values whereas the *InNSE* values of the other models fall below zero. (4) Implementing the Muskingum-Cunge method does not add additional value to runoff simulation at a daily time step in the study area as reflected by the unchanged value of *NSE* and *InNSE* between GROne and GRTwo.

The runoff seasonality is of high concern by hydrologists for water management. The monthly mean runoff is shown in Fig. 3(a) and the deviations of the five models from the observed values are shown in Fig. 3(b). It is seen that the model errors of LWhole and SBand exhibit a stronger seasonal pattern than GROne and GRTwo. Less water is predicted in pre-flooding seasons and more floods are predicted to occur in high flow seasons. In consequence LWhole and SBand have a tendency to amplify risks of drought and flooding and to hint a depressing situation for water resources. Although all five model structures have good total *RME* values of less than 3%, GROne and GRTwo are more reliable in overall evaluation.

4.2. Discharge estimation at interior points

One of big benefits of using distributed models is that they can explicitly account for spatial variability inside a basin and have the

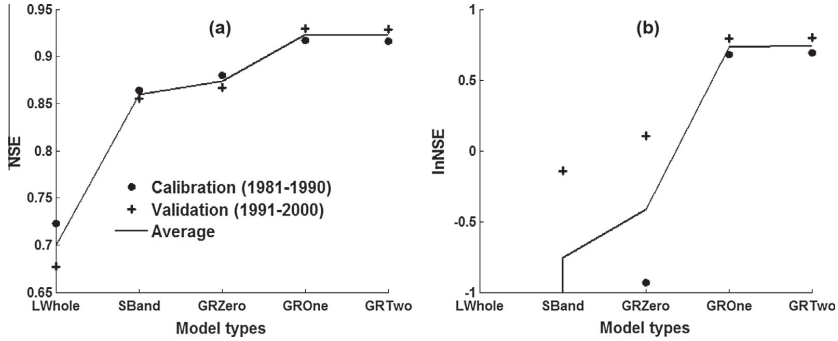

Fig. 2. The *NSE* (a) and *lnNSE* (b) values of different spatial discretisation schemes for calibration and validation periods at the outlet. Average is the mean of the *NSE* values for the calibration and the validation. In (b), the values, which are not shown, −46.12 for calibration, −13.32 for validation, −29.72 as the average of LWhole, and −1.37 for calibration of SBand.

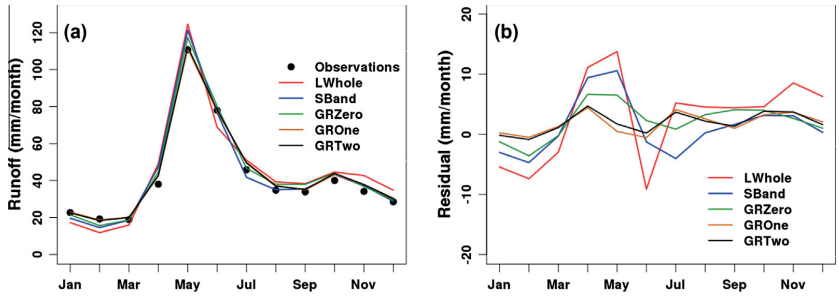

Fig. 3. Monthly mean runoff for the validation period at the outlet. (a) Comparison of simulations by the five models and the observations. (b) The residuals of the simulations.

ability to produce simulations at interior points without explicit calibration at these points. However, by transferring the parameter values and areal mean inputs, the lumped models can also estimate runoff at interior points. Then all the models can be evaluated at interior points; therefore we treat the performance of LWhole as a benchmark for the assessment of the other models, because we simply run LWhole in the sub-catchments with the parameter values calibrated at the catchment outlet and the time series of areal mean inputs. The forcing data in the sub-catchments for LWhole are the same as in the entire Norsfoss catchment.

There are six sub-catchments in total and results are presented in Fig. 4 and Table 3. It is noteworthy that only the discharge of the Norsfoss station was used in the calibration. Generally, the *NSE* values of all models increase with increasing catchment area. In the sub-catchments larger than 1646 km^2 (less than 10% of the area of the Norsfoss catchment) the *NSE* values of all the models except LWhole are larger than 0.6.

The mean and coefficient of variance (*CV*) of the *NSE* values of the five models are shown in Table 3. High mean with low *CV* indicates a good model performance. As expected, LWhole gives the lowest efficiency among the five models. GRTwo is the best with the largest mean *NSE* and the smallest *CV*. GROne and GRTwo are more likely to be capable than other three models.

4.3. Internal variables

Involving other variables in model evaluation is essential to make a breakthrough in model structure identification and process

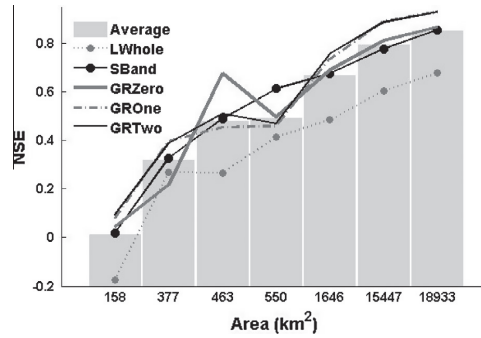

Fig. 4. The *NSE* values of six sub-catchments and the entire study area of five model structures for the validation period. Average is the mean of the *NSE* values of different model structures. The catchment with the largest area (18,933 km^2) is the entire study area.

Table 3
The mean value (mean) and *CV* of *NSE* on six sub-catchments and the entire study area in the validation period.

	LWhole	SBand	GRZero	GROne	GRTwo
Mean	0.363	0.536	0.543	0.564	0.576
CV	0.722	0.498	0.527	0.499	0.482

understanding. Simulations of evapotranspiration, SWE and groundwater are compared either among the five models or with observed data.

4.3.1. Evapotranspiration

It can be seen from Fig. 5 that the simulations of evapotranspiration by the five models are very close. Slight differences occur during the summer time, especially at the peaks in July. In the winter time, all the simulated evapotranspiration values are zero or close to zero. In humid area, evapotranspiration highly depends on the available energy for evaporation and vegetation growth. Thus evapotranspiration increases from January to July, when it is the warmest month and biological activity is intense (Beldring et al., 2003), and decreases from July to December. The calculated evapotranspiration is 352 mm/year and accounts for 40% of annual precipitation. This reflects a typical water balance situation at the east side of high mountains in central southern Norway.

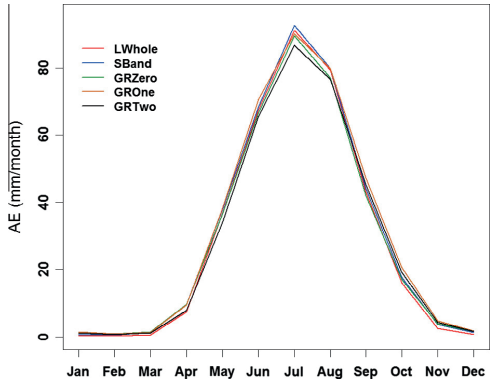

Fig. 5. Monthly mean evaportransipiration simulated by the five models for the validation period for the entire study area.

4.3.2. SWE

The SWE time series measured by three snow pillows and the simulations of three grids where the snow pillows are located by three grid-models are shown in Fig. 6. All the grid-models can give reasonable pattern of snow storage both by visual inspection and by the R values in Table 4. The models capture the time of accumulation and melting. However, all the three models do not accurately estimate the SWE amount. At the Kvarstadseter snow pillow site, all the models compute more snow than the observations; however, the results of the models are inconsistent at the Vauldalen snow pillow site. GRZero gives the highest R value at the three sites.

The areal mean monthly SWE simulations are presented in Fig. 7. It shows that the models can be roughly grouped into three classes. LWhole is the first class; SBand and GRZero are in the second class; and GROne and GRTwo are in the third class. There is more SWE calculated by the models of the third class than others.

4.3.3. Groundwater

In the HBV model, groundwater is simulated as areal mean volume of groundwater storage, whereas in practice, groundwater level is measured by piezometers. However, the storage and depth are highly correlated. Assuming a homogeneous aquifer and horizontal water table, the storage of the aquifer can be calculated by Eq. (11).

$$S_a = (H - H_0) \times \phi = H \times \phi - H_0 \times \phi \tag{11}$$

where S_a is the storage of aquifer per unit area in depth; H is the groundwater level; H_0 is the reference level, which is usually thought as the lowest groundwater level; ϕ is the effective porosity in relative volume.

The R between observed groundwater level and simulated groundwater storage is used to evaluate groundwater models in this study. The seven groundwater piezometers as presented in Table 1 and Fig. 1 are used. Weekly observations are available for the period from 1981 to 2000 with some missing values. In total, there are 5702 observations. All the measured aquifers are

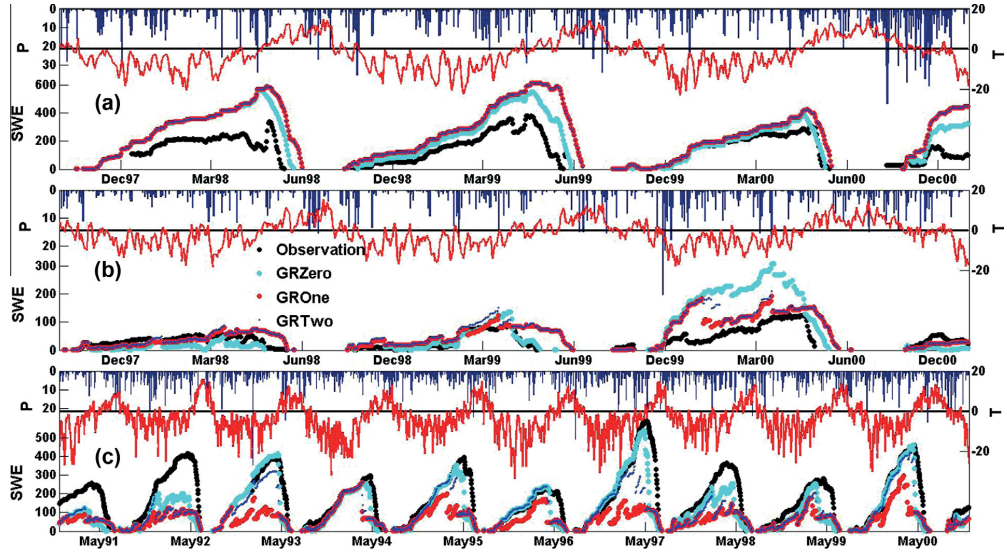

Fig. 6. Observations of SWE by the snow pillows, Kvarstadseter (a), Fokstugu (b) and Vauldalen (c) and the simulations of SWE of the grids where the snow pillows are located. P is the daily precipitation in mm/day. SWE is the daily observation and simulations in mm. T is the daily temperature in °C.

Table 4
The *R* values between snow pillow measurements and grid-model simulations.

Snow pillow	GRZero	GROne	GRTwo
Kvarstadseter	0.8	0.68	0.68
Fokstugu	0.73	0.7	0.69
Vauldalen	0.77	0.61	0.64
Mean	0.77	0.66	0.67

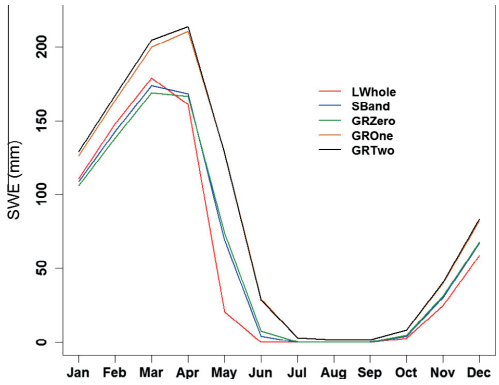

Fig. 7. Monthly mean SWE by the five models for the entire study area.

unconfined. *R* is calculated between the observed time series and the simulated time series of the grid where the piezometer is located.

Fig. 8 presents the results against the mean groundwater depth at the piezometers sites, elevation and slope of the grids where the piezometers are located. Firstly, all the grid-models give lower correlation coefficients at the piezometers with the deepest groundwater depth. Secondly, the patterns against elevation seem quite complex. The correlation coefficients go up with increased elevation and then down. The highest correlation coefficients are at approximately 600 m. Thirdly, there is an up trend against slope with large spread. The mean of all the *R* is 0.53 and the values of *R* of the three grid-models are comparable in magnitude.

5. Discussions

5.1. Runoff simulations

In rainfall–runoff modelling, runoff is indeed the most crucial output. As expected, the model performance improves most from LWhole to SBand and minor improvement occurs from the semi-distributed model, SBand to the grid distributed model, GRZero. This confirms the previous studies by Lindström et al. (1997), Das et al. (2008) and Wrede et al. (2013). The spatial variability in the forcing data, particularly temperature and precipitation must be accounted in hydrological modelling in mountainous and cold catchments. This is quite different from the catchment used by Michaud and Sorooshian (1994) and the DMIP catchments by Reed et al. (2004) and Butts et al. (2004).

The improvements both in the *NSE* and *lnNSE* from GRZero to GROne show that distributed hillslope routing is essential in runoff modelling, especially for simulating the low flow. In the hillslope routing, the water routes from an upstream grid to the outlet rather than directly add to its runoff volume. This process prolongs the response time and more water drains in the low flow seasons than in high flow seasons. This hypothesis is confirmed by Fig. 3. The models except GROne and GRTwo overestimate the high flow and underestimate the low flow.

The low efficiency of channel routing is caused by the high slope and sparse vegetation. Most runoff flows out within two days (Li et al., 2014). It is difficult to include this fast channel response in a daily simulation. The data error in observed discharge and aggregation of precipitation and temperature (Montanari and Baldassarre, 2013) is another possible reason.

The up trend of model efficiency with size of sub-catchments is the same as what was reported by Varado et al. (2006). A primary contributing factor to this may be that smaller basins have less capacity to deal with data error either in forcing data or discharge series. Besides, observations in small basins indeed exhibit more variability and dynamics in responses functions (Varado et al., 2006) than in larger basins, making accurate simulation more difficult (Reed et al., 2004). Another reason is that in this study the models are calibrated for the outlet station, and large sub-catchments share more common features with the one used for calibration.

5.2. Internal variables' simulation

Validating models on internal variables is always difficult and of primary importance. The first reason is that most internal variables, such as soil moisture and groundwater depth are measured at point scale. Simulations by hydrological models, even distributed models at a very fine resolution are areal mean values. The second reason is the less satisfactory length and quality of measurements compared to runoff data. However, this approach is required to assess the general behaviour of hydrological models and identification of model structures, especially in cases when runoff simulations by different models are close.

All grid-simulations are at a regular grid of 1 km. It is the most adopted spatial resolution in catchment hydrology studies and global datasets, for example, Hydro1k (EROS, 1996). These results will

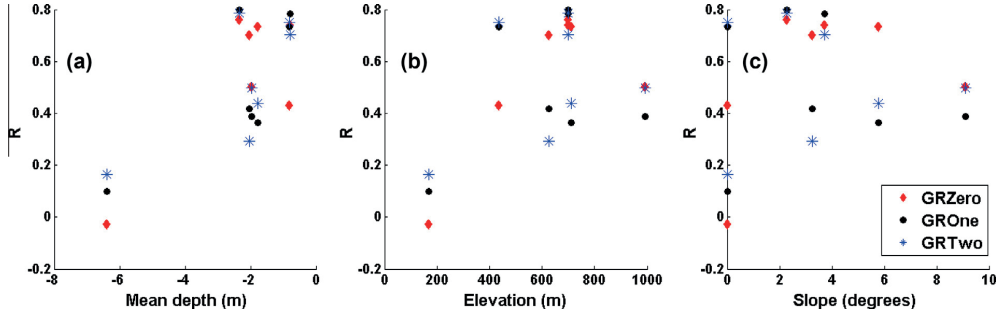

Fig. 8. The *R* values between measured groundwater level series and the simulated groundwater storage series.

give insights of other researchers and will be compared to on-going research.

5.2.1. Evapotranspiration

Evapotranspiration is a crucial term to connect a water balance model and a land surface energy balance model (Xu et al., 2005; Xu and Singh, 2005). The best available technology for observing evapotranspiration is a weighing lysimeter. However, establishing and maintaining a lysimeter for a long time period is very costly (Xu and Chen, 2005). Therefore, evapotranspiration is usually estimated using other methods, such as the Penman-Monteith method, reference evapotranspiration based methods, hydrological models (water balance method) and complementary relationship based methods (Gao et al., 2012). Recently, remote sensing data have been gradually used to estimate actual evapotranspiration (EI Hai EI Tahir et al., 2012; Yang et al., 2012; Corbari et al., August 2014). The most conceptually simple tool is the hydrological modelling, especially when regional estimation is required (Xu and Singh, 2005).

Although no observations of evapotranspiration are available, the simulated patterns are considered to be reasonable. The five models produced similar results. This can be explained from the water balance, because all five models used the same precipitation and discharge data and the model reproduced almost same runoff volume. The leftover of precipitation after runoff is the evaporation, if water storage of catchment does not change. Another reason is that the five models used the same temperature based method with the same areal mean temperature.

5.2.2. SWE

In Norway, almost half of the precipitation falls as snow, and it appreciably influences the hydrological responses. The most severe flood in southeast Norway in recent times occurred in the year 1995 and was fed from extensive snow covered high-mountain areas (Sorteberg et al., 2001).

Table 5
Ranks in the descending order of the five most sensitive parameters for each model. Other parameters are found insensitive.

Rank	LWhole	SBand	GRZero	GROne	GRTwo
1	*ALFA*	*SMELTR*	*EPOT*	*ALFA*	*ALFA*
2	*SMELTR*	*EPOT*	*SMELTR*	*KUZ*	*KUZ*
3	*EPOT*	*ALFA*	*ALFA*	*EPOT*	*EPOT*
4	*KLZ*	*KLZ*	*KLZ*	*SMELTR*	*SMELTR*
5	*MELTT*	*FC*	*FC*	*MELTT*	*FC*

The data errors existing in the measurements by snow pillow and in the grid temperature make the model simulation less accurate than other variables. For example, at the Kvarstadseter snow pillow site, there was a melting event on April 4th, 1998 according to the observations (Fig. 6). Contradictorily all models responded as an accumulation. The temperature of this grid was −7.5 °C in April 4th, 1998. Therefore, the models are believed to function well to the forcing data. The error may be investigated from the uncertainty of forcing data and measurements, or the sub-grid variability (Gisnås et al., 2013).

5.2.3. Groundwater

Bergström and Sandberg (1983) have shown that the HBV model is able to model groundwater level of unconfined aquifers after calibration with an objective function to achieve the maximum R between observed groundwater level and simulated groundwater storage. Their research provides confidence in the model and a benchmark in presenting our results. The values of R were around 0.8 and higher in most cases. However, Bergström and Sandberg (1983) used the average values of the stations at the study catchment and closeness of simulated and observed groundwater depth was the objective function of calibration. Varado et al. (2006) gave an example of model efficiency of a conceptual hydrological model (REW-v4.0) when it was only calibrated with discharge data. The model efficiency was very low and they concluded that was caused by the lack of presentation of the processes in the unsaturated zone.

Although our models produce lower R than the model of Bergström and Sandberg (1983), no groundwater data are used in calibration in our study. Additionally, the observed groundwater depth series are individually compared to the model produced series of the grid where they are located. If counting these differences, our models give equivalent performance.

The HBV model is a conceptual rainfall–runoff model. Therefore, it shows less capability in simulating groundwater levels of deeper depth, which are less relevant to runoff peaks and total runoff volume. Additionally, the three stations with low efficiency are located at approximately 200 m amsl, where human effects are stronger than at other stations with higher elevations.

In cold mountainous catchments, groundwater aquifers are recharged by rainfall and snow melt. At higher elevation places, snow melt has large proportion. Less accuracy in snow melt produced by models than the input precipitation is a possible explanation of low R at around the 1000 m height.

The trend of R against slope would be misleading. If the three stations at the 200 m height (R of which are below 0.2) are removed, there is no trend any more.

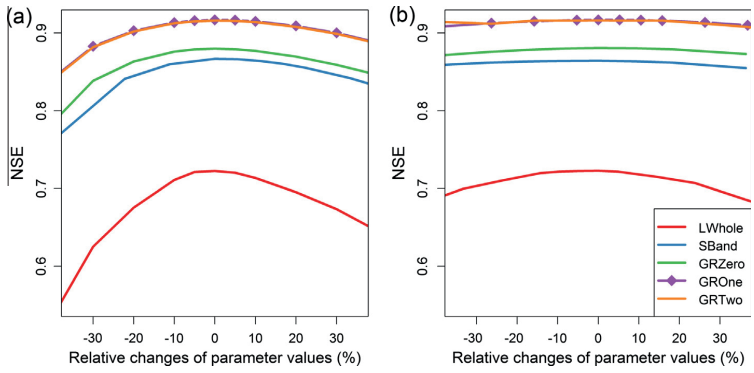

Fig. 9. Sensitivities of *SMELTR* (a) and *MELTT* (b). Other parameters are kept in their optimised values in each model.

5.3. Parameter analysis

Complex models are easily required to prove that their good efficiency is not achieved by adding additional parameters and the best solution should be supported by deliberate measurements of hydrological processes (Vaché and McDonnell, 2006). Otherwise, the optimised parameter values likely provide high evidence of parameter identifiability. As shown in Table 2, the optimised values of the selected parameters are considered to be in their plausible ranges. There are interdependence between certain parameters. *MELTT* and *SMELTR* are strongly correlated and positively associated. However, the soil parameters *FC* and *BETA* are negatively associated.

Parameter sensitivity is difficult to quantify due to the non-linear response of runoff to parameters and parameter interactions (Seibert, 1997; Tang et al., 2007). The sensitivities are impacted by selection of analysis method and the physical characteristic of study area (Tang et al., 2007). Thereby, we define the parameter sensitivity as the changes of *NSE* against the relative changes of the parameter values. Shown in Table 5, *SMELTR*, *ALFA* and *EPOT* are among the five most sensitive parameters for every model. It can be concluded that the ranks of parameter sensitivity for the five models are similar. For an illustrative purpose, the sensitivities of a sensitive parameter (*SMELTR*) and a less sensitive parameter (*MELTT*) are plotted in Fig. 9(a) and (b), respectively.

6. Conclusions

The aim of this paper is to test the hypothesis that with appropriate structures, increasing complexity would increase the model efficiency either in runoff simulation or other internal variables. Five variants of the HBV model, i.e. a lumped model (LWhole), a semi-distributed model with elevation bands (SBand), a grid-model without routing (GRZero), a grid-model with hillslope routing (GROne), and a grid-model with both hillslope and channel routing (GRTwo) are compared in a cold and mountainous catchment in central southern Norway. The five models are compared according to runoff simulation either at the catchment outlet or interior points as well as internal variables, i.e. actual evapotranspiration, snow water equivalent and groundwater depth. The following conclusions are drawn from this study.

According to the Nash–Sutcliffe efficiency (*NSE*) and the inverse Nash–Sutcliffe efficiency (*InNSE*) of the outlet discharge, the rank of model efficiency in the descending order is GRTwo, GROne, GRZero, SBand and LWhole both in the calibration and validation mode. Applying the parameter values calibrated at the outlet to the six sub-catchments within the study area, GRTwo is still the best but with less superiority than in producing the outlet discharge. The *NSE* values increase with the areas of the sub-catchments.

Three internal variables are compared with observations measured at several sites and among models. The areal mean actual evapotranspiration simulations are very similar. Considerable differences exist among areal mean monthly SWE. The *R* values between the measurements by three snow pillows and grid-simulations show that GRZero is slightly better than GROne and GRTwo. Moreover, the three grid-models are comparable in simulations of groundwater levels; model performances are affected by the groundwater depth and elevation of ground piezometers.

It is worth noting that this study is performed only in one catchment. Robustness of the results needs to be tested by, for example, performing the study in other catchments and/or applying the models in non-stationary conditions. The latter can be done by calibrating and validating the models in different seasons or under different climate conditions. This kind of research will be done in the ongoing research.

Acknowledgements

This study is funded by the Research Council of Norway through the research project-JOINTINDNOR (project number 203867). The provision of the meteorological data by met.no, and the discharge and the spatial data by NVE are gratefully acknowledged. The authors are also grateful to the editor and the reviewers for their valuable comments and suggestions, which eventually lead to a substantial improvement of the paper.

Appendix A

see Table A1.

Table A1
Meanings of the parameters and the calibrated values. The *MannR* was only used in the Muskingum-Cunge channel routing method and calibrated for each land cover in calibration. Parameters are subscripted with *b* for the bog, *f* for the forest, *a* for the alpine, *r* for the rock, *h* for the heather, *o* for the open land, *g* for the glacier. The parameters of LWhole for the other land and soil were the same as those for the open land.

Group	Parameters	Meaning	Unit	LWhole	SBand	GRZero	GROne	GRTwo
Lake	*EPOT_L*	Potential evaporation capacity	m/day/°C	0.000001	0.000097	0.000010	0.000971	0.000980
	KLAKE	Rating curve constant	–	0.006224	0.035225	0.015674	0.031472	0.066361
	NLAKE	Rating curve exponent	–	0.560846	1.619736	1.025064	0.512362	0.164502
	MannR	Manning roughness coefficient	–	–	–	–	–	0.030000
Land	INT_MAX_o	Maximum interception storage	m/day	0.005017	0.009845	0.009943	0.002957	0.002488
	$EPOT_o$	Potential evaporation capacity	m/day/°C	0.000291	0.000334	0.000331	0.000196	0.000204
	$MELTT_o$	Melting temperature of snow	°C	−1.977322	−1.399138	−1.400558	1.517349	1.542897
	$SMELTR_o$	Temperature index of snow melting rate	m/day/°C	0.002267	0.002491	0.002488	0.003125	0.003190
	$MannR_o$	Manning roughness coefficient	–	–	–	–	–	0.050000
	INT_MAX_b	Maximum interception storage	m/day	–	0.000528	0.000282	0.007291	0.000733
	$EPOT_b$	Potential evaporation capacity	m/day/°C	–	0.000040	0.000036	0.000175	0.000105
	$MELTT_b$	Melting temperature of snow	°C	–	2.313019	2.300974	−1.470627	−1.890260
	$SMELTR_b$	Temperature index of snow melting rate	m/day/°C	–	0.008284	0.008275	0.008171	0.006826
	$MannR_b$	Manning roughness coefficient	–	–	–	–	–	0.040000
	INT_MAX_f	Maximum interception storage	m/day	–	0.009845	0.009943	0.002957	0.002488
	$EPOT_f$	Potential evaporation capacity	m/day/°C	–	0.000334	0.000331	0.000196	0.000204
	$MELTT_f$	Melting temperature of snow	°C	–	−1.399138	−1.400558	1.517349	1.542897
	$SMELTR_f$	Temperature index of snow melting rate	m/day/°C	–	0.002491	0.002488	0.003125	0.003190
	$MannR_f$	Manning roughness coefficient	–	–	–	–	–	0.010000

Table A1 (*continued*)

Group	Parameters	Meaning	Unit	LWhole	SBand	GRZero	GROne	GRTwo
	INT_MAX_a	Maximum interception storage	m/day	–	0.000600	0.000159	0.000108	0.000100
	$EPOT_a$	Potential evaporation capacity	m/day/°C	–	0.000267	0.000308	0.002000	0.001202
	$MELTT_a$	Melting temperature of snow	°C	–	−1.324652	−1.402145	−2.000000	−0.974982
	$SMELTR_a$	Temperature index of snow melting rate	m/day/°C	–	0.015644	0.014929	0.100000	0.100000
	$MannR_a$	Manning roughness coefficient	–	–	–	–	–	0.025000
	INT_MAX_h	Maximum interception storage	m/day	–	0.009845	0.009943	0.002957	0.002488
	$EPOT_h$	Potential evaporation capacity	m/day/°C	–	0.000334	0.000331	0.000196	0.000204
	$MELTT_h$	Melting temperature of snow	°C	–	−1.399138	−1.400558	1.517349	1.542897
	$SMELTR_h$	Temperature index of snow melting rate	m/day/°C	–	0.002491	0.002488	0.003125	0.003190
	$MannR_h$	Manning roughness coefficient	–	–	–	–	–	0.050000
	INT_MAX_r	Maximum interception storage	m/day	–	0.009845	0.009943	0.002957	0.002488
	$EPOT_r$	Potential evaporation capacity	m/day/°C	–	0.000334	0.000331	0.000196	0.000204
	$MELTT_r$	Melting temperature of snow	°C	–	−1.399138	−1.400558	1.517349	1.542897
	$SMELTR_r$	Temperature index of snow melting rate	m/day/°C	–	0.002491	0.002488	0.003125	0.003190
	$MannR_r$	Manning roughness coefficient	–	–	–	–	–	0.030000
	INT_MAX_g	Maximum interception storage	m/day	–	0.009845	0.009943	0.002957	0.002488
	$EPOT_g$	Potential evaporation capacity	m/day/°C	–	0.000334	0.000331	0.000196	0.000204
	$MELTT_g$	Melting temperature of snow	°C	–	−1.399138	−1.400558	1.517349	1.542897
	$SMELTR_g$	Temperature index of snow melting rate	m/day/°C	–	0.002491	0.002488	0.003125	0.003190
	$MannR_g$	Manning roughness coefficient	–	–	–	–	–	0.030000
Soil	FC_o	Field capacity	m	1.292544	0.854174	0.852845	0.149419	0.170029
	$BETA_o$	Shape coefficient of soil moisture	–	0.395717	0.632809	0.621915	10.000000	9.905496
	KUZ_o	Recession coefficient of the upper zone	1/day	0.133252	0.031759	0.000075	1.000000	1.000000
	$ALFA_o$	Non-linear drainage coefficient of the upper zone	–	0.976138	2.500000	2.374286	1.208677	1.217343
	$PERC_o$	Percolation from upper zone to the lower zone	–	0.012520	0.022951	0.023132	0.001013	0.001000
	KLZ_o	Recession coefficient of the lower zone	1/day	0.035208	0.089434	0.089466	0.020157	0.011136
	FC_b	Field capacity	m	–	0.195487	0.264188	1.300000	1.300000
	$BETA_b$	Shape coefficient of soil moisture	–	–	6.254378	8.313165	50.000000	50.000000
	KUZ_b	Recession coefficient of the upper zone	1/day	–	0.973313	0.998324	0.871973	0.770876
	$ALFA_b$	Non-linear drainage coefficient of the upper zone	–	–	1.784086	1.796010	1.979247	1.826975
	$PERC_b$	Percolation from upper zone to the lower zone	–	–	0.003896	0.004053	0.001000	0.001000
	KLZ_b	Recession coefficient of the lower zone	1/day	–	0.007228	0.006526	0.014653	0.026939
	FC_f	Field capacity	m	–	0.854174	0.852845	0.149419	0.170029
	$BETA_f$	Shape coefficient of soil moisture	–	–	0.632809	0.621915	10.000000	9.905496
	KUZ_f	Recession coefficient of the upper zone	1/day	–	0.005303	0.217543	1.000000	1.000000
	$ALFA_f$	Non-linear drainage coefficient of the upper zone	–	–	2.500000	2.374286	1.208677	1.217343
	$PERC_f$	Percolation from upper zone to the lower zone	–	–	0.022951	0.023132	0.001013	0.001000
	KLZ_f	Recession coefficient of the lower zone	1/day	–	0.089434	0.089466	0.020157	0.011136
	FC_a	Field capacity	m	–	0.444265	0.544096	0.050000	0.050000
	$BETA_a$	Shape coefficient of soil moisture	–	–	0.538706	0.568572	10.000000	10.000000
	KUZ_a	Recession coefficient of the upper zone	1/day	–	0.277815	0.322954	0.132547	0.018076
	$ALFA_a$	Non-linear drainage coefficient of the upper zone	–	–	2.500000	2.500000	2.477734	2.500000
	$PERC_a$	Percolation from upper zone to the lower zone	–	–	0.008084	0.007916	0.122702	0.084411
	KLZ_a	Recession coefficient of the lower zone	1/day	–	0.007617	0.008469	0.022254	0.013849
	FC_h	Field capacity	m	–	0.854174	0.852845	0.149419	0.170029
	$BETA_h$	Shape coefficient of soil moisture	–	–	0.632809	0.621915	10.000000	9.905496
	KUZ_h	Recession coefficient of the upper zone	1/day	–	1.000000	0.146038	1.000000	1.000000
	$ALFA_h$	Non-linear drainage coefficient of the upper zone	–	–	2.500000	2.374286	1.208677	1.217343
	$PERC_h$	Percolation from upper zone to the lower zone	–	–	0.022951	0.023132	0.001013	0.001000
	KLZ_h	Recession coefficient of the lower zone	1/day	–	0.089434	0.089466	0.020157	0.011136
	FC_r	Field capacity	m	–	0.854174	0.852845	0.149419	0.170029
	$BETA_r$	Shape coefficient of soil moisture	–	–	0.632809	0.621915	10.000000	9.905496
	KUZ_r	Recession coefficient of the upper zone	1/day	–	1.000000	0.312415	0.294833	1.000000
	$ALFA_r$	non linear drainage coefficient of the upper zone	–	–	2.500000	2.374286	1.208677	1.217343
	$PERC_r$	Percolation from upper zone to the lower zone	–	–	0.022951	0.023132	0.001013	0.001000
	KLZ_r	Recession coefficient of the lower zone	1/day	–	0.089434	0.089466	0.020157	0.011136
	FC_g	Field capacity	m	–	0.854174	0.852845	0.149419	0.170029
	$BETA_g$	Shape coefficient of soil moisture	–	–	0.632809	0.621915	10.000000	9.905496
	KUZ_g	Recession coefficient of the upper zone	1/day	–	0.466374	1.000000	0.014564	0.048685
	$ALFA_g$	Non-linear drainage coefficient of the upper zone	–	–	2.500000	2.374286	1.208677	1.217343
	$PERC_g$	Percolation from upper zone to the lower zone	–	–	0.022951	0.023132	0.001013	0.001000
	KLZ_g	Recession coefficient of the lower zone	1/day	–	0.089434	0.089466	0.020157	0.011136

References

Abebe, N.A., Ogden, F.L., Pradhan, N.R., 2010. Sensitivity and uncertainty analysis of the conceptual HBV rainfall–runoff model: implications for parameter estimation. J. Hydrol. 389, 301–310. http://dx.doi.org/10.1016/j.jhydrol.2010.06.007.

Alley, W.M., 1984. On the treatment of evapotranspiration, soil moisture accounting, and aquifer recharge in monthly water balance models. Water Resour. Res. 20, 1137–1149. http://dx.doi.org/10.1029/WR020i008p01137.

Atkinson, S., Sivapalan, M., Woods, R., Viney, N., 2003. Dominant physical controls on hourly flow predictions and the role of spatial variability: Mahurangi catchment, New Zealand. Adv. Water Resour. 26, 219–235. http://dx.doi.org/10.1016/S0309-1708(02)00183-5.

Beldring, S., 2002a. Multi-criteria validation of a precipitation runoff model. J. Hydrol. 257, 189–211. http://dx.doi.org/10.1016/S0022-1694(01)00541-8.

Beldring, S., 2002b. Runoff generating processes in boreal forest environments with glacial tills. Nord. Hydrol. 33, 347–372. http://dx.doi.org/10.2166/nh.2002.021.

Beldring, S., Engeland, K., Roald, L.A., Slthun, N.R., Voks, A., 2003. Estimation of parameters in a distributed precipitation-runoff model for Norway. Hydrol. Earth Syst. Sci. 7, 304–316. http://dx.doi.org/10.5194/hess-7-304-2003.

Bergström, S., 1976. Development and Application of a Conceptual Runoff Model for Scandinavian Catchments. Technical Report 07 Swedish Meteorological and Hydrological Institute. <http://books.google.no/books?id=vRyeQAAACAAJ>.

Bergström, S., Sandberg, G., 1983. Simulation of groundwater response by conceptual models. Nord. Hydrol. 14, 71–84. http://dx.doi.org/10.2166/nh.1983.007.

Bookhagen, B., Burbank, D.W., 2010. Toward a complete Himalayan hydrological budget: spatiotemporal distribution of snowmelt and rainfall and their impact on river discharge. J. Geophys. Res.: Earth Surf. 115, F03019. http://dx.doi.org/10.1029/2009JF001426.

Boyle, D.P., Gupta, H.V., Sorooshian, S., Koren, V., Zhang, Z., Smith, M., 2001. Toward improved streamflow forecasts: value of semidistributed modeling. Water Resour. Res. 37, 2749–2759. http://dx.doi.org/10.1029/2000WR000207.

Bruland, O., Frevåg, Å., Steinsland, I., Liston, G.E., Sand, K., 2015. Weather SDM – a model for estimating snow density with high precision using snow depth and local climate. Hydrol. Res. http://dx.doi.org/10.2166/nh.2015.059 (in press).

Butts, M.B., Payne, J.T., Kristensen, M., Madsen, H., 2004. An evaluation of the impact of model structure on hydrological modelling uncertainty for streamflow simulation. J. Hydrol. 298, 242–266. http://dx.doi.org/10.1016/j.jhydrol.2004.03.042.

Corbari, C., Mancini, M., Su, Z., Li, J., August 2014. Evapotranspiration estimate from water balance closure using satellite data for the Upper Yangtze River basin. Hydrol. Res. 45, 603–614. http://dx.doi.org/10.2166/nh.2013.016.

Coron, L., Andréassian, V., Perrin, C., Lerat, J., Vaze, J., Bourqui, M., Hendrickx, F., 2012. Crash testing hydrological models in contrasted climate conditions: an experiment on 216 Australian catchments. Water Resour. Res. 48, W05552. http://dx.doi.org/10.1029/2011WR011721.

Das, T., Bádossy, A., Zehe, E., He, Y., 2008. Comparison of conceptual model performance using different representations of spatial variability. J. Hydrol. 356, 106–118. http://dx.doi.org/10.1016/j.jhydrol.2008.04.008.

Doherty, J., 2005. PEST Model-Independent Parameter Estimation User Manual. Watermark Numerical Computing, fifth ed. <http://www.pesthomepage.org/Downloads.php>.

Doherty, J., Johnston, J.M., 2003. Methodologies for calibration and predective analysis of a watershed model 1. J. Am. Water Resour. Assoc. 39, 251–265. http://dx.doi.org/10.1111/j.1752-1688.2003.tb04381.x.

Duan, Q., Sorooshian, S., Gupta, V., 1992. Effective and efficient global optimization for conceptual rainfall–runoff models. Water Resour. Res. 28, 1015–1031. http://dx.doi.org/10.1029/91WR02985.

Ehret, U., Götzinger, J., Bárdossy, A., Pegram, G.G., 2008. Radar-based flood forecasting in small catchments, exemplified by the Goldersbach catchment, Germany. Int. J. River Basin Manage. 6, 323–329. http://dx.doi.org/10.1080/15715124.2008.9635359.

El Hai El Tahir, M., Wang, W., Xu, C.-Y., Zhang, Y., Singh, V., 2012. Comparison of methods for estimation of regional actual evapotranspiration in data scarce regions: Blue Nile Region, Eastern Sudan. J. Hydrol. Eng. 17, 578–589. http://dx.doi.org/10.1061/(ASCE)HE.1943-5584.0000429.

Engelhardt, M., Schuler, T.V., Anderson, L.M., 2012. Evaluation of gridded precipitation for Norway using glacier mass-balance measurements. Geografiska Ann.: Ser. A, Phys. Geogr. 94, 501–509. http://dx.doi.org/10.1111/j.1468-0459.2012.00473.x.

Engelhardt, M., Schuler, T.V., Andreassen, L.M., 2013. Glacier mass balance of Norway 1961–2010 calculated by a temperature-index model. Ann. Glaciol. 54, 32–40. http://dx.doi.org/10.3189/2013AoG63A245.

EROS, 1996. Hydro1k Elevation Derivative Database. <http:s://lta.cr.usgs.gov/HYDRO1K>.

Fekete, B.M., Vörösmarty, C.J., Lammers, R.B., 2001. Scaling gridded river networks for macroscale hydrology: development, analysis, and control of error. Water Resour. Res. 37, 1955–1967. http://dx.doi.org/10.1029/2001WR900024.

Fleig, A.K., 2013. Norwegian Hydrological Reference Dataset for Climate Change Studies. Technical Report 02 Norwegian Water Resources and Energy Directorate. <http://webby.nve.no/publikasjoner/rapport/2013/rapport201302.pdf>.

Gao, G., Xu, C.-Y., Chen, D., Singh, V., 2012. Spatial and temporal characteristics of actual evapotranspiration over Haihe River basin in China. Stoch. Environ. Res. Risk Assess. 26, 655–669. http://dx.doi.org/10.1007/s00477-011-0525-1.

Gisnås, K., Etzelmüller, B., Farbrot, H., Schuler, T.V., Westermann, S., 2013. CryoGRID 1.0: Permafrost distribution in Norway estimated by a spatial numerical model. Permafrost Periglac. Process. 24, 2–19. http://dx.doi.org/10.1002/ppp.1765.

Gong, L., Widén-Nilsson, E., Halldin, S., Xu, C.-Y., 2009. Large-scale runoff routing with an aggregated network-response function. J. Hydrol. 368, 237–250. http://dx.doi.org/10.1016/j.jhydrol.2009.02.007.

Hailegeorgis, T.T., Alfredsen, K., 2015. Comparative evaluation of performances of different conceptualisations of distributed HBV runoff response routines for prediction of hourly streamflow in boreal mountainous catchments. Hydrol. Res. http://dx.doi.org/10.2166/nh.2014.051 (in press).

Han, J., Huang, G., Zhang, H., Li, Z., Li, Y., 2014. Effects of watershed subdivision level on semi-distributed hydrological simulations: case study of the SLURP model applied to the Xiangxi River watershed, China. Hydrol. Sci. J. 59, 108–125. http://dx.doi.org/10.1080/02626667.2013.854368.

Harlin, J., Kung, C., 1992. Parameter uncertainty and simulation of design floods in Sweden. J. Hydrol. 137, 209–230. http://dx.doi.org/10.1016/0022-1694(92)90057-3.

Jiang, T., Chen, Y.D., Xu, C.-Y., Chen, X., Chen, X., Singh, V., 2007. Comparison of hydrological impacts of climate change simulated by six hydrological models in the Dongjiang Basin, South China. J. Hydrol. 336, 316–333. http://dx.doi.org/10.1016/j.jhydrol.2007.01.010.

Krysanova, V., Bronstert, A., Müller-Wohlfeil, D.-I., 1999. Modelling river discharge for large drainage basins: from lumped to distributed approach. Hydrol. Sci. J. 44, 313–331. http://dx.doi.org/10.1080/02626669909492224.

L'Abée-Lund, J., Eie, J., Faugli, P., Haugland, S., Hvidsten, N., Jensen, A., Melvold, K., Pettersen, V., Saltveit, S., 2009. Rivers of Europe. Rivers in Boreal Uplands. Academic Press, pp. 577–606. <http://www.sciencedirect.com/science/book/9780123694492> (chapter).

Lawrence, D., Haddeland, I., Langsholt, E., 2009. Calibration of HBV Hydrological Models Using PEST Parameter Estimation. Technical Report 01 Norwegian Water Resources and Energy Directorate. <http://www.nve.no/Global/Publikasjoner/Publikasjoner>.

Li, H., Beldring, S., Xu, C.-Y., 2014. Implementation and testing of routing algorithms in the distributed Hydrologiska Byråns Vattenbalansavdelning model for mountainous catchments. Hydrol. Res. 45, 322–333. http://dx.doi.org/10.2166/nh.2013.009.

Lindström, G., Johansson, B., Persson, M., Gardelin, M., Bergström, S., 1997. Development and test of the distributed HBV-96 hydrological model. J. Hydrol. 201, 272–288. http://dx.doi.org/10.1016/S0022-1694(97)00041-3.

Mayr, E., Hagg, W., Mayer, C., Braun, L., 2013. Calibrating a spatially distributed conceptual hydrological model using runoff, annual mass balance and winter mass balance. J. Hydrol. 478, 40–49. http://dx.doi.org/10.1016/j.jhydrol.2012.11.035.

Michaud, J., Sorooshian, S., 1994. Comparison of simple versus complex distributed runoff models on a midsized semiarid watershed. Water Resour. Res. 30, 593–605. http://dx.doi.org/10.1029/93WR03218.

Mohr, M., 2008. New Routines for Gridding of Temperature and Precipitation Observations for seNorge. no. Technical Report 08 Norwegian Meteorological Institute. <http://met.no/Forskning/Publikasjoner/Publikasjoner2008/filestore/NewRoutinesforGriddingofTemperature.pdf>.

Montanari, A., Baldassarre, G.D., 2013. Data errors and hydrological modelling: the role of model structure to propagate observation uncertainty. Adv. Water Resour. 51, 498–504. http://dx.doi.org/10.1016/j.advwatres.2012.09.007.

Nash, J., Sutcliffe, J., 1970. River flow forecasting through conceptual models part I-A discussion of principles. J. Hydrol. 10, 282–290. http://dx.doi.org/10.1016/0022-1694(70)90255-6.

NVE. The National River Network Database (ELVIS). <http://www.nve.no/en/Water/NVEs-geographic-databases/The-National-River-Network-Database-ELVIS/> (accessed in 02.15).

O'Callaghan, J.F., Mark, D.M., 1984. The extraction of drainage networks from digital elevation data. Comput. Vis., Graph., Image Process. 28, 323–344. http://dx.doi.org/10.1016/S0734-189X(84)80011-0.

Perrin, C., Michel, C., Andréassian, V., 2001. Does a large number of parameters enhance model performance? Comparative assessment of common catchment model structures on 429 catchments. J. Hydrol. 242, 275–301. http://dx.doi.org/10.1016/S0022-1694(00)00393-0.

Petersen-verleir, A., Soot, A., Reitan, T., 2009. Bayesian rating curve inference as a streamflow data quality assessment tool. Water Resour. Manage 23, 1835–1842. http://dx.doi.org/10.1007/s11269-008-9354-5.

Praskievicz, S., Chang, H., 2009. A review of hydrological modelling of basin-scale climate change and urban development impacts. Prog. Phys. Geogr. 33, 650–671. http://dx.doi.org/10.1177/0309133309348098.

Pushpalatha, R., Perrin, C., Moine, N.L., Andréassian, V., 2012. A review of efficiency criteria suitable for evaluating low-flow simulations. J. Hydrol. 420–421, 171–182. http://dx.doi.org/10.1016/j.jhydrol.2011.11.055.

Reed, S., Koren, V., Smith, M., Zhang, Z., Moreda, F., Seo, D.-J., Participants, D., 2004. Overall distributed model intercomparison project results. J. Hydrol. 298, 27–60. http://dx.doi.org/10.1016/j.jhydrol.2004.03.031.

Slthun, N.R. 1996. The Nordic HBV model. Technical Report 07 Norwegian Water Resources and Energy Directorate. <http://folk.uio.no/nilsroar/gf247/hbvmod.pdf>.

Seibert, J., 1997. Estimation of parameter uncertainty in the HBV model. Nord. Hydrol. 28, 247–262. http://dx.doi.org/10.2166/nh.1997.015.

Seibert, J., 1999. Regionalisation of parameters for a conceptual rainfall–runoff model. Agric. For. Meteorol. 98–99, 279–293. http://dx.doi.org/10.1016/S0168-1923(99)00105-7.

Singh, V., Woolhiser, D., 2002. Mathematical modeling of watershed hydrology. J. Hydrol. Eng. 7, 270–292. http://dx.doi.org/10.1061/(ASCE)1084-0699(2002)7:4(270).

Skahill, B.E., Doherty, J., 2006. Efficient accommodation of local minima in watershed model calibration. J. Hydrol. 329, 122–139. http://dx.doi.org/10.1016/j.jhydrol.2006.02.005.

Smith, M.B., Seo, D.-J., Koren, V.I., Reed, S.M., Zhang, Z., Duan, Q., Moreda, F., Cong, S., 2004. The distributed model intercomparison project (DMIP): motivation and experiment design. J. Hydrol. 298, 4–26. http://dx.doi.org/10.1016/j.jhydrol.2004.03.040.

Sorteberg, H., Engeset, R., Udnas, H., 2001. A national network for snow monitoring in Norway: snow pillow verification using observations and models. Phys. Chem. Earth, Part C: Solar, Terrestr. Planet. Sci. 26, 723–729. http://dx.doi.org/10.1016/S1464-1917(01)95016-0.

Strahler, A.N., 1957. Quantitative analysis of watershed geomorphology. Trans., Am. Geophys. Union 38, 913–920. http://dx.doi.org/10.1029/TR038i006p00913.

Tang, Y., Reed, P., Wagener, T., van Werkhoven, K., 2007. Comparing sensitivity analysis methods to advance lumped watershed model identification and evaluation. Hydrol. Earth Syst. Sci. 11, 793–817. http://dx.doi.org/10.5194/hess-11-793-2007.

Todini, E., 2007. A mass conservative and water storage consistent variable parameter Muskingum-Cunge approach. Hydrol. Earth Syst. Sci. 11, 1645–1659. http://dx.doi.org/10.5194/hess-11-1645-2007.

Uhlenbrook, S., Seibert, J., Leibundgut, C., Rodhe, A., 1999. Prediction uncertainty of conceptual rainfall–runoff models caused by problems in identifying model parameters and structure. Hydrol. Sci. J. 44, 779–797. http://dx.doi.org/10.1080/02626669909492273.

Vaché, K.B., McDonnell, J.J., 2006. A process-based rejectionist framework for evaluating catchment runoff model structure. Water Resour. Res. 42, W02409. http://dx.doi.org/10.1029/2005WR004247.

Varado, N., Braud, I., Galle, S., Le Lay, M., Seguis, L., Kamagate, B., Depraetere, C., 2006. Multi-criteria assessment of the Representative Elementary Watershed approach on the Donga catchment (Benin) using a downward approach of model complexity. Hydrol. Earth Syst. Sci. 10, 427–442. http://dx.doi.org/10.5194/hess-10-427-2006.

Vormoor, K., Skaugen, T., 2013. Temporal disaggregation of daily temperature and precipitation grid data for Norway. J. Hydrometeorol. 14, 989–999. http://dx.doi.org/10.1175/JHM-D-12-0139.1.

Wagener, T., Boyle, D.P., Lees, M.J., Wheater, H.S., Gupta, H.V., Sorooshian, S., 2001. A framework for development and application of hydrological models. Hydrol. Earth Syst. Sci. 5, 13–26. http://dx.doi.org/10.5194/hess-5-13-2001.

Wrede, S., Seibert, J., Uhlenbrook, S., 2013. Distributed conceptual modelling in a Swedish lowland catchment: a multi-criteria model assessment. Hydrol. Res. 44, 318–333. http://dx.doi.org/10.2166/nh.2012.056.

Xu, C.-Y., Chen, D., 2005. Comparison of seven models for estimation of evapotranspiration and groundwater recharge using lysimeter measurement data in Germany. Hydrol. Process. 19, 3717–3734. http://dx.doi.org/10.1002/hyp.5853.

Xu, C.-Y., Singh, V., 2005. Evaluation of three complementary relationship evapotranspiration models by water balance approach to estimate actual regional evapotranspiration in different climatic regions. J. Hydrol. 308, 105–121. http://dx.doi.org/10.1016/j.jhydrol.2004.10.024.

Xu, C.-Y., Widén, E., Halldin, S., 2005. Modelling hydrological consequences of climate change–progress and challenges. Adv. Atmos. Sci. 22, 789–797. http://dx.doi.org/10.1007/BF02918679.

Yan, C., Zhang, W., 2014. Effects of model segmentation approach on the performance and parameters of the Hydrological Simulation Program Fortran (HSPF) models. Hydrol. Res. 45, 893–907. http://dx.doi.org/10.2166/nh.2014.182.

Yang, X., Ren, L., Singh, V., Liu, X., Yuan, F., Jiang, S., Yong, B., 2012. Impacts of land use and land cover changes on evapotranspiration and runoff at Shalamulun River watershed, China. Hydrol. Res. 43, 23–37. http://dx.doi.org/10.2166/nh.2011.120.

3 Article III

– **Li, H.**, Beldring, S., Xu, C.-Y., Huss, M., Melvold, K., Jain, S. (2015): Integrating a glacier retreat model into a hydrological model—case studies on three glacierised catchments in Norway and Himalayan region—*Journal of Hydrology*, **527**: 656–667, doi:10.1016/j.jhydrol.2015.05.017.

Journal of Hydrology 527 (2015) 656–667

Contents lists available at ScienceDirect

Journal of Hydrology

journal homepage: www.elsevier.com/locate/jhydrol

Integrating a glacier retreat model into a hydrological model – Case studies of three glacierised catchments in Norway and Himalayan region

Hong Li [a], Stein Beldring [b], C.-Y. Xu [a,*], Matthias Huss [c,d], Kjetil Melvold [b], Sharad K. Jain [e]

[a] Department of Geosciences, University of Oslo, Norway
[b] Norwegian Water Resources and Energy Directorate, Norway
[c] Department of Geosciences, University of Fribourg, Switzerland
[d] Laboratory of Hydraulics, Hydrology and Glaciology, ETH Zurich, Switzerland
[e] National Institute of Hydrology, Roorkee, India

ARTICLE INFO

Article history:
Received 16 December 2014
Received in revised form 8 May 2015
Accepted 10 May 2015
Available online 19 May 2015
This manuscript was handled by Konstantine P. Georgakakos, Editor-in-Chief, with the assistance of Daqing Yang, Associate Editor

Keywords:
Himalaya
Glaciers
Glacier retreat model
HBV
Norway

SUMMARY

Glaciers are crucial in many countries where meltwater from glaciers is an important source of water for drinking water supply, irrigation, hydropower generation and the ecological system. Glaciers are also important indicators of climate change. They have been significantly altered due to the global warming and have subsequently affected the regional hydrological regime. However, few models are able to parameterise the dynamics of the glacier system and consequent runoff processes in glacier fed basins with desirable performance measures. To narrow this gap, we have developed an integrated approach by coupling a hydrological model (HBV) and a glacier retreat model (Δh-parameterisation) and tested this approach in three basins with different glacier coverage and subject to different climate and hydrologic regimes. Results show that the coupled model is able to give satisfactory estimations of runoff and glacier mass balance in the Nigardsbreen basin where the measured data are available to verify the results. In addition, the model can provide maps of snowpack distribution and estimate runoff components from glaciers.

1. Introduction

Glaciers are essential in the water system. They store about 75% of the fresh water on the earth. Approximately 99.5% of the ice volume store in ice sheets and the remaining 0.5% in mountain glaciers (Khadka et al., 2014). Although the mountain glaciers are relatively small, they are critically important to the humanity (Beniston, 2003; Arora et al., 2014). Firstly, mountain glaciers are relevant to humankind because of their proximity to populated areas (Singh et al., 2006). During 14th to 19th century, a period known as the Little Ice Age, advancing glaciers periodically extended down into valleys and destroyed communities, crops, and livelihoods (Carey, 2007). Glacier recession also induces a series of natural hazards (Carey, 2005). Secondly, mountain glaciers indeed substantially contribute to the development of society and economy (Beniston, 2003). For example, glaciers only cover approximately 1% area of mainland Norway. However, 15% of its electricity is generated by runoff from these glacierised basins (Andreassen et al., 2005). Thirdly, glacier meltwater is an important water resource (Burlando et al., 2002) and a supplement to streamflow under drought conditions (Marshall, 2014).

Furthermore, glaciers are considered as one of the most sensitive indicators of climate change (Burlando et al., 2002). That is because runoff from a glacierised basin is more dependent on the available energy than from a non-glacierised basin. Therefore, a modification of the prevalent climate, particularly of air temperature, can considerably affect the hydrologic regime (Burlando et al., 2002; Radić and Hock, 2014).

Glacier responses to climate change are of concern for both scientific research and public communities (Hagg et al., 2007; Barnett et al., 2005). In many regions of the earth, glaciers are retreating and seasonal snowfalls are diminishing as shown by observations and modelling (Bolch et al., 2012; Barnett et al., 2005). Zemp et al. (2008) reported that the global average annual mass was −0.58 m water equivalent (w.e.) year^{-1} for the decade 1996–2005. Assuming a minor change in precipitation, ice- and

* Corresponding author.
E-mail address: c.y.xu@geo.uio.no (C.-Y. Xu).

http://dx.doi.org/10.1016/j.jhydrol.2015.05.017
0022-1694/

snow-covered areas are predicted to decrease at accelerating rates due to increased melting of snowpack and ice as well as due to reduced accumulation of snow and decreased surface albedo (Radić and Hock, 2014). The expected climate change and its serious implications demand interdisciplinary research on different topics including glaciers.

The response of glaciers to global warming is generally stated as: due to the release of water from glacial storage, runoff initially increases especially during late spring and summer, and after complete removal of the glacier ice, runoff stabilizes and drops below the previous level (Huss et al., 2008). Theoretically, the total amount of runoff cannot be changed by the disappearance of glaciers compared to stable glacier conditions. However, changes in seasonal distribution of runoff have significant impacts on water availability, ecosystems and human well-being (Jain et al., 2011).

The inhomogeneity among mountain glaciers, however, makes this generalisation not applicable for all glaciers (Jain et al., 2011). This inhomogeneity is significant among different climate regimes, even among the glaciers in a close neighbourhood (Horton et al., 2006). The rate of glacier retreat depends on both large-scale and time-invariant factors, and small-scale and time-dependent factors (Burlando et al., 2002; Khadka et al., 2014). Geographical, topographical and climatic conditions act at large scales and relatively stable, whereas the size, location of glaciers and study period of research are at a small spatial scale and time dependent (Bolch, 2007; Marshall, 2014).

The processes of melt water from glaciers draining to the catchment outlet are very complex. Glaciologists and hydrologists have made many efforts to describe and model them by employing glaciological methods and hydrological methods or by integrated knowledge. The methods used can be categorised into three types: glaciological, hydrological and interdisciplinary approaches.

From a glaciological point of view, it is essential to simulate response of glaciers to climate change and contribution to streamflow by glacier wastage. This approach mainly uses models to relate meteorological measurements to accumulation and ablation rates on the glacier surface. These mass balance models vary in complexity, including conceptual models and or more complicated models based on the energy balance (Gottlieb, 1980; Arnold et al., 1996; Klok and Oerlemans, 2002; Hock, 2005) and models for ice dynamics (Greuell, 1992; Hubbard et al., 1998; Jouvet et al., 2009). They have been validated by in-situ glacier measurements, such as surface mass balance or ice thickness change. Then glacier mass loss can be compared with discharge downstream of the glacier (Kotlarski et al., 2010). However, glacier melt water is only a raw volume input into the hydrological system, similar to rainfall. The discharge is further modified by, e.g. evaporation and groundwater storage. Therefore, the direct comparison leads to an overestimation of glacier contribution to discharge (Kaser et al., 2010), unless contributions from non-glacierised areas are also considered.

Many diverse approaches have been used in developing hydrological models for a better representation of snow processes and ice melting (Bergström, 1976; Shrestha et al., 2012; Wrede et al., 2013). The models mainly use the meteorological data, satellite data of snow cover and climate scenarios to study effects of climate change on glaciers (Khadka et al., 2014; Jasper et al., 2004). Among the models, the Snowmelt Runoff Model (SRM) (Khadka et al., 2014; Immerzeel et al., 2009) and the HBV model (Mayr et al., 2013; Hagg et al., 2006; Akhtar et al., 2008) are widely used. However, these studies did not take into account the change in the glacier area to the imposed climatic changes. Although these studies provide valuable insights into the possible range of the future options, they suffer from a large uncertainty about the plausibility of the future evolution of glaciers (Immerzeel et al., 2012). This limits the time scale over which the results could apply. Several studies using the HBV model considered the retreat of glaciers (Hagg et al., 2006; Akhtar et al., 2008) but, since the change of glacier extent were arbitrarily assigned, they can be considered as rather simple and non-dynamic experiments not allowing to account for the transient evolution.

The coupled models with both descriptions of glacier and hydrology are quite new. Several of such models have been reported to link glacier dynamics and hydrological processes. Horton et al. (2006) studied the climate change impacts on the runoff regimes in the Swiss Alps by a conceptual reservoir-based hydrological model. The glacier extent was updated by a conceptual model based on the accumulation area ratio (AAR) method, which assumes that the accumulation area of a glacier occupies a fixed proportion of the total glacier area. However, the AAR method is not able to reproduce the transient response of glaciers to a changing climate as it assumes the glacier to be permanently in steady-state (Huss et al., 2008). Huss et al. (2008) ran a distributed model to simulate the daily surface mass balance on three highly glacierised catchments in Switzerland. The model included the water balance calculation and a parameterisation of glacier retreat. The model was validated with monthly runoff and decadal ice volume change. Stahl et al. (2008) proposed and applied a methodology for estimating changes in streamflow associated with the coupled effects of climatic change and associated glacier response, with a specific focus on transient responses. The authors combined the HBV model with a model of the glacier area evolution based on volume-area scaling. However, as shown by Lüthi (2009) and Radić and Hock (2014), volume-area scaling cannot describe a critical time lag between the area and the volume response to the prevailing climate. Immerzeel et al. (2012) suggested a combined approach consisting of a simple precipitation-runoff model and an ice dynamics model including basal sliding for a glacierised Himalayan catchment in Nepal. The model was first calibrated using the recent location of the glacier terminus and then by using discharge observations. Naz et al. (2014) published a physically-based, spatially distributed hydrological model coupled to a shallow ice dynamics model. A common drawback of the currently available physically-based models is a high demand of input data and computational power, which hampers their applicability to large-scale catchments.

This paper aims at presenting a coupled model for hydrology and glacier retreat suitable for large catchments with low data demand. The combined model explicitly simulates glacier evolution and major hydrological processes at a high spatial resolution.

2. Methodology

The general framework is to couple a distributed HBV model with a mass-conserving glacier retreat model. The HBV model calculates the accumulation and ablation of snow and glacier ice for every grid at a daily time step and the glacier retreat model describes glacier surface elevation changes and updates glacier area in response to the total amount of glacier mass change calculated by the HBV model.

2.1. Hydrological model

The HBV model concept was initially developed for runoff simulation in the Scandinavian countries in the 1970s (Bergström, 1976). So far, the HBV model has been applied in more than 80 countries and is used as a standard tool for flood forecasting and for simulating inflow to hydropower reservoirs in Norway as well as many other European areas. The scientific basis and applicability of the model have been verified at many sites in Europe (Uhlenbrook et al., 1999; Götzinger and Bárdossy, 2005;

Hailegeorgis and Alfredsen, in press) and Asia (Akhtar et al., 2008; Li et al., 2014b). The algorithms have been described in details (e.g., Bergström, 1976; Lindström et al., 1997; Beldring et al., 2003); therefore, we present here only the equations of special significance to our research.

The model version used in this study was first published by Beldring et al. (2003). It is a distributed model considering the spatial distribution of meteorological data at a daily time step. The main inputs are precipitation, temperature and surface elevation. The station precipitation is firstly corrected for under catch (Eq. (1)). Then the corrected precipitation and air temperature series are interpolated for every grid using the inverse distance weighting (IDW) method considering elevation effects (Eq. (2)). Finally water balance is computed by the HBV algorithms for every grid.

$$P_c = \begin{cases} K_r \cdot P_o & \text{if rainfall} \\ K_s \cdot K_r \cdot P_o & \text{if snowfall} \end{cases} \quad (1)$$

where P_c is corrected precipitation (mm day^{-1}) and P_o is precipitation measured at the weather station (mm day^{-1}). K_r and K_s are free parameters respectively for rainfall and snowfall correction.

$$P_g = \sum_{i=1}^{n} W_i \cdot P_i \cdot \gamma_p^{(H_g - H_i)/100}$$
$$T_g = \sum_{i=1}^{n} W_i \cdot \left(T_i + \gamma_t \times \frac{H_g - H_i}{100} \right) \quad (2)$$

where P_g and T_g are precipitation (mm day^{-1}) and temperature (°C) at each grid. W_i is the weight of station i calculated by the IDW method. H_g and H_i are the elevations in meters above mean sea level (m amsl) of grid and station i. n is the number of stations used for interpolation. γ_t (°C per 100 m) and γ_p are free parameters that describe elevation effects on temperature and precipitation, respectively.

Snow accumulates when the air temperature is below the threshold temperature of snow accumulation (T_{acc},°C) and there is precipitation. Snow melting is calculated by a degree-day method based on temperature according to Eq. (3) (Lindström et al., 1997). Glacier melting starts when there is no snow coverage and the air temperature is higher than the melting threshold temperature (T_t). The melting rate of ice ($Melt_{ice}$) is based on the same method, but another melting factor (MF_{ice}) as shown in Eq. (4). At the end of melting season (i.e. 31st August) existing snow on the glacier is transformed into ice, and then the glacier gains mass.

$$Melt_{snow} = MF_{snow} \cdot (T - T_t) \quad T > T_t \quad (3)$$

$$Melt_{ice} = MF_{ice} \cdot (T - T_t) \quad T > T_t \quad (4)$$

where T is air temperature (°C) and T_t is the threshold temperature of snow melting; $Melt_{snow}$ and $Melt_{ice}$ are melting rate of snow and glacier (m day^{-1}) obtained with the degree-day factors MF_{snow} and MF_{ice}, respectively (both in m day^{-1} °C^{-1}).

2.2. Glacier retreat model

The Δh-parameterisation for modelling the changes in surface elevation and extent for retreating glaciers owes its origin to varying thinning rates over a glacier (Huss et al., 2010). For a certain mass change, surface elevation changes are smallest in the accumulation area and the largest near the terminus of mountain glaciers. This has been confirmed by measurements (Arendt et al., 2002; Bauder et al., 2007) and numerical modelling (Jóhannesson et al., 1989). The Δh-parameterisation describes the surface elevation changes as a function of elevation and the ice volume change, as Eq. (5).

$$h_r = \frac{h_{max} - h}{h_{max} - h_{min}}$$
$$\Delta h = (h_r + a)^\gamma + b \cdot (h_r + a) + c \quad (5)$$

where h is the glacier surface elevation (m amsl); h_{max} and h_{min} are the maximum and minimum elevations (both in m amsl); h_r is the normalised elevation; Δh is the normalised surface elevation change. γ, a, b and c are parameters and their values can be derived from glacier surface maps of different years, or calibration (Huss et al., 2010).

Integration of the dimensionless Δh function (Eq. (5)) over the entire glacier, taking into account the area distribution and the ice density ρ_{ice} (900 kg m^{-3}) must equal the total glacier mass change B_a (kg) calculated by the HBV model in a given time interval:

$$B_a = f_s \cdot \rho_{ice} \cdot \sum_{i=1}^{n} A_i \cdot \Delta h_i \quad (6)$$

where Δh_i is the normalised elevation change of grid i; A_i is its area (m^2); n is the number of glacier grids. Further, f_s is a factor that scales the magnitude of the dimensionless ice thickness change. It is chosen for each time interval such that Eq. (6) is satisfied. Then the glacier surface is changed as:

$$h_1 = h_0 + f_s \cdot \Delta h_i \quad (7)$$

where h_0 is the elevation (m amsl) in the previous time step and h_1 is the updated elevation (m amsl). In the last step, the change in glacier extent is determined by the updated glacier surface elevation. The glacier disappears for grids where the thickness is not greater than zero.

The required inputs are the initial ice thickness and surface elevation. The algorithm runs for individual glaciers, but all glaciers in a basin share the same values of the parameters. In this research, the glacier flow sheds are constructed from the surface elevation according to the D8 (deterministic eight-node) algorithms (O'Callaghan and Mark, 1984) and the grids having the same terminus point belong to one glacier. Glacier area has a slower climate response than runoff (Lüthi, 2009). Therefore, glacier extent is updated at a yearly scale, at the end of every melting season, i.e. 31st August.

The Δh-parameterisation avoids high demand of field data and computation resources such as an ice dynamics model (Jouvet et al., 2009) and can provide similar estimates as a 3D finite element ice flow model as shown by Huss et al. (2010).

2.3. Calibration and criteria

The combined model is calibrated by a model independent calibration package (PEST). PEST is available for free download (Doherty, 2005) and has been widely used in environmental and hydrological modelling (Doherty and Johnston, 2003; Immerzeel et al., 2012; Li et al., 2014a). The objective function is to obtain the minimum of a weighted least square sum of the discrepancies between simulated and observed series, i.e. daily discharge (m^3 s^{-1}) and if available, glacier annual mass balance (m year^{-1}) where the weight of an annual mass balance value is assumed 10,000 times of a discharge value. When glacier data are not available, the sum of the discharge series is additionally used to control the volume error.

The criteria used for evaluating precision of streamflow simulation are the Nash–Sutcliffe efficiency (NSE) (Nash and Sutcliffe, 1970) and relative mean error (RME), while the Pearson correlation coefficient (COR) is used to evaluate mass balance simulation. The criteria are shown by Eq. (8).

$$NSE = 1 - \frac{\sum_{i=1}^{n}(O_i - S_i)^2}{\sum_{i=1}^{n}(O_i - \overline{O})^2}$$
$$RME = \frac{\sum_{i=1}^{n}(S_i - O_i)}{\sum_{i=1}^{n}O_i} \times 100 \quad (8)$$
$$COR = \frac{\sum_{i=1}^{n}(O_i - \overline{O})(S_i - \overline{S})}{\sqrt{\sum_{i=1}^{n}(O_i - \overline{O})^2}\sqrt{\sum_{i=1}^{n}(S_i - \overline{S})^2}}$$

where O_i is the observed series; S_i is the simulated series; n is the length of series; $\overline{O}$ and $\overline{S}$ are the mean values of observed series and simulated series.

3. Study sites and data

Data of three basins are used to test the coupled model: (1) the Nigardsbreen basin in Norway (Fig. 1), (2) the Chamkhar Chhu basin in Bhutan (Fig. 2) and (3) the Beas basin in India (Fig. 2). The area of the basins ranges from 65 to 3201 km^2 and the glacier-covered fractions are between 15% and 73% (Table 1). Hydrographs of all basins show a similar discharge pattern characterised by a peak occurring between May and August (Fig. 3).

3.1. Nigardsbreen basin

The Nigardsbreen basin is a glacierised watershed in the high mountains in western Norway (Fig. 1). It has a small area of 65 km^2, but with a large range of elevation. The highest point is 1957 m amsl and the lowest in only 285 m amsl. The climate is humid, as it is influenced by the moist currents from the ocean. In addition, the climate is locally modified by the presence of the glacier. The mean annual air temperature is −0.47 °C and the mean precipitation reaches 3736 mm year^{-1}, with a large amount falling in winter as snow (Andreassen et al., 2005). Streamflow is largely determined by melting of snow and ice in the warm period of the year.

Nigardsbreen is one of the largest outlet glaciers from Jostedalsbreen (the largest ice cap in mainland Europe). The glacier is exposed towards the southeast and extends from approximately 315 to 1957 m amsl. Approximately 73% of the basin area is covered by ice (Andreassen et al., 2012). Nigardsbreen is well-known in the scientific community as it is one of the most studied alpine glaciers in Northern Europe (Oerlemans, 1986, 1997, 2007; Engelhardt et al., 2012).

The climate data are spatially interpolated maps of precipitation and temperature produced by the Norwegian Meteorological Institute (met.no) using 24-h mean temperature and accumulated precipitation measured at meteorological stations (NVE, 2015). These datasets are in a grid format at 1 km resolution and have been evaluated and used in many studies covering mainland Norway, such as hydrological modelling (Beldring et al., 2003; Li et al., 2014a), glacier mass balance estimation (Engelhardt et al., 2012, 2013), permafrost evolution (Gisnæas et al., 2013) and snow depth estimation (Vormoor and Skaugen, 2013). The areal mean value of the Nigardsbreen basin is assigned to a virtual station located at the middle of the basin.

The daily discharge is obtained from the national hydrological database, which is collected and managed by NVE. The series are transformed from the in-situ measured water depth by the Bayesian Rating Curve Fitting method (Petersen-Øverleir et al., 2009) and its quality is ensured by the NVE hydrological quality control system. The mass changes of the glacier are derived from the direct glaciological method or stakes-and-pits method, which is traditionally used by glaciologists to measure glacier mass balance (Østrem and Brugman, 1991; Hagg et al., 2004). Stakes are used to measure the changes in thickness and pits are selected sites for measuring the density at different depth. The measurements are interpolated over the glacier to obtain the total amount of glacier mass change. According to the experience of NVE, the measurements are suspected to be subject to a slight positive bias for the Norwegian coastal glaciers and the reason is not clear yet (Andreassen et al., 2011). However, no better dataset is available at present. The mass balance data have been extensively used for glacier modelling purposes (Oerlemans, 1986, 1997, 2007; Engelhardt et al., 2012).

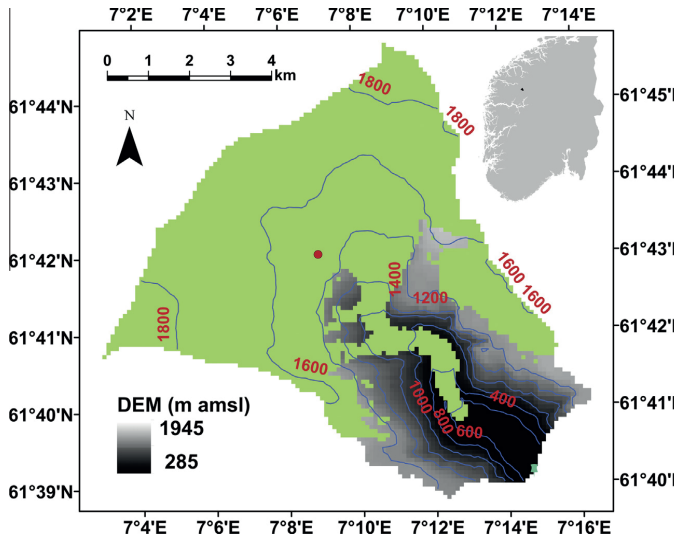

Fig. 1. Location and digital surface elevation models (DEM) of the Nigardsbreen basin at the Nigardsbreen station. The light green indicates glacier covered area. The contours are elevations (m amsl). The red dot denotes the location of the virtual meteorological station and the cyan pin marks the location of the discharge gauging station. (For interpretation of the references to colour in this figure legend, the reader is referred to the web version of this article.)

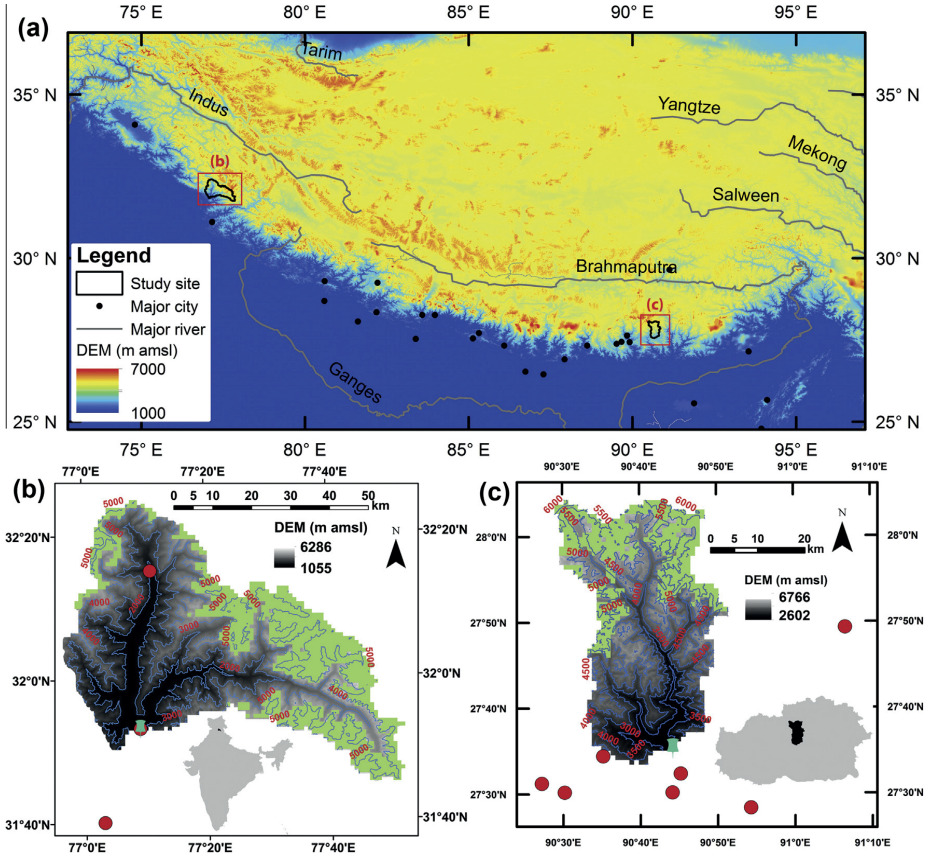

Fig. 2. Maps of the Chamkhar Chhu and Beas basins. (a) Map of the Himalaya showing the orography, major rivers and major cities and the locations of the study sites (Joshi, 2007, 2008, 2011). (b) The Beas basin at the Bhuntar gauging station. (c) The Chamkhar Chhu basin at the Kurjey gauging station. The range of DEM in (a) is assigned to give a better presentation rather than the minimum and maximum for the displaying area. Other signs are same as in Fig. 1.

Table 1
A short summary of the basins. Note: A is area of the basin in km^2. ME is median elevation in m amsl. GF is glacier fraction in %. P is annual precipitation in mm year^{-1}. T is annual mean temperature in °C.

Basin	(Lon(E), Lat(N))	A	ME	GF	P	T
Nigardsbreen	(7.24, 61.67)	65	1542	72.8	3736	−0.47
Chamkhar Chhu	(90.74, 27.59)	1353	4479	15.0	1786	1.75
Beas	(77.15, 31.88)	3202	4213	32.7	1116	−1.04

Maps of bedrock and glacier surface elevation are provided by the Norwegian Water Resources and Energy Directorate (NVE). The profiles were measured by the Radio-Echo Sounding (RES) method during spring and early summer in the years 1981, 1984 and 1985 (Sætrang and Wold, 1986). The bedrock map is obtained through interpolation of the measured profiles and the open valley. The glacier surface elevation at a spatial resolution of 25 m are derived from complete or partial aerial photos taken within the

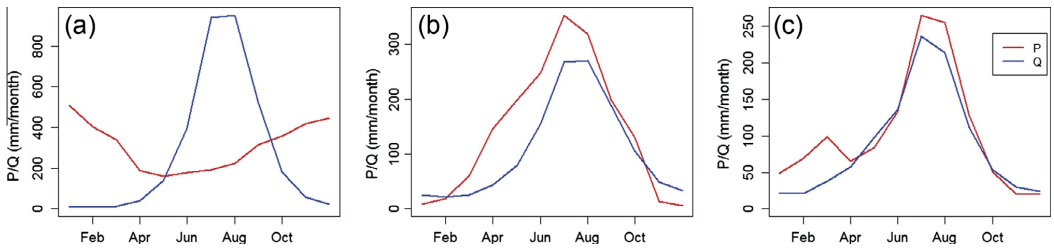

Fig. 3. Monthly mean precipitation and runoff of (a) the Nigardsbreen basin, (b) the Chamkhar Chhu basin, and (c) the Beas basin. Calculations are based on the sum of calibration and validation periods (Table 1).

Table 2
Summary of model settings. The last column indicates the observed series used in calibration and validation. *Q* means daily discharge and *M* means annual mass balance.

Basin	Resolution	Spin-up	Calibration	Validation	Series
Nigardsbreen	100 m	1989.09.01	1991.01.01–2002.12.31	2003.01.01–2012.12.31	*Q*, *M*
Chamkhar Chhu	1 km	1993.09.01	1998.01.01–2004.12.31	2005.01.01–2008.12.31	*Q*
Beas	1 km	1993.09.01	1997.01.01–2002.12.31	2003.01.01–2005.09.19	*Q*

Table 3
Numerical criteria of model calibration and validation. *Q* means daily discharge and *M* means annual mass balance.

Basin	Variable	Criteria	Calibration	Validation
Nigardsbreen	*Q*	NSE	0.90	0.90
		RME	4.61	5.38
	M	COR	0.90	0.92
Chamkhar Chhu	*Q*	NSE	0.87	0.85
		RME	−0.02	10.32
Beas	*Q*	NSE	0.65	0.73
		RME	2.07	−22.38

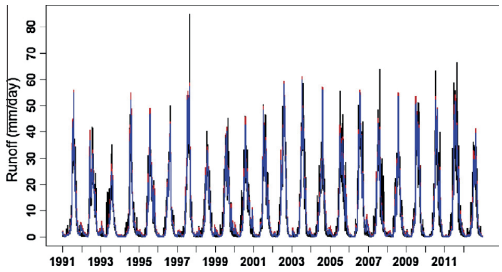

Fig. 4. Runoff components of the Nigardsbreen basin. Runoff below the blue line is the from the glacierised area. The red is the simulation of total runoff. The black is the observed time series. (For interpretation of the references to colour in this figure legend, the reader is referred to the web version of this article.)

period 1984–2009. The ice thickness is calculated as the difference between the glacier surface and bedrock for each grid. The thickness map is further aggregated at a resolution of 100 m, which is the spatial resolution of the HBV model for the Nigardsbreen basin. The starting date of the HBV model simulations is 1st September, 1989, which is roughly the middle of the period of the aerial photos (Table 2).

3.2. Chamkhar Chhu basin

The Chamkhar Chhu basin is located in central Bhutan (Fig. 2) and is the source of one of the major national rivers. The basin has three branches originating from the glaciers of the Gangkar Punsum region and the glaciers of the Monla Karchung La region. The river flows south-easterly and finally joins the Brahmaputra River in India. The basin area above the Kurjey gauging station is 1353 km^2. The elevation ranges from 6653 m amsl in the upper northern glacial region to 2643 m amsl in the southern low-land. The northern part above 4000 m amsl is mainly occupied by glaciers (Fig. 2(c)) whereas the southern low-land is covered by forests.

The climate is strongly influenced by elevation and monsoon; therefore it varies from the southeast to the northwest. Based on observations in the period from 1998 to 2008, the mean precipitation is 1786 mm year^{-1} and the mean annual air temperature is 1.75 °C. The monsoon normally starts in June and lasts until early September. It brings significant amounts of rainfall and warm weather. Subsequently, river flow rises due to the rainfall and melting of snow and ice. As the monsoon proceeds or retreats, there are four clear seasons, spring (March to May), summer (June to August), autumn (September to November), and winter (December to the following February).

The climate data are measured by in-situ meteorological stations, as shown in Fig. 2. Data of seven stations are used; however none of them lies inside the basin. The mean of daily maximum and minimum temperatures is taken by the HBV model as input of daily air temperature. The discharge series of the Kurjey station are obtained from the national authorities, which are in charge of collecting hydrological data. The measurements are available for the period 1998–2008 and have been used for evaluating climate change impacts on hydropower development (Beldring, 2011).

Glacier ice thickness distribution for the Chamkhar Chhu basin is a part of the global dataset produced by Huss and Farinotti (2012) using a method based on glacier mass turnover and principles of ice-flow mechanics (Farinotti et al., 2009). Required input data are a digital elevation model and glacier outlines. For each individual glacier ice thickness distribution is determined for about the year 2000 depending on the date of the utilised glacier inventory data (Pfeffer et al., 2014). The starting date for modelling is mainly determined by the observation period of the meteorological data and is set to 1st September, 1993.

The elevation and land use data are obtained from the Department of Hydromet Services, Bhutan. The original data are at a spatial resolution of 25 m and are rescaled at 1 km. The land use data are reclassified into three broad classes, high biomass (including broadleaf forest, coniferous forest and scrub), low biomass (including erosion, pasture, rock) and human affected (agriculture and urban).

3.3. Beas basin

The Beas River is an important branch of the Indus River system in northern India (Fig. 2). It originates at the southern side of the Rohtang Pass in the Himalaya. The river is 470 km long and has a drainage area of 12,916 km^2 (Gupta et al., 1982). This area is extremely rich in hydroelectricity resources. In total, there are 11 hydroelectric plants projects and three of them are ongoing or have been finished (SANDRP, 2015). To avoid the effects of flow regulation and to have a large study area, the Bhuntar gauging station is selected. The station lies downstream of the confluence with the eastern branch, the Parbati River. Only the Malana Hydel Scheme, with a capacity of 86 MW, was running during the study period of 1997–2005. The area above the station is 3202 km^2. The elevation decreases from 6288 m amsl in the northern mountains to 1055 m amsl. The area above 4500 m amsl is occupied by permanent snow and glaciers (Fig. 2(b)).

The climate is a result of a combined effect of elevation and monsoon. The northern part is much colder and drier than the low valleys. Influenced by the monsoon, there are four seasons, winter (January to March), pre-monsoon (April to June), monsoon (July to September) and post-monsoon (October to December) (Singh and Kumar, 1997). The monsoon strength is a major indicator of magnitude of precipitation and temperature. The air currents

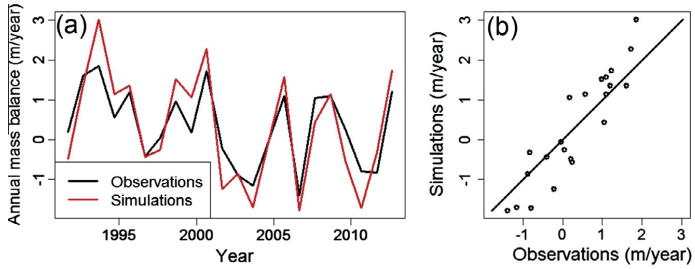

Fig. 5. Comparison of the observed and simulate annual mass balance of Nigardsbreen. The correlation coefficients are 0.90 for the calibration period and 0.92 for the validation period, as tabulated in Table 3.

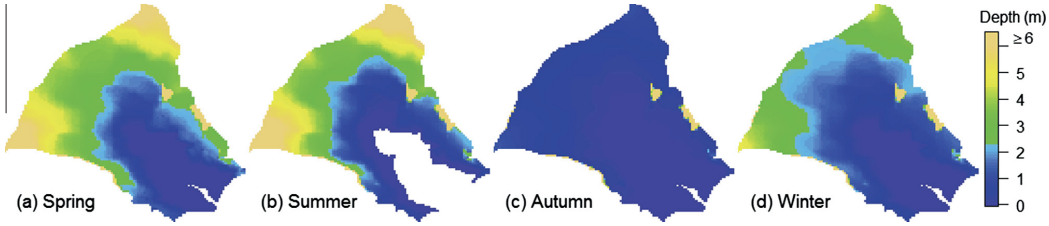

Fig. 6. Seasonal mean snowpack depth (m w.e.) in the Nigardsbreen basin. The white region is snow free. The snow-cover fractions are respectively 99.4% in (a) spring, 84.0% in (b) summer and 99.4% in (c) autumn and 99.4% in (d) winter.

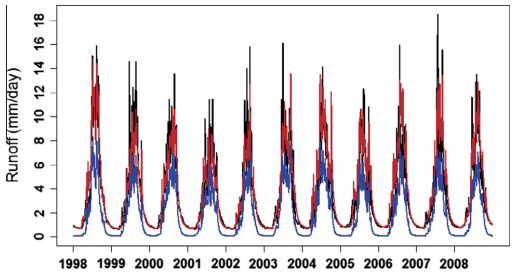

Fig. 7. Runoff components of the Chamkhar Chhu basin. Runoff below the blue line is the from the glacierised area. The red line is the simulation of total runoff. The black line is the observed runoff. (For interpretation of the references to colour in this figure legend, the reader is referred to the web version of this article.)

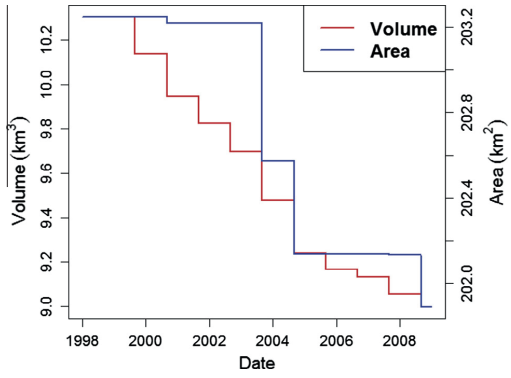

Fig. 8. Simulations of volume and area of the glaciers in the Chamkhar Chhu basin.

of the monsoon originate in the Bay of Bengal and they are weaker after striking east Himalaya and a long westward travel than in the Chamkhar Chhu basin (Singh and Kumar, 1997). Therefore, the precipitation decreases with height. Based on the observations during the period from 1997 to 2005, the mean precipitation is 1116 mm year^{-1} and the mean annual air temperature is −1.04 °C.

Three meteorological stations measure precipitation, and daily maximum and minimum temperature. Two of the stations are located in the selected area, respectively at the north valley and the Bhuntar station. The mean of daily maximum and minimum temperature is utilised by the HBV model as temperature input. The daily discharge series only cover the period 1997–2005 and the data quality is largely unknown. Quality control is visually conducted and points of suspicious errors are not included in model calibration and validation.

The ice thickness data are also a part of the dataset provided by Huss and Farinotti (2012). The DEMs are downloaded from the Hydro1k global datasets (EROS, 1996).

4. Results

4.1. Nigardsbreen basin

The model is run at a daily time step and at a spatial resolution of 100 m. The model is calibrated for the period from 1991 to 2002 using discharge and annual mass balance and is validated for the period from 2003 to 2012. The numerical values of NSE and RME are tabulated in Table 3 which shows a high model efficiency. Fig. 4 visually shows the good performance of the model in reproducing the historical daily flow series. The annual mass balance simulations also fit well with the observations (Fig. 5). The cumulative mass change in the period 1991–2012 is +7255 mm w.e. by observations and +7231 mm w.e. according to the simulation.

As shown in Fig. 6, summer is the season with the least snow cover, with approximately 84% of the total basin area. For autumn,

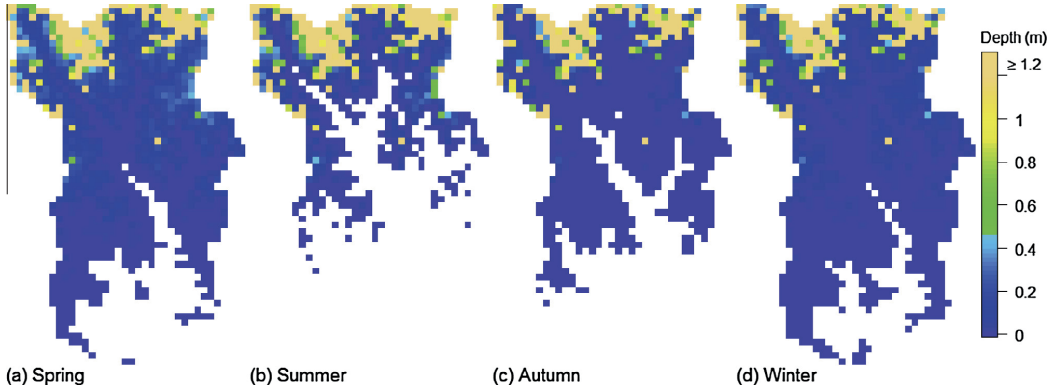

Fig. 9. Seasonal mean snowpack depth (m w.e.) in the Chamkahar Chhu basin. The white region is snow free. The snow-cover fractions are respectively 82.1% in (a) spring, 47.2% in (b) summer, 67.5% in (c) autumn and 87.7% in (d) winter.

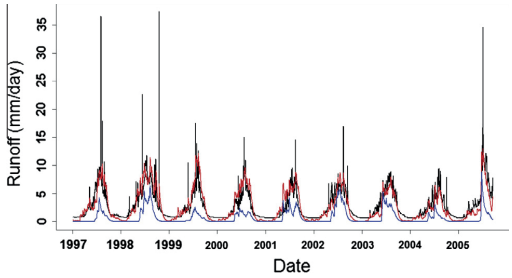

Fig. 10. Runoff components of the Beas basin. Runoff below the blue line is from the glacierised area. The red line is the simulation of total runoff. The black line is the observed time series. (For interpretation of the references to colour in this figure legend, the reader is referred to the web version of this article.)

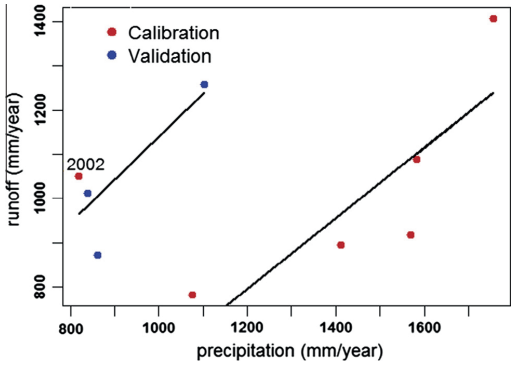

Fig. 11. Scatter plot of annual precipitation and annual runoff of the Beas basin. The right regression is based on the red dots except the year 2002. The left regression is based on the remaining dots. (For interpretation of the references to colour in this figure legend, the reader is referred to the web version of this article.)

the model produces a thinner snowpack than for summer, but a larger snow-covered area. The thinner pattern is because on 31st August, the model removes snow on glaciers and accumulation and ablation are relatively small for the autumn months. However, the summer pattern is a result of accumulation and ablation effects for each hydrological year. The spatial distribution of snow is in agreement with the seNorge snow modelling product (NVE, 2015).

4.2. Chamkhar Chhu basin

The model is run at a daily time step at a spatial resolution of 1 km. The calibration period is from 1998 to 2004 and the validation period is from 2005 to 2008 against discharge. The graphs of observed and simulated discharge are shown in Fig. 7. The NSE values for the calibration and validation are not less than 0.85 (Table 3), which indicates a very good simulation of runoff.

As shown in Fig. 8, the glaciers continued to retreat and mass balance was negative, roughly -0.51 m w.e. year^{-1} for the period 1998–2008. The maps of seasonal mean snowpack are shown in Fig. 9. They show similar model response as the Nigardsbreen basin.

4.3. Beas basin

The model is run at a daily time step on a spatial resolution of 1 km. The model is calibrated against discharge in the period from 1997 to 2002 and validation is performed for the period 2003–2005. The model efficiency is the lowest among the three basins (Table 3). As shown in Fig. 10, the model cannot capture the peaks in the observed hydrograph and significantly overestimates the low flow. The low quality of the data is likely one of the main reasons for this, as the extreme peaks are more than three times of normal high flow and most of them are only sustained for one day.

To further explore the reasons of the relatively low model efficiency, we plot the relationship between annual precipitation and runoff in Fig. 11. The year 2002 can be considered as a turning point and the relationships of precipitation and runoff are substantially modified since this year. The reasons cannot be conclusively stated by examining the annual temperature and precipitation. The shift is possibly due to some sub-daily events or changes in glacier energy balance. For the Himachal Pradesh (Western Himalaya, India) region, Azam et al. (2012) also reported a particularly negative mass balance since the year 2002 compared to the data collected during the period 1987–1989.

Fig. 12 shows the simulated snow pattern of the Beas basin. In addition to the similar model responses of the Nigardsbreen and

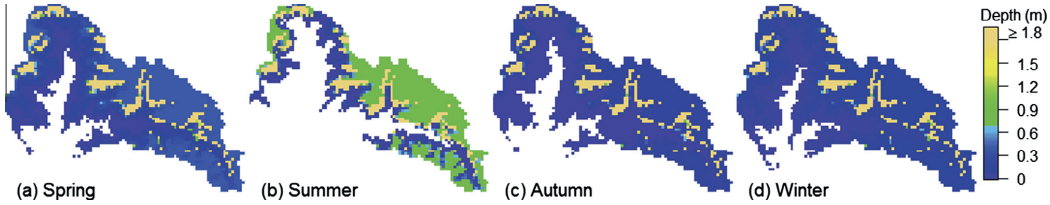

Fig. 12. Seasonal mean snowpack depth (m w.e.) in the Beas basin. The white region is snow free. The snow-cover fractions for the four seasons are respectively 85.5% in (a) spring, 58.0% in (b) summer, 82.6% in (c) autumn and 90.8% in (d) winter.

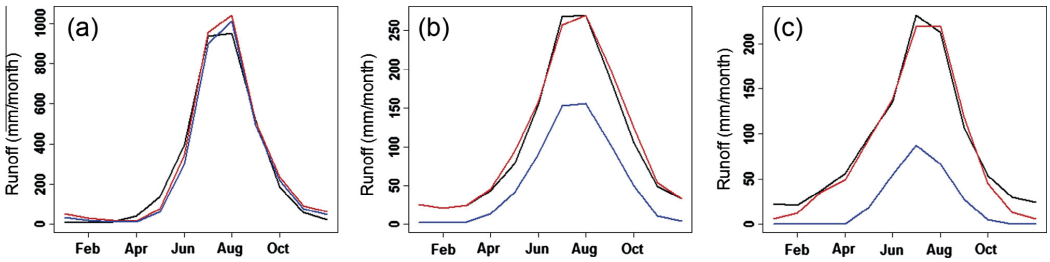

Fig. 13. Runoff components of the three basins, (a) the Nigardsbreen basin, (b) the Chamkhar Chhu basin, and (c) the Beas basin. Runoff below the blue line is from the glacierised area. The red line is the simulated total runoff. The black line is the observed runoff. (For interpretation of the references to colour in this figure legend, the reader is referred to the web version of this article.)

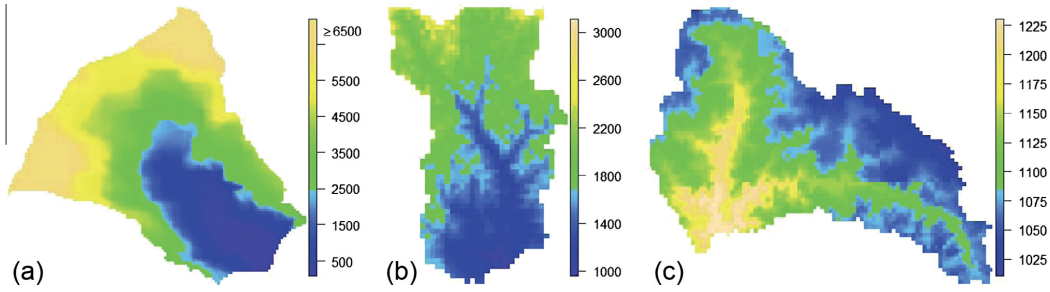

Fig. 14. Annual mean precipitation (mm year^{-1}) of (a) the Nigardsbreen basin, (b) the Chamkhar Chhu basin, and (c) the Beas basin.

Table 4
Table of the selected HBV parameters and their values. T_t and MF_{snow} for the Chamkhar Chhu basin are land cover dependent; therefore the areal mean is given.

Name	Unit	Nigardsbreen	Chamkhar Chhu	Beas
K_f		1.00*	1.06	1.06
K_s		1.00*	1.14	0.96
γ_p		1.32	1.00	1.00
γ_t	°C per 100 m	−0.90	−0.60	−0.69
T_{acc}	°C	0*	−2.5*	−2.5*
T_t	°C	2.49	0.37	3.07
MF_{snow}	m day^{-1} °C^{-1}	8.32E−3	4.55E−3	1.78E−1
MF_{ice}	m day^{-1} °C^{-1}	9.93E−3	4.79E−3	2.26E−1

* Indicates that the value is assigned by experience and the remaining values are optimised.

Chamkhar Chhu basins, the eastern part in the summer receives more snow than in the spring. This confirms that significant snow accumulation occurs during the summer months. The snow pattern of the Beas basin is the most complex among the three basins.

5. Discussions

5.1. Model performance

The model evaluation is based on discharge and available mass balance measurements. The results given in Table 3 show that the coupled model is able to accurately simulate both daily discharge and annual glacier mass balance in the Nigardsbreen basin. Though there are no mass balance measurements in the Chamkhar Chhu basin, the numerical criteria of NSE are higher than or equal 0.85 for the calibration and validation modes, which is considered as very good simulation. The model efficiency of the Beas basin is much lower than for the other two basins, but results are considered as acceptable, considering the availability and quality of the data.

Mapping the spatial distribution of internal variables, such as snowpack, is an advantage of distributed modelling. In the three basins, the snow storage increases from the lower elevations to the higher elevations. As stated before, the model transforms the snow remaining on glaciers to ice by 31st August, which means

that snow on glaciers is zero at the end of every summer. However, if glaciers are misrepresented by the model, the simulated snow could be misleading and should be interpreted carefully. The misrepresentation can be introduced by errors in the initial ice thickness data or generated during simulating glacier area.

5.2. Glacier runoff

The glacierised areas are considered to be very valuable for water resources and hydropower management (Barnett et al., 2005). Most glaciers are located at high elevation, which results in a high hydropower potential (hydraulic head). Additionally, the evaporation rate is small and the specific runoff is high in these areas.

Glacier runoff is defined as the runoff from the glacierised area, including all melt of snow and glacier ice/firn, and rain water in the most general sense (Radić and Hock, 2014; Bliss et al., 2014). Fig. 13 shows the monthly mean runoff of the three basins. The ranking of glacier contribution to runoff in the descending order is the Nigardsbreen basin (92.5%), the Chamkhar basin (48.1%) and the Beas basin (27.5%). The main reason for the highest contribution for the Nigardsbreen basin is its largest glacierisation. Additionally, the glacier contribution also depends on climate, especially the spatial distribution of precipitation within a watershed. The more precipitation falls on the glacierised areas, the higher the glacier's contributions to runoff. As shown in Fig. 14, the precipitation decreases from upstream to downstream in the Nigardsbreen basin and in the Chamkhar Chhu basin. However, in the Beas basin, more precipitation falls in the valleys compared to the high mountains. As a result of these spatial distribution patterns of precipitation, the ratio of the glacier's contribution is higher in the Chamkhar Chhu basin than in the Beas basin, even though the latter has a higher glacierisation.

There is no doubt that runoff of these basins is strongly defined by both glaciers and precipitation. Glacier melting is dominant in the Nigardsbreen basin, whereas precipitation is the main contributor in the Chamkhar Chhu and Beas basins. For a given increase in temperature, the three basins are expected to respond differently in terms of runoff and glacier existence. The sensitivity of a basin to climate change and effects on runoff can be studied by running the model with climate projections and this is an on-going research.

5.3. Uncertainties

Uncertainties can inherit from data, models and their parameters; small uncertainties can accumulate into considerable uncertainties in the target outputs through the modelling processes (Seiller and Anctil, 2014; Bastola et al., 2011).

The quality of climate data is very important in hydrological modelling. In the studies of the Chamkhar Chhu and Beas basins, the meteorological stations are sparsely distributed and mainly located at low elevation places. This distribution leads to a low representativeness of the spatial precipitation and temperature. Though in the interpolation of the station measurements, elevation effects have been considered, the exposure to the sun also influences snow and ice melt. For very high mountain glaciers, air temperature is seldom above the melting point and due to thin atmospheres, it is a humble indicator of energy (Hock, 2003; Sicart et al., 2008). The accumulated ice flows to lower elevations due to ice dynamics. The accumulation and melting should be carefully interpreted in their total amount rather than the spatial details.

The discharge series are essential to calibrate and validate hydrological models. Therefore, their accuracy and length should be adequate. However, the available discharge series of the Himalayan basins typically have a length of only ten years. In addition, the accuracy is affected by the measurement methodology and quality is not ensured, particularly for the Beas basin.

Initial conditions provide a starting point for a model system. The initial conditions of the hydrological models are determined by model simulations, usually referred to as model "spin-up". However, this method cannot be used to construct the glacier state in current climate. A glacier forms over many years and recent warming has induced melting for most glaciers globally. Considerable uncertainties exist in the initial state of glaciers in the three basins.

For the Δh-parameterisation, a limitation is that this model is only valid for retreating glaciers, which is generally true for most mountain glaciers at present and for the near future. At present no scheme is implemented that allows describing the expansion of glaciers following positive mass change; they just increase the total glacier volume. The four parameters of the Δh-parameterisation are only calibrated according to discharge in the Chamkhar Chhu and Beas basins. How well they are identified needs further evaluations. For the HBV parameters, the optimised values are given in Table 4, which shows that the parameters values are in general within their empirical ranges except few parameters for the Beas basin.

6. Conclusions

Glaciers strongly influence hydrology in glacierised areas. However, these effects have not been well understood and well simulated quantitatively at present due to imperfect tools and data scarcity. In this study, we integrated a simple approach for simulating glacier geometry change, the Δh-parameterisation into the HBV model, to study the dynamics of hydrological processes in glacierised basins. The combined model requires easily accessible inputs data (precipitation, temperature and initial ice thickness) and provides the dynamics of glacier system and consequent runoff processes. The model can be used for estimating runoff, snow and glacier mass balance in past and future.

The coupled model is tested in three high mountain basins with different climates and data quantity and quality. Among the basins, the Nigardsbreen basin has the longest time series of discharge data and observed annual glacier mass balance. Comparisons of model simulations with the observations show that the model yields very high model efficiency in simulation of discharge and annual mass balance for the Nigardsbreen basin. The least model efficiency is found for the Beas basin possibly due to uncertainties in input data and the changed precipitation-runoff relationship since the year 2002. Additionally, the model can provide maps of snowpack distribution and estimate runoff components from glaciers.

Acknowledgements

This study is funded by the Research Council of Norway through the research project-JOINTINDNOR (Project Number 203867) and the Department of Science and Technology, Govt. of India. All the data of the Chamkhar Chhu basin are provided by the Department of Hydromet Services, Ministry of Economic Affairs, Royal Government of Bhutan. Thanks also go to Norwegian Water Resources and Energy Directorate for providing the data of the Nigardsbreen basin and computational facility, and helps in Geographic Information System and the Bhakra Beas Management Board for providing the data of the Beas basin. The authors are also grateful to the reviewers for their valuable comments and suggestions, which are very helpful to the substantial improvement of this paper.

References

Akhtar, M., Ahmad, N., Booij, M., 2008. The impact of climate change on the water resources of Hindukush–Karakorum–Himalaya region under different glacier coverage scenarios. J. Hydrol. 355, 148–163. http://dx.doi.org/10.1016/j.jhydrol.2008.03.015.

Andreassen, L.M., Elvehy, H., Jackson, M., Kjllmoen, B., Giesen, R.H., 2011. Glaciological Investigations in Norway in 2010. Report 03 Norwegian Water Resources and Energy Directorate. <http://webby.nve.no/publikasjoner/report/2011/report201103.pdf>.

Andreassen, L.M., Elvehy, H., Kjllmoen, B., Engeset, R.V., Haakensen, N., 2005. Glacier mass-balance and length variation in Norway. Ann. Glaciol. 42, 317–325. http://dx.doi.org/10.3189/172756405781812826.

Andreassen, L.M., Winsvold, S.H., Paul, F., Hausberg, J.E., 2012. Inventory of Norwegian Glaciers. Report 38 Norwegian Water Resources and Energy Directorate. <http://webby.nve.no/publikasjoner/rapport/2012/rapport201238.pdf>.

Arendt, A.A., Echelmeyer, K.A., Harrison, W.D., Lingle, C.S., Valentine, V.B., 2002. Rapid wastage of Alaska glaciers and their contribution to rising sea level. Science 297, 382–386. http://dx.doi.org/10.1126/science.1072497.

Arnold, N., Willis, I., Sharp, M., Richards, K., Lawson, W., 1996. A distributed surface energy-balance model for a small valley glacier. I. Development and testing for Haut Glacier d'Arolla, Valais, Switzerland. J. Glaciol. 42, 77–89, <http://www.igsoc.org/journal.old/42/140/igsjournalvol42issue140pg77-89.pdf>.

Arora, M., Kumar, R., Kumar, N., Malhotra, J., 2014. Assessment of suspended sediment concentration and load from a large Himalayan glacier. Hydrol. Res. 45, 292–306. http://dx.doi.org/10.2166/nh.2013.129.

Azam, M.F., Wagon, P., Ramanathan, A., Vincent, C., Sharma, P., Arnaud, Y., Linda, A., Pottakkal, J.G., Chevallier, P., Singh, V.B., Berthier, E., 2012. From balance to imbalance: a shift in the dynamic behaviour of Chhota Shigri glacier, western Himalaya, India. J. Glaciol. 58, 315–324. http://dx.doi.org/10.3189/2012JoG11J123.

Barnett, T.P., Adam, J.C., Lettenmaier, D.P., 2005. Potential impacts of a warming climate on water availability in snow-dominated regions. Nature 438, 303–309. http://dx.doi.org/10.1038/nature04141.

Bastola, S., Murphy, C., Sweeney, J., 2011. The role of hydrological modelling uncertainties in climate change impact assessments of Irish river catchments. Adv. Water Resour. 34, 562–576. http://dx.doi.org/10.1016/j.advwatres.2011.01.008.

Bauder, A., Funk, M., Huss, M., 2007. Ice-volume changes of selected glaciers in the Swiss Alps since the end of the 19th century. Ann. Glaciol. 46, 145–149. http://dx.doi.org/10.3189/172756407782871701.

Beldring, S., 2011. Climate Change Impacts on the Flow Regimes of Rivers in Bhutan and Possible Consequences for Hydropower Development. Report 04 Norwegian Water Resources and Energy Directorate. <http://www.nve.no/Global/Publikasjoner/Publikasjoner>.

Beldring, S., Engeland, K., Roald, L.A., Selthun, N.R., Voks, A., 2003. Estimation of parameters in a distributed precipitation-runoff model for Norway. Hydrol. Earth Syst. Sci. 7, 304–316. http://dx.doi.org/10.5194/hess-7-304-2003.

Beniston, M., 2003. Climatic change in mountain regions: a review of possible impacts. Climatic Change 59, 5–31. http://dx.doi.org/10.1023/A:1024458411589.

Bergström, S., 1976. Development and Application of a Conceptual Runoff Model for Scandinavian Catchments. Report 07 Swedish Meteorological and Hydrological Institute. <http://books.google.no/books?id=vRyeQAAACAAJ>.

Bliss, A., Hock, R., Radić, V., 2014. Global response of glacier runoff to twenty-first century climate change. J. Geophys. Res. Earth Surf. 119, 717–730. http://dx.doi.org/10.1002/2013JF002931.

Bolch, T., 2007. Climate change and glacier retreat in northern Tien Shan (Kazakhstan/Kyrgyzstan) using remote sensing data. Glob. Planet. Change 56, 1–12. http://dx.doi.org/10.1016/j.gloplacha.2006.07.009.

Bolch, T., Kulkarni, A., Kääb, A., Huggel, C., Paul, F., Cogley, J.G., Frey, H., Kargel, J.S., Fujita, K., Scheel, M., Bajracharya, S., Stoffel, M., 2012. The state and fate of Himalayan glaciers. Science 336, 310–314. http://dx.doi.org/10.1126/science.1215828.

Burlando, P., Pellicciotti, F., Strasser, U., 2002. Modelling mountainous water systems between learning and speculating looking for challenges. Nord. Hydrol. 33, 47–74. http://dx.doi.org/10.2166/nh.2002.004.

Carey, M., 2005. Living and dying with glaciers: people's historical vulnerability to avalanches and outburst floods in Peru. Glob. Planet. Change 47, 122–134. http://dx.doi.org/10.1016/j.gloplacha.2004.10.007.

Carey, M., 2007. The history of ice: how glaciers became an endangered species. Environ. Hist. 12, 497–527. http://dx.doi.org/10.1093/envhis/12.3.497.

Doherty, J., 2005. PEST Model-Independent Parameter Estimation User Manual. Watermark Numerical Computing, fifth ed. <http://www.pesthomepage.org/Downloads.php>.

Doherty, J., Johnston, J.M., 2003. Methodologies for calibration and predective analysis of a watershed model[1]. J. Am. Water Resour. Assoc. 39, 251–265. http://dx.doi.org/10.1111/j.1752-1688.2003.tb04381.x.

Engelhardt, M., Schuler, T.V., Anderson, L.M., 2012. Evaluation of gridded precipitation for Norway using glacier mass-balance measurements. Geogr. Ann. Ser. A Phys. Geogr. 94, 501–509. http://dx.doi.org/10.1111/j.1468-0459.2012.00473.x.

Engelhardt, M., Schuler, T.V., Andreassen, L.M., 2013. Glacier mass balance of Norway 1961–2010 calculated by a temperature-index model. Ann. Glaciol. 54, 32–40. http://dx.doi.org/10.3189/2013AoG63A245.

EROS, 1996. Hydro1k Elevation Derivative Database. <https://lta.cr.usgs.gov/HYDRO1K>.

Farinotti, D., Huss, M., Bauder, A., Funk, M., Truffer, M., 2009. A method to estimate the ice volume and ice-thickness distribution of alpine glaciers. J. Glaciol. 55, 422–430. http://dx.doi.org/10.3189/002214309788816759.

Gisnas, K., Etzelmüller, B., Farbrot, H., Schuler, T.V., Westermann, S., 2013. CryoGRID 1.0: permafrost distribution in Norway estimated by a spatial numerical model. Permafrost Periglac. Process. 24, 2–19. http://dx.doi.org/10.1002/ppp.1765.

Gottlieb, L., 1980. Development and applications of a runoff model for snowcovered and glacierized basins. Nord. Hydrol. 11, 255–272. http://dx.doi.org/10.2166/nh.1980.020.

Götzinger, J., Bárdossy, A., 2005. Integration and calibration of a conceptual rainfall–runoff model in the framework of a decision support system for river basin management. Adv. Geosci. 5, 31–35. http://dx.doi.org/10.5194/adgeo-5-31-2005.

Greuell, W., 1992. Hintereisferner, Austria: mass-balance reconstruction and numerical modelling of the historical length variations. J. Glaciol. 38, 233–244, <http://www.igsoc.org:8080/journal/38/129/igsjournalvol38issue129pg233-244.pdf>.

Gupta, R., Duggal, A., Rao, S., Sankar, G., Singhal, B., 1982. Snow-cover area vs. snowmelt runoff relation and its dependence on geomorphology? – A study from the Beas catchment (Himalayas, India). J. Hydrol. 58, 325–339. http://dx.doi.org/10.1016/0022-1694(82)90042-7.

Hagg, W., Braun, L., Kuhn, M., Nesgaard, T., 2007. Modelling of hydrological response to climate change in glacierized Central Asian catchments. J. Hydrol. 332, 40–53. http://dx.doi.org/10.1016/j.jhydrol.2006.06.021.

Hagg, W., Braun, L., Weber, M., Becht, M., 2006. Runoff modelling in glacierized Central Asian catchments for present-day and future climate. Nord. Hydrol. 37, 93–105. http://dx.doi.org/10.2166/nh.2006.001.

Hagg, W.J., Braun, L.N., Uvarov, V.N., Makarevich, K.G., 2004. A comparison of three methods of mass-balance determination in the Tuyuksu glacier region, Tien Shan, Central Asia. J. Glaciol. 50, 505–510. http://dx.doi.org/10.3189/172756504781829783.

Hailegeorgis, T.T., Alfredsen, K., 2015. Comparative evaluation of performances of different conceptualisations of distributed HBV runoff response routines for prediction of hourly streamflow in boreal mountainous catchments. Hydrol. Res. (in press). http://dx.doi.org/10.2166/nh.2014.051.

Hock, R., 2003. Temperature index melt modelling in mountain areas. J. Hydrol. 282, 104–115. http://dx.doi.org/10.1016/S0022-1694(03)00257-9.

Hock, R., 2005. Glacier melt: a review of processes and their modelling. Prog. Phys. Geogr. 29, 362–391. http://dx.doi.org/10.1191/0309133305 pp453ra.

Horton, P., Schaefli, B., Mezghani, A., Hingray, B., Musy, A., 2006. Assessment of climate-change impacts on alpine discharge regimes with climate model uncertainty. Hydrol. Process. 20, 2091–2109. http://dx.doi.org/10.1002/hyp.6197.

Hubbard, A., Blatter, H., Nienow, P., Mair, D., Hubbard, B., 1998. Comparison of a three-dimensional model for glacier flow with field data from Haut Glacier d'Arolla, Switzerland. J. Glaciol. 44, 368–378, <http://www.igsoc.org:8080/journal/44/147/igsjournalvol44issue147pg368-378.pdf>.

Huss, M., Farinotti, D., 2012. Distributed ice thickness and volume of all glaciers around the globe. J. Geophys. Res. Earth Surf. 117, F04010. http://dx.doi.org/10.1029/2012JF002523.

Huss, M., Farinotti, D., Bauder, A., Funk, M., 2008. Modelling runoff from highly glacierized alpine drainage basins in a changing climate. Hydrol. Process. 22, 3888–3902. http://dx.doi.org/10.1002/hyp.7055.

Huss, M., Jouvet, G., Farinotti, D., Bauder, A., 2010. Future high-mountain hydrology: a new parameterization of glacier retreat. Hydrol. Earth Syst. Sci. 14, 815–829. http://dx.doi.org/10.5194/hess-14-815-2010.

Immerzeel, W., Droogers, P., de Jong, S., Bierkens, M., 2009. Large-scale monitoring of snow cover and runoff simulation in Himalayan river basins using remote sensing. Rem. Sens. Environ. 113, 40–49. http://dx.doi.org/10.1016/j.rse.2008.08.010.

Immerzeel, W.W., van Beek, L., Konz, M., Shrestha, A., Bierkens, M., 2012. Hydrological response to climate change in a glacierized catchment in the Himalayas. Climatic Change 110, 721–736. http://dx.doi.org/10.1007/s10584-011-0143-4.

Jain, S.K., Thakural, L., Singh, R., Lohani, A., Mishra, S., 2011. Snow cover depletion under changed climate with the help of remote sensing and temperature data. Nat. Hazards 58, 891–904. http://dx.doi.org/10.1007/s11069-010-9696-1.

Jasper, K., Calanca, P., Gyalistras, D., Fuhrer, J., 2004. Differential impacts of climate change on the hydrology of two alpine river basins. Clim. Res. 26, 113–129. http://dx.doi.org/10.3354/cr026113.

Jóhannesson, T., Raymond, C., Waddington, E., 1989. Time-scale for adjustment of glaciers to changes in mass balance. J. Glaciol. 35, 355–369, <http://www.igsoc.org:8080/journal/35/121/igsjournalvol35issue121pg355-369.pdf>.

Joshi, G., 2007. Major Cities of Hindu Kush Himalayan (HKH) Region (accessed in January 2015). <http://rds.icimod.org/Home/DataDetail?metadataId=3434&searchlist=True>.

Joshi, G., 2008. Major River Systems of Hindu Kush Himalayan (HKH) Region. (accessed in January 2015). <http://rds.icimod.org/Home/DataDetail?metadataId=2956&searchlist=True>.

Joshi, G., 2011. Digital Elevation Model of Hindu Kush Himalayan (HKH) Region (accessed in January 2015). <http://rds.icimod.org/Home/DataDetail?metadataId=8744&searchlist=True>.

Jouvet, G., Huss, M., Blatter, H., Picasso, M., Rappaz, J., 2009. Numerical simulation of Rhonegletscher from 1874 to 2100. J. Comput. Phys. 228, 6426–6439. http://dx.doi.org/10.1016/j.jcp.2009.05.033.

Kaser, G., Grohauser, M., Marzeion, B., 2010. Contribution potential of glaciers to water availability in different climate regimes. Proc. Nat. Acad. Sci. 104, 20223–20227. http://dx.doi.org/10.1073/pnas.1008162107.

Khadka, D., Babel, M.S., Shrestha, S., Tripathi, N.K., 2014. Climate change impact on glacier and snow melt and runoff in Tamakoshi basin in the Hindu Kush Himalayan (HKH) region. J. Hydrol. 511, 49–60. http://dx.doi.org/10.1016/j.jhydrol.2014.01.005.

Klok, E.L., Oerlemans, J., 2002. Model study of the spatial distribution of the energy and mass balance of Morteratschgletscher, Switzerland. J. Glaciol. 48, 505–518. http://dx.doi.org/10.3189/172756502781831133.

Kotlarski, S., Jacob, D., Podzun, R., Paul, F., 2010. Representing glaciers in a regional climate model. Clim. Dyn. 34, 27–46. http://dx.doi.org/10.1007/s00382-009-0685-6.

Li, H., Beldring, S., Xu, C.-Y., 2014a. Implementation and testing of routing algorithms in the distributed Hydrologiska Byrans Vattenbalansavdelning model for mountainous catchments. Hydrol. Res. 45, 322–333. http://dx.doi.org/10.2166/nh.2013.009.

Li, H., Beldring, S., Xu, C.-Y., Jain, S., October 2014b. Modelling runoff and its components in Himalayan basins. In: Hydrology in a Changing World: Environmental and Human Dimensions number 363 in FRIEND-Water. Montpellier, France, pp. 158–164. <http://iahs.info/Publications-News.do>.

Lindström, G., Johansson, B., Persson, M., Gardelin, M., Bergström, S., 1997. Development and test of the distributed HBV-96 hydrological model. J. Hydrol. 201, 272–288. http://dx.doi.org/10.1016/S0022-1694(97)00041-3.

Lüthi, M.P., 2009. Transient response of idealized glaciers to climate variations. J. Glaciol. 55, 918–930. http://dx.doi.org/10.3189/002214309790152519.

Marshall, S.J., 2014. Meltwater runoff from Haig Glacier, Canadian Rocky Mountains, 2002–2013. Hydrol. Earth Syst. Sci. Discuss. 11, 8355–8407. http://dx.doi.org/10.5194/hessd-11-8355-2014.

Mayr, E., Hagg, W., Mayer, C., Braun, L., 2013. Calibrating a spatially distributed conceptual hydrological model using runoff, annual mass balance and winter mass balance. J. Hydrol. 478, 40–49. http://dx.doi.org/10.1016/j.jhydrol.2012.11.035.

Nash, J., Sutcliffe, J., 1970. River flow forecasting through conceptual models Part I – A discussion of principles. J. Hydrol. 10, 282–290. http://dx.doi.org/10.1016/0022-1694(70)90255-6.

Naz, B.S., Frans, C.D., Clarke, G.K.C., Burns, P., Lettenmaier, D.P., 2014. Modeling the effect of glacier recession on streamflow response using a coupled glacio-hydrological model. Hydrol. Earth Syst. Sci. 18, 787–802. http://dx.doi.org/10.5194/hess-18-787-2014.

NVE. seNorge.no (accessed in March 2015). <http://www.senorge.no/aboutSeNorge.html?show=on>.

O'Callaghan, J.F., Mark, D.M., 1984. The extraction of drainage networks from digital elevation data. Comput. Vis. Graph. Image Process. 28, 323–344. http://dx.doi.org/10.1016/S0734-189X(84)80011-0.

Oerlemans, J., 1986. An attempt to simulate historic front variations of Nigardsbreen, Norway. Theoret. Appl. Climatol. 37, 126–135. http://dx.doi.org/10.1007/BF00867846.

Oerlemans, J., 1997. A flowline model for Nigardsbreen, Norway: projection of future glacier length based on dynamic calibration with the historic record. J. Glaciol. 24, 382–389, <http://dspace.library.uu.nl/handle/1874/22126>.

Oerlemans, J., 2007. Estimating response times of Vadret da Morteratsch, Vadret da Palü, Briksdalsbreen and Nigardsbreen from their length records. J. Glaciol. 53, 357–362. http://dx.doi.org/10.3189/002214307783258387.

Østrem, G., Brugman, M., 1991. Glacier Mass-Balance Measurements: A Manual for Field and Office Work. Report 04 National Hydrology Reseacrch Institute. <http://www.wgms.ch/downloads/OestremBrugmanGlacierMassBalanceMeasurements1991.pdf>.

Petersen-verleir, A., Soot, A., Reitan, T., 2009. Bayesian rating curve inference as a streamflow data quality assessment tool. Water Resour. Manage. 23, 1835–1842. http://dx.doi.org/10.1007/s11269-008-9354-5.

Pfeffer, W.T., Arendt, A.A., Bliss, A., Bolch, T., Cogley, J.G., Gardner, A.S., Hagen, J.-O., Hock, R., Kaser, G., Kienholz, C., Miles, E.S., Moholdt, G., Mölg, N., Paul, F., Radić, V., Rastner, P., Raup, B.H., Rich, J., Sharp, M.J., 2014. The Randolph Glacier Inventory: a globally complete inventory of glaciers. J. Glaciol. 60, 537. http://dx.doi.org/10.3189/2014JoG13J176.

Radić, V., Hock, R., 2014. Glaciers in the Earth's hydrological cycle: assessments of glacier mass and runoff changes on global and regional scales. Surv. Geophys. 35, 813–837. http://dx.doi.org/10.1007/s10712-013-9262-y.

Setrang, A.C., Wold, B., 1986. Results from the radio echo-sounding on parts of the Jostedalsbreen ice cap, Norway. Ann. Glaciol. 8, 156–158, <http://www.igsoc.org:8080/annals/8/igsannalsvol08year1985pg156-158.pdf>.

SANDRP. Hydro Electric Projects in Beas River Basin (accessed in February 2015). <http://sandrp.in/basinmaps/HydropowerProjectsinBeasBasin.pdf>.

Seiller, G., Anctil, F., 2014. Climate change impacts on the hydrologic regime of a canadian river: comparing uncertainties arising from climate natural variability and lumped hydrological model structures. Hydrol. Earth Syst. Sci. 18, 2033–2047. http://dx.doi.org/10.5194/hess-18-2033-2014.

Shrestha, M., Wang, L., Koike, T., Xue, Y., Hirabayashi, Y., 2012. Modeling the spatial distribution of snow cover in the Dudhkoshi region of the Nepal Himalayas. J. Hydrometeorol. 13, 204–222. http://dx.doi.org/10.1175/JHM-D-10-05027.1.

Sicart, J.E., Hock, R., Six, D., 2008. Glacier melt, air temperature, and energy balance in different climates: the Bolivian Tropics, the French Alps, and northern Sweden. J. Geophys. Res. 113 (December), D24113. http://dx.doi.org/10.1029/2008JD010406.

Singh, P., Haritashya, U.K., Kumar, N., Singh, Y., 2006. Hydrological characteristics of the Gangotri Glacier, central Himalayas, India. J. Hydrol. 327, 55–67. http://dx.doi.org/10.1016/j.jhydrol.2005.11.060.

Singh, P., Kumar, N., 1997. Effect of orography on precipitation in the western Himalayan region. J. Hydrol. 199, 183–206. http://dx.doi.org/10.1016/S0022-1694(96)03222-2.

Singh, P., Kumar, N., 1997. Impact assessment of climate change on the hydrological response of a snow and glacier melt runoff dominated Himalayan river. J. Hydrol. 193, 316–350. http://dx.doi.org/10.1016/S0022-1694(96)03142-3.

Stahl, K., Moore, R.D., Shea, J.M., Hutchinson, D., Cannon, A.J., 2008. Coupled modelling of glacier and streamflow response to future climate scenarios. Water Resour. Res. 44, W02422. http://dx.doi.org/10.1029/2007WR005956.

Uhlenbrook, S., Seibert, J., Leibundgut, C., Rodhe, A., 1999. Prediction uncertainty of conceptual rainfall–runoff models caused by problems in identifying model parameters and structure. Hydrol. Sci. J. 44, 779–797. http://dx.doi.org/10.1080/02626669909492273.

Vormoor, K., Skaugen, T., 2013. Temporal disaggregation of daily temperature and precipitation grid data for Norway. J. Hydrometeorol. 14, 989–999. http://dx.doi.org/10.1175/JHM-D-12-0139.1.

Wrede, S., Seibert, J., Uhlenbrook, S., 2013. Distributed conceptual modelling in a Swedish lowland catchment: a multi-criteria model assessment. Hydrol. Res. 44, 318–333. http://dx.doi.org/10.2166/nh.2012.056.

Zemp, M., Roer, I., Kääb, A., Hoelzle, M., Paul, F., Haeberli, W., 2008. Global Glacier Changes: Facts and Figures. The United Nations Environment Programme and The World Glacier Monitoring Service. <http://www.grid.unep.ch/glaciers/>.

4 Article IV

– **Li, H.**, Xu, C.-Y., Beldring, S., Tallaksen, L., Jain, S. (2015): Water Resources under Climate Change of Himalayan Basins—*Water Resources Management*, submitted.

Water Resources Management manuscript No.
(will be inserted by the editor)

Water Resources under Climate Change in Himalayan Basins

Hong Li · Chongyu Xu* · Stein Beldring · Lena Merete Tallaksen · Sharad K. Jain

Received: date / Accepted: date

Abstract Global warming has significant implications for glacier changes and water resources in the Himalayan region. There is an urgent need to improve our current knowledge and methods in quantifying water resources changes. This paper used an integrated approach that couples a hydrological model and a glacier retreat model to assess the future water resources for two Himalayan basins. They are the Chamkhar Chhu basin in Bhutan (eastern Himalaya) and the Beas basin in India (western Himalaya). The future climate is simulated by two Regional Climate Models (RCMs) for South Asia. In total, there are six climate projections for three Representative Concentration Pathways (Rcp2.6, Rcp4.5 and Rcp8.5). The climate projections for the period 2010–2100 indicate significant warming effects; however, changes in precipitation are not consistent. Discrepancies in precipitation are noteworthy between the RCMs and CO_2 scenarios. The glaciers in the Chamkhar Chhu basin are predicted to disappear or reduce to a small size

Funded by the Research Council of Norway through the research project, JOINTINDNOR (203867).

H. Li; C.-Y. Xu

Department of Geosciences, University of Oslo, Norway

Tel.: +47-22-855825 Fax: +47-22-854215 E-mail: chongyu.xu@geo.uio.no

S. Beldring

Norwegian Water Resources and Energy Directorate, Norway

L. Tallaksen

Department of Geosciences, University of Oslo, Norway

S. Jain

National Institute of Hydrology, Roorkee, India

before the 2050s, whereas the glaciers in the Beas basin are expected to lose mass before the 2060s, and afterwards to accumulate under Rcp2.6 and Rcp4.5 or to melt at a high rate under Rcp8.5. The available water resources per capita of two basins are projected to decrease in the period 2010–2050 which jointly results due to climate change and population growth. The latter is responsible for roughly 40% of the water declines. Both basins are facing serious water shortages at present and the water shortages will intensify in the future.

Keywords climate change · CORDEX · hydro-glacial modelling · glacier retreat · Himalaya · water resources

1 Introduction

As the largest cryosphere outside the polar areas and source of rivers supporting more than 800 million people, the state of Hindukush—Karakorum—Himalaya (HKH) glaciers is of concern for both scientists and the general public. There is a long-term increase in the global average near surface temperature and most glaciers are losing mass at accelerated rates according to instrument measurements. For example, by using ice core data, Kehrwald et al (2008) demonstrated that the Naimona'nyi Glacier at 6,050 meters above mean sea level (m amsl) started losing mass at least since the year 1950. Recent satellite imagery has also revealed a large spread of glacier wastages in the early 21^{st} century (Kääb et al, 2012; Ding et al, 2006). The subsequently changes in runoff have profound and long-term impacts on water resources for the lives and livelihoods of people living within this area and the downstream places of the rivers.

Available water resources in the HKH region are expected to decrease significantly caused by recession of glaciers (Barnett et al, 2005; Immerzeel et al, 2010). Rupper et al (2012) suggested that even if climate remained at the mean values of the period 1980–2000, almost 10% of Bhutanese glacierised area would vanish and melt water flux would drop by as much as 30%. In addition to the drops in streamflow, Immerzeel et al (2010) showed that there would be a shift in runoff seasonality of the Indus and Brahmaputra basins in the period 2046–2065 compared to the period 2000–2007 by the SRES (Special Report on Emissions Scenarios) A1B scenarios. However, these estimations assume a static condition of glaciers without changes in dynamics and extent, which

is not valid for shrinking glaciers.

In general, three steps are involved to assess water resources for the future. Firstly, Global Climate Models (GCMs) are used to generate the future climate at the global scale and a sparse spatial resolution under certain assumptions about CO_2 emissions. The future climate is subsequently downscaled by Regional Climate Models (RCMs) and/or statistical methods to account for temporal and spatial variability in topography and vegetation. Finally, hydrological models convert climate conditions to water volumes at scales suitable for water resources assessment (Xu, 1999; Xu et al, 2005; Kizza et al, 2013). However, most hydrological models do not have a proper representation of glacier (Horton et al, 2006; Stahl et al, 2008).

This study builds on the development a hydro-glacial model, which can simulate retreat of glaciers and runoff process (Li et al, 2015). This model makes use of the HBV model, which computes water balance and glacier mass change, and the Δh-parametrisation, which automatically updates glacier surface elevation and extent according to the mass change calculated by the HBV model. The model has been applied to three basins, one basin in Norway and two Himalayan basins in this study. Results show that the model is able to correctly reproduce major hydrological processes and glacier evolution at a high spatial scale. This research further uses this hydro-glacial model to estimate the future water resources in the Himalayan basins.

Additionally, we desire to use the most recent state of the art of regional climate modelling and contribute to globally available knowledge, especially for water resources management in regions with limited data. Therefore, the World Climate Research Programme (WCRP) Coordinated Regional Downscaling Experiment (CORDEX) project is selected for provision of the future climate. GCMs follow the same experiment protocols and the simulations are downscaled to 14 CORDEX domains by RCMs and they are available for free download. The purpose of the CORDEX project is to produce climate projections for use in impact and adaptation studies (Jacob et al, 2014). However, no research results have been published particularly for South Asia, even though there have been approximately 30 peer-reviewed publications since the year 2005 (CORDEX, 2015).

Therefore, the objectives of this study are twofold. The first is to obtain fair water resource projections for the selected basins by an integrated model including a hydrological model and a glacier retreat model. The second is to evaluate and to use the CORDEX datasets for the Himalaya basins in climate change studies for water resources assessment.

2 Methodology

For assessing climate change impacts on water resources, we run the hydro-glacial model forced by the future climate projections for the two Himalayan basins. The model was calibrated for historical period (Li et al, 2015) and then the runoff scenarios are generated by the hydro-glacial model forced by bias corrected CORDEX data. Finally with population projections, the water resources per capita (Wp) for the future can be estimated.

2.1 Hydro-glacial Model

The hydro-glacial model is based on the HBV model (Bergström, 1976; Beldring et al, 2003) and Δh-parametrisation (Huss et al, 2008). The HBV is a conceptual hydrological model, containing three main routines, i.e. snow, soil and groundwater responses. The glacier surface elevation and extent are modelled by the Δh-parametrisation (Huss et al, 2008, 2010). It describes the varying thinning rates over a glacier: surface elevation changes are smallest in the accumulation area and the largest near the terminus of mountain glaciers. The model has been proved to be able to give similar performance as a 3D ice flow model (Huss et al, 2010), but avoids high requirements in data and computation resources. The HBV model calculates the accumulation and ablation of snow and glacier ice for every grid. The glacier retreat model updates glacier surface elevation and extent in response to the total amount of glacier mass change for a given time interval calculated by the HBV model (Li et al, 2015). The required inputs are precipitation, temperature, surface elevation maps and initial ice thickness. In most places, they can be easily accessed; therefore this hydro-glacial model can be used in large regions.

2.2 Water Resources

Water resources are defined as the annual runoff excluding the environmental water requirement (EWR), which should not consumed by the humanity in order to keep rivers healthy avoid harmful environmental consequence. EWR includes the minimum water requirement of fish and other aquatic species and for maintenance of river channel, wetland and riparian vegetation (Smakhtin et al, 2004). According to Smakhtin et al (2004), EWR can be calculated as a fraction of annual mean runoff. As an initial guess, EWR can be assumed as 30% of annual mean runoff (Hagemann et al, 2013) of observed periods. Assuming EWR would not change significantly in the future, the total available water resources can be calculated for the future.

2.3 Bias Correction

Many a time, RCM outputs have certain bias and it is important to reduce the bias from the RCM results. The most popular approaches are statistical transformations that adjust the probability distribution of modelled results to resemble observations. Following the recommendations of Gudmundsson et al (2012), seven methods (Table 1) are selected and applied to the data for each month. To account for changes of seasons, the previous month and the following month are also used in calibration. The method with the least value of the Mean Absolute Error (MAE) is selected for the target month. The meteorological observations during the period 1981–2005, which is the reference period of the CORDEX project, are used to get the parameter values.

The bias correction methods are good at presenting the mean state of the reference period. However, they may modify climate signals or trends from climate projections (Hempel et al, 2013), whereas the modifications have significant hydrological implications. To avoid this problem, we additionally employ a trend preserving method proposed by Hempel et al (2013). A multiplicative correction and additive correction are respectively used for precipitation and temperature as shown in Equations 1 and 4. Their code in the programming language R (CRAN, 2015a) can be freely downloaded (Li, 2015).

$$\lambda_{\mathrm{p}} = \frac{\bar{P}}{\bar{P}_0} \tag{1}$$

$$\widehat{P} = f(\frac{P}{\lambda_{\mathrm{p}}}) \times \lambda_{\mathrm{p}} \tag{2}$$

where λ_{p} is the precipitation correction factor; P and P_0 are modelled precipitation respectively for the future and reference period. f is the bias correction method.

$$\lambda_{\mathrm{t}} = \bar{T} - \bar{T_0} \tag{3}$$

$$\widehat{T} = f(T - \lambda_{\mathrm{t}}) + \lambda_{\mathrm{t}} \tag{4}$$

where λ_{t} is the temperature correction factor; T and T_0 are modelled precipitation respectively for the future and reference period. f is the bias correction method.

2.4 Hypothesis Test

The changes in annual mean temperature and precipitation are statistically tested by the two-tailed Mann-Whitney test (Bauer, 1972). It is a non-parametric statistical hypothesis test used when the data samples are independent without assuming them to follow the normal distribution (CRAN, 2015b) . The method is based on rank statistics, which indicates that the differences are between medians. It is more widely applicable than independent samples Student's t-test (Wikipedia, 2015). For the reference period, the annual means of 25-years data are derived from the historical simulations of each RCM. For the future, the annual means of 30-years data for each period are derived from simulations of each RCM under assumed CO_2 emission scenarios. The null hypothesis is that the mean does not change and a significant level of 5% is selected for the tests.

2.5 Numerical Criteria

There is a large variety of numerical criteria available to evaluate model simulations in an efficient and reproducible way. However, depending on their formulations, the criteria underscore certain aspects of the set of analysed values. Thus, it is important to combine several complementary

criteria for a comprehensive assessment. In addition, standard and common criteria should be compulsory to conform evaluation and comparison studies. With these considerations, the criteria are carefully chosen to correspond with the series, such as temperature and streamflow. The criteria and their formula are tabulated in Table 2. To rate the bias correction methods, four criteria are used. Among them, *bias* measures the volume error; MAE and normalised mean square error ($NMSE$) measures the absolute error respectively in mean and squared errors. The NSE (Nash and Sutcliffe, 1970) and relative mean error (RME) are used to assess precision of modelling streamflow.

3 Study Area and Data

The Chamkhar Chhu basin at the Kurjey gauging station and the Beas basin at the Bhuntar gauging station are respectively located in eastern and western Himalaya (Fig. 1 and Table 3). The basins are selected to obtain a better understanding of climatic and hydrologic variability cross the Himalaya region. Access to discharge data is another factor to consider. The accesses are restricted by local authorities due to the sensitivity for hydropower and sale of data for commercial purposes. The data used are provided by the project partners and can only be used for research and education purposes within the research group according to agreement.

3.1 Chamkhar Chhu Basin

The Chamkhar Chhu basin is located in central Bhutan as shown in Fig. 1. There are has three branches originating from the glaciers of the Gangkar Punsum region and the glaciers of the Monla Karchung La region. The river is one of the national rivers and it flows south-easterly until joining the Brahmaputra River in India. Above the the Kurjey gauging station, the area is 1,353 km^2 with elevation ranging from 6,653 meters above mean sea level (m amsl) to 2,643 m amsl. The high mountains lie in the northern part and they are mainly occupied by glaciers above 4,000 m amsl. The southern part is lower and occupied by forests.

The Chamkhar Chhu basin belongs to the temperate climatic zone, which is characterised as

cold in winter (-5.65°C in January) and warm and humid in summer (7.43°C in July). The annual precipitation is 1,786 mm/year with a large fractions in the monsoon months. The monsoon starts in June and lasts until early September. It brings warm weather and significant amounts of rainfall. As the monsoon proceeds or retreats, there are four clear seasons, spring (March to May), summer (June to August), autumn (September to November), and winter (December to the following February).

3.2 Beas Basin

The Beas River located in northern India is an important river of the Indus River system (Fig. 1). In total, the Beas River is 470 km long and has a drainage area of 12,916 km^2 (Gupta et al, 1982). As a hydropower hotspot, there are 11 hydroelectric plants projects, out of which three are under construction (SANDRP, 2015). To avoid hydrologic alternations and to have a large study area, the Bhuntar gauging station is selected. This station lies downstream of the confluence with the eastern branch, the Parbati River. During the study period 1997–2005, only the Malana Hydel Scheme with a capacity of 86 megawatt was running. The basin area is 3,202 km^2 with elevations ranging from 6,288 m amsl to 1,055 m amsl. The areas above 4,500 m amsl is are mainly covered by permanent snow and glaciers.

The climate is cold and dry with annual temperature of -1.04°C and annual precipitation of 1,116 mm/year. As influenced by the monsoon, there are four seasons, winter (January to March), pre-monsoon (April to June), monsoon (July to September) and post-monsoon (October to December) (Singh and Kumar, 1997b). Additionally, the monsoon strength is a major indicator of the magnitudes of precipitation and temperature. Compared with in Chamkhar Chhu basin, the air currents originating in the Bay of Bengal are relatively weak after striking east Himalaya and a long westward travel (Singh and Kumar, 1997a).

3.3 Data

The initial ice thickness is a part of the global dataset produced by Huss and Farinotti (2012) using a method based on glacier mass turnover and principles of ice-flow mechanics (Farinotti

et al, 2009). Required input data are DEMs and glacier outlines. For each individual glacier ice thickness distribution is determined for about the year 2000 depending on the date of the utilised glacier inventory data (Pfeffer et al, 2014). The starting date for modelling is mainly determined by the observation period of the meteorological data and is set to 1^{st} September, 1993.

The observed precipitation and temperature are measured by in situ meteorological stations. As shown in Fig. 1, seven stations are used in the Chamkhar Chhu basin and three in the Beas basin. The daily mean temperature is calculated as the mean of observed daily maximum and minimum temperature. For the Chamkhar Chhu basin, measurements of the stations did not start at the same time (Table 4); therefore, the interpolation for each grid only takes the available observations. For the Beas basin, all temperature observations after 19^{st}, September 2005 are missing and they are filled by the RCMs simulations.

In the CORDEX data portal, two RCMs at the daily time step and in regular grids for South Asia are available. They are respectively produced by the Swedish Meteorological and Hydrological Institute, Sweden and the Max Planck Society, Germany. The Swedish datasets are generated by the EC-Earth and the Rossby Center Regional Climate model (RCA4) (Samuelsson et al, 2011; SMHI, 2015). The German datasets are generated by the Max Planck Society for Meteorology-Earth System Model (MPI-ESM) and the most recent hydrostatic REMO (Jacob et al, 2012, 2014).

The data are produced by downscaling the new Coupled Model Intercomparison Project Phase 5 (CMIP5) global climate projections and the new three Representative Concentration Pathways (Rcps) to a spatial resolution of 0.44°, roughly 50 km (Teichmann et al, 2013). The historical climate simulations for the period from 1950 to 2005 are driven by observed anthropogenic forcings. The large-scale forcing of the RCMs is taken from the global reanalysis data of ERA-Interim at a horizontal resolution of approximately 0.7°. The climate projections are driven by projected anthropogenic forcings according to Rcp2.6, Rcp4.5 and Rcp8.5, which respectively prescribe the low, middle, and high concentrations (Teichmann et al, 2013). The natural forcings are the same as in the historical experiment, except for volcanic aerosols, which are set to zero. Other

anthropogenic and natural forcings such as ozone and aerosols are kept constant (Jacob et al, 2012). Hydrological simulations for the period 2006–2100 are forced by the climate projections.

Population estimations at a catchment scale are not available and have to be estimated from national population projections. A national population estimation and projection for the period 1960–2050 can be freely downloaded from World Bank (2014). This dataset was produced in the year 2012 and there is no error for the following year (World Bank, 2014). However, the projections for the year 2014 were 2.5% and 4.4% higher than the estimations by CIA (2015), respectively for India and Bhutan. Population distribution maps at a spatial resolution of 1 km (Balk et al, 2006) are available for the years, 1990, 1995 and 2000. The quality of maps are difficulty to quantify, particularly in the Himalayan basins. The correlation between the maps and the observations reached 0.6 in Cambodia and Vietnam (Gaughan et al, 2013) and the map quality of two Himalayan basins are suspected to be worse due to their remote locations and less development.

4 Results

4.1 Historical Simulations

In general, the hydro-glacial model is able to reproduce the daily runoff series with high model efficiency criteria (Table 5), particularly for the Chamkhar Chhu basin. For this basin, the model is calibrated for the period 1998–2004 and validated for the period 2005–2008. The NSE values are up to 0.85 and absolute RME values are not more than 10% for both calibration and validation modes. For the Beas basin, the model is calibrated for the period 1997–2002 and validated for the period 2003–2005 based on the observed data. The NSE values are 0.65 and 0.73 respectively for calibration and validation.

4.2 Bias Correction

The performance of the bias correction methods is shown in Fig. 3. For precipitation, the methods are very similar for precipitation in terms of MAE and the mean of MAE is 4.6 mm/day with

the lowest by $M6$ (scale, 4.53 mm/day) and the highest by $M3$ (linear, 4.66 mm/day). However, these methods give different inefficiencies in bias correcting temperature. The lowest error is given by $M3$ (linear, 2.29°C) followed by $M1$ (empirical, 2.30°C) and the highest is given by $M7$ (power, 5.73°C). Fig. 4 shows comparison between the final downscaled series and the original grid series of the RCMs. For both precipitation and temperature, the bias correction significantly reduce the differences between the in situ observations and the simulations of the RCMs. The improvements are found in variance shown by sd, total volume shown by $bias$ and absolute errors in mean (MAE) and square ($NMSE$).

4.3 Future Climate

The changes of temperature at every station are presented in Fig. 5. It shows that the future periods are much warmer than the control period and the warming effects increase with more emissions and in the further future except under Rcp2.6. The statistics of the Mann-Whitney test suggest that all the changes are significant except at the Torngsa station by RCA4 under Rcp8.5 and Rcp4.5 in the period 2011–2040. Similarly, the changes of precipitation are shown in Fig. 6. Among the 180 tests, only 49 tests are significant and but there are no clear patterns against emission or time. The wettest conditions are given by RCA4 under Rcp8.5 except at the Bhuntar and Manali stations in the Beas basin. At the same stations, the differences between the wettest and driest do not increase with time whereas they become larger at other stations.

The areal mean precipitation and temperature in ten-years moving average (MA) are depicted in Fig. 7. It shows the similar information by the last two figures. Annual temperature increases under Rcp4.5 and Rcp8.5, as well as Rcp2.6 before the 2050s. Under Rcp8.5, the changes of annual temperature are approximately +0.05 °C/year and they are substantially warmer than under Rcp4.5. For precipitation, there are large differences between the two RCMs and it is difficult to say which is more reliable. At the end of the 21^{st} century, the wettest and driest conditions are respectively by given RCA4 and REMO under Rcp8.5. Generally, the predictions indicate that the Chamkhar Chhu basin will become wetter and the Beas basin will get drier compared to their respective baseline periods.

4.4 Glaciers Change

The changes of glaciers are simultaneously affected by changes of temperature and precipitation. The annual mean temperature is above the melting point and much warmer than the Beas basin. With the increase in temperature, the glaciers of the Chamkhar Chhu basin are predicted to continuously lose mass before the 2050s until they disappear or reduce to a small size in the 2050s (Fig. 8). Among the six projections, the fastest mass loss is given by REMO under Rcp8.5 and the slowest is given by RCA4 under Rcp8.5, but their differences are modest. In the Beas basin, the glaciers respond very differently. They are likely to experience mass loss before the 2060s but the estimates by two RCMs under three Rcps show large variations. Afterwards, the glaciers are predicted to grow under Rcp2.6 and Rcp4.5 but may experience mass loss under Rcp8.5.

Glaciers have significant influence on runoff both the total amount and its temporal distribution. As shown in Fig. 8, the glaciers of the Chamkhar Chhu basin are predicted to continuously lose mass before the 2050s until they disappear or reduce to a small size in the 2050s. Fig. 9 compares the monthly precipitation and runoff for two periods, from 2010 to 2049 and from 2050 to 2089. Runoff of the later period has a smaller total amount, even suggested by RCA4 that more precipitation is projected. The changes are very notable in July and August, when the ice melting rates are the highest.

Additionally, we compared monthly mean runoff for selected two-decades in Fig. 10. It shows that there is a large variety among the different periods as well as between the two RCMs. Similarly the changes in the summer months are more significant than in the winter months. Additionally, the differences among the Rcps get larger against time and the differences between the RCMs get larger against time and with more CO_2 emission. Therefore, the largest change ranges are given under Rcp8.5.

4.5 Water Resources

Wp depends on both the total available water and population growth. Therefore, we estimated basin population and available water resources and the latter is estimated by excluding mean EWR from the total water resources. For population, a linear relationship is found between the basin population of the grid data (Balk et al, 2006) and the country population (World Bank, 2014) for three years, 1990, 1995 and 2000. The errors of this linear function are tabulated in Table 6. The maximum RME is 7.9% for the Chamkhar Chhu basin, whereas it is only 0.1% for the Beas basin. The basin population projections for the period 2000–2050 are plotted in Fig. 11. The basin population is predicted to continuously grow in the period 2000–2050. The population in the Chamkhar Chhu basin almost doubles and in the Beas basin, the population increases by 50%.

Considering the possible inaccuracy in the used population data, we additionally present the ranges if there are ±20% errors in Fig. 11. Their difference accounts for 40% of the total population and it is very noteworthy when the total population is large. For example, the differences are 153,878 persons in the Beas basin in the year 2050. Consequently, the uncertainties is accumulating in estimations of the available water resources per capita.

As shown in Fig. 12, there are significant decreases with considerable fluctuations by all projections for the two basins. In the Chamkhar Chhu basin, Wp will drop from approximately 137 m^3/year in the 2010s to 78 m^3/year in the 2040s, whereas it is predicted to decrease from 21 m^3/year to 14 m^3/year in the Beas basin. Effects of climate change and population growth are split by assuming that the population, conservatively, would not grow after the period 2011–2015 and the remaining is caused by climate change. The water declines are respectively reduced to 34 m^3/year in the Chamkhar Chhu basin and 4 m^3/year in the Beas basin. Therefore, the population growth is approximately responsible for 42% in the Chamkhar Chhu basin and 43% in the Beas basin. The two basins are facing absolute water scarcity, less than 500 m^3/year (Schewe et al, 2014) and the water scarcity will intensify in the future.

The ranges of Wp caused by RCMs, Rcps and possible population inaccuracy are given in Table 7. The differences among RCMs and Rcps count less than 30% of the mean of Wp. They range from 12.0% (14.8 m^3/year) to 35.7% (36.2 m^3/year) in the Chamkhar Chhu basin and from 11.4% (1.9 m^3/year) to 43.5% (9.0 m^3/year) in the Beas basin. However, when considering ±20% inaccuracy in population estimations, the uncertainties mount up to 68% in the Chamkhar Chhu basin and 73% in the Beas basin. For the period 2016–2020 in the Beas basin, the best water resource scenario is given by REMO under Rcp4.5 and the worst by RCA4 under Rcp4.5. The differences between the best with 80% population estimation and the worst with 120% population estimation reach 18 m^3/year and account for 86.6% of the mean of six the estimations. The uncertainties caused by ±20% population inaccuracy are much more than caused by RCMs and Rcps.

5 Discussions

5.1 Uncertainties

Uncertainties are suspected in the data used for calibrating model parameters and the algorithms of the glacier retreat model (Li et al, 2015). The data related uncertainties include the sparse distribution of the meteorological stations and the short length of the observed time series as well as the initial ice thickness. Though the model performance for the historical periods is satisfying, these uncertainties are suspected to be significant in long term simulation.

For the estimation of Wp, we used the leftover streamflow of EWR. Actually, both the Chamkhar Chhu and the Beas basins are located in upstream of a large watershed. The domestics living in the basins should not deplete the total runoff. Additionally, Pastor et al (2014) compared five environmental flow methods and they showed that Wp calculated by Smakhtin et al (2004) method was lower than the locally calculated values for rivers with variable flows. Moreover, the value used (30%) is a conservative estimation compared with the global average, 37%. The available water resources would be less when considering reservoir storages, flooding and streamflow seasonality.

For predicting water resources per capita, population estimations introduce additional uncertainties. Prediction of population growth for a country or region involves large uncertainty, particularly for small and developed areas (Balk et al, 2006). Moreover, population and runoff are calculated at different scales. Runoff is estimated for a catchment whereas population is counted for an administrative region. The discrepancies in scales may lead to inaccuracy in projection of the future water resources per capita.

5.2 Implications

The two RCMs give similar results for temperature but show large differences in estimation of precipitation under different CO_2 scenarios. For example, the changes of temperature are approximately +0.05 °C/year under Rcp8.5, which is similar to the global average temperature trends (Rogelj et al, 2012). The climate under Rcp8.5 is substantially warmer than under Rcp4.5, which is similar to the EUROCORDEX for the Europe (Jacob et al, 2014). However, for precipitation, no evidence shows which RCM is more reasonable. The possible reason is the two RCMs have higher skills in reproducing the temperature features than in precipitation (Chaturvedi et al, 2012). The performance of the RCMs in reproducing precipitation is additionally hampered by the lack of observational data (Jacob et al, 2012).

The response of a glacier to climate change is highly related to its location in the Himalaya region. The glacier AX010 (maximum elevation is 5,360 m amsl) in Nepal was predicted to disappear by the year 2060 even under the climate condition of the period 1992–1996 (Fujita et al, 2001). However, the Langtang Lirung glacier extending from 3,800 up to 7,234 m amsl was predicted to lose 75% of its area of the year 2000 by the year 2088 under the SRES A1B scenario (Immerzeel et al, 2012). The Chamkhar Chhu basin located in eastern Himalaya is warmer and wetter than the Beas basin located in western Himalaya. The glaciers in Bhutan are losing mass due to the climate change (Bajracharya et al, 2014) and the wastage rates are expected to increase in the future (Rupper et al, 2012; Kääb et al, 2012). However, in the Karakoram and western Himalaya, the thinning rates are very small and some glaciers are even growing (Kääb et al, 2012). As shown by Azam et al (2012), the Chhota Shigri glacier in western Himalaya

gained mass in the years 2008 and 2009. Both temperature and precipitation play important roles in glacier responses to climate change.

Fig. 8 shows that the volume of the glaciers in the Chamkhar Chhu basin linearly decreased with time, which means a constant contribution to runoff. This is different from conclusion of Singh and Kumar (1997b) that glacier runoff increased linearly with temperature in the Spiti River basin, which is a part of the Indus River system. This is likely because they did not consider changes in glacier extent and the future climate was constructed by a delta change method. However, glaciers shrink with mass loss and the total runoff from glacierised area become less with decreasing area when the specific mass balance is constant. Additionally, Akhtar et al (2008) showed that the delta change method was not suitable for the HKH region due to the poor observed data. For long-term runoff simulation in basins with considerable glacier coverage, proper presentation of glaciers in hydrological models is a key factor for reliability of results.

6 Conclusions

To assess the water resources for the future, we used a hydro-glacial model for two basins respectively located in eastern and western Himalaya with considerable glacierised coverage. The model was forced by six downscaled CORDEX datasets following the CMIP5 protocols and new CO_2 scenarios. Changes of precipitation and temperature were investigated as well as the glacier effects on runoff. Excluding EWR and using a proper population projection method, we eventually predicted Wp.

There are high consistencies between the two RCMs in terms of annual temperature for the three CO_2 scenarios. The warming effetcs are more obvious with more emissions. Under Rcp8.5, the changes in annual air temperature are around $+0.05°C$/year for the period 2010–2100. However, the increasing trends under Rcp2.6 will only last to the 2050s. For the same period, most projections do not show significant trends in annual precipitation and the changes in annual precipitation are not consistent.

In the Chamkhar Chhu basin, the glaciers are predicted to disappear or reduce to a very small size in the 2050s, whereas the glaciers in the Beas basin are predicted to lose mass before the 2060s. Afterwards they are predicted to accumulate under Rcp2.6 and Rcp4.5 or lose mass at a high rate under Rcp8.5. Though precipitation is the largest contributor to streamflow, the impacts of glaciers on runoff are noteworthy.

For water resources, all projections reveal significantly less water which jointly results due to population growth and climate change. Wp are predicted to drop from 137 m^3/year in the 2010s down to 78 m^3/year in the 2040s in the Chamkhar Chhu basin and from 21 m^3/year to 14 m^3/year in the Beas basin. The population growth is responsible for roughly 40% of the water declines. In interpretation of the results, it is important to keep uncertainties in mind, which is the same for any other research for climate change impacts. Though various modelling efforts have made a big progress in the HKH region, a highly accurate assessment remains largely unaccomplished.

Acknowledgements We thank Department of Hydromet Services, Ministry of Economic Affairs, Royal Government of Bhutan for provision of the data of the Chamkhar Chhu basin. Thanks also go to Norwegian Water Resources and Energy Directorate for providing computational facility, and helps in Geographic Information System, and the Bhakra Beas Management Board (India) for providing the data of the Beas basin and Dr. Huss in Department of Geosciences, University of Fribourg, Switzerland for provision of glacier data.

Conflict of Interest

No conflict of interest.

References

Akhtar M, Ahmad N, Booij M (2008) The impact of climate change on the water resources of Hindukush—Karakorum—Himalaya region under different glacier coverage scenarios. Journal of Hydrology 355(1-4):148 – 163, DOI 10.1016/j.jhydrol.2008.03.015

Azam MF, Wagon P, Ramanathan A, Vincent C, Sharma P, Arnaud Y, Linda A, Pottakkal JG, Chevallier P, Singh VB, Berthier E (2012) From balance to imbalance: a shift in the dynamic

behaviour of Chhota Shigri glacier, western Himalaya, India. Journal of Glaciology 58(208):315 – 324, DOI 10.3189/2012JoG11J123

Bajracharya SR, Maharjan SB, Shrestha F (2014) The status and decadal change of glaciers in Bhutan from the 1980s to 2010 based on satellite data. Annals of Glaciology 55(66):159 – 166, DOI 10.3189/2014AoG66A125

Balk D, Deichmann U, Yetman G, Pozzi F, Hay S, Nelson A (2006) Determining Global Population Distribution: Methods, Applications and Data 62:119 – 156, DOI 10.1016/S0065-308X(05)62004-0

Barnett TP, Adam JC, Lettenmaier DP (2005) Potential impacts of a warming climate on water availability in snow-dominated regions. Nature 438(7066):303 – 309, DOI 10.1038/nature04141

Bauer DF (1972) Constructing Confidence Sets Using Rank Statistics on JSTOR. Journal of the American Statistical Association 67(39):687 – 690, URL http://www.jstor.org/stable/2284469?seq=1#page_scan_tab_contents

Beldring S, Engeland K, Roald LA, Sælthun NR, Voksø A (2003) Estimation of parameters in a distributed precipitation-runoff model for Norway. Hydrology and Earth System Sciences 7(3):304 – 316, DOI 10.5194/hess-7-304-2003

Bergström S (1976) Development and application of a conceptual runoff model for Scandinavian catchments. Tech. Rep. 07, Swedish Meteorological and Hydrological Institute, URL http://books.google.no/books?id=vRyeQAAACAAJ

Chaturvedi RK, Joshi J, Jayaraman M, Bala G, Ravindranath N (2012) Multi-model climate change projections for India under representative concentration pathways. Current Science 103(7):791 – 802, URL http://wcrp-cordex.ipsl.jussieu.fr/images/pdf/peer_rev_pub/2012_Chaturvedi.pdf

CIA (2015) The World Factbook. URL https://www.cia.gov/library/publications/resources/the-world-factbook/docs/contact.html

CORDEX (2015) Peer reviewed publications. URL http://wcrp-cordex.ipsl.jussieu.fr/index.php/cordex-peer-review-publications

CRAN (2015a) An Introduction to R. URL http://cran.r-project.org/doc/manuals/R-intro.html#The-array_0028_0029-function

CRAN (2015b) Wilcoxon Rank Sum and Signed Rank Tests. URL https://stat.ethz.ch/R-manual/R-patched/library/stats/html/wilcox.test.html

Ding Y, Liu S, Li J, Shangguan D (2006) The retreat of glaciers in response to recent climate warming in western China. Annals of Glaciology 43(1):97 – 105, DOI 10.3189/172756406781812005

Farinotti D, Huss M, Bauder A, Funk M, Truffer M (2009) A method to estimate the ice volume and ice-thickness distribution of alpine glaciers. Journal of Glaciology 55(191):422 – 430, DOI 10.3189/002214309788816759

Fujita K, Kadota T, Rana B, Kayastha RB, Ageta Y (2001) Shrinkage of Glacier AX010 in Shrong region, Nepal Himalayas in the 1990s. Bulletin of Glaciological Research 18:51 – 54, URL http://www.seppyo.org/bgr/pdf/18/BGR18P51.PDF

Gaughan AE, Stevens FR, Linard C, Jia P, Tatem AJ (2013) High resolution population distribution maps for Southeast Asia in 2010 and 2015. PloS one 8(2):e55,882, DOI 10.1371/journal.pone.0055882

Gudmundsson L, Bremnes JB, Haugen JE, Engen-Skaugen T (2012) Technical Note: Downscaling RCM precipitation to the station scale using statistical transformations—a comparison of methods. Hydrology and Earth System Sciences 16(9):3383 – 3390, DOI 10.5194/hess-16-3383-2012

Gupta R, Duggal A, Rao S, Sankar G, Singhal B (1982) Snow-cover area vs. snowmelt runoff relation and its dependence on geomorphology?—A study from the Beas catchment (Himalayas, India). Journal of Hydrology 58(3-4):325 – 339, DOI 10.1016/0022-1694(82)90042-7

Hagemann S, Chen C, Clark DB, Folwell S, Gosling SN, Haddeland I, Hanasaki N, Heinke J, Ludwig F, Voss F, Wiltshire AJ (2013) Climate change impact on available water resources obtained using multiple global climate and hydrology models. Earth System Dynamics 4(1):129 – 144, DOI 10.5194/esd-4-129-2013

Hempel S, Frieler K, Warszawski L, Schewe J, Piontek F (2013) A trend-preserving bias correction—the ISI-MIP approach. Earth System Dynamics 4(2):219 – 236, DOI 10.5194/esd-4-219-2013

Horton P, Schaefli B, Mezghani A, Hingray B, Musy A (2006) Assessment of climate-change impacts on alpine discharge regimes with climate model uncertainty. Hydrological Processes

20(10):2091 – 2109, DOI 10.1002/hyp.6197

Huss M, Farinotti D (2012) Distributed ice thickness and volume of all glaciers around the globe. Journal of Geophysical Research: Earth Surface 117(F4):F04,010, DOI 10.1029/2012JF002523

Huss M, Farinotti D, Bauder A, Funk M (2008) Modelling runoff from highly glacierized alpine drainage basins in a changing climate. Hydrological processes 22(19):3888 – 3902, DOI 10.1002/hyp.7055

Huss M, Jouvet G, Farinotti D, Bauder A (2010) Future high-mountain hydrology: a new parameterization of glacier retreat. Hydrology and Earth System Sciences 14(5):815 – 829, DOI 10.5194/hess-14-815-2010

Immerzeel WW, van Beek LPH, Bierkens MFP (2010) Climate Change Will Affect the Asian Water Towers. Science 328(5984):1382 – 1385, DOI 10.1126/science.1183188

Immerzeel WW, van Beek L, Konz M, Shrestha A, Bierkens M (2012) Hydrological response to climate change in a glacierized catchment in the Himalayas. Climatic Change 110(3-4):721 – 736, DOI 10.1007/s10584-011-0143-4

Jacob D, Elizalde A, Haensler A, Hagemann S, Kumar P, Podzun R, Rechid D, Remedio AR, Saeed F, Sieck K, Teichmann C, Wilhelm C (2012) Assessing the Transferability of the Regional Climate Model REMO to Different COordinated Regional Climate Downscaling EXperiment (CORDEX) Regions. Atmosphere 3(1):181 – 199, DOI 10.3390/atmos3010181

Jacob D, Petersen J, Eggert B, Alias A, Christensen OB, Bouwer L, Braun A, Colette A, Deque M, Georgievski G, Georgopoulou E, Gobiet A, Menut L, Nikulin G, Haensler A, Hempelmann N, Jones C, Keuler K, Kovats S, Kroner N, Kotlarski S, Kriegsmann A, Martin E, van Meijgaard E, Moseley C, Pfeifer S, Preuschmann S, Radermacher C, Radtke K, Rechid D, Rounsevell M, Samuelsson P, Somot S, Soussana JF, Teichmann C, Valentini R, Vautard R, Weber B, Yiou P (2014) EURO-CORDEX: new high-resolution climate change projections for European impact research. Regional Environmental Change 14(2):563 – 578, DOI 10.1007/s10113-013-0499-2

Joshi G (2007) Major Cities of Hindu Kush Himalayan (HKH) Region. URL `http://rds.icimod.org/Home/DataDetail?metadataId=3434&searchlist=True`

Joshi G (2008) Major River Systems of Hindu Kush Himalayan (HKH) Region. URL `http://rds.icimod.org/Home/DataDetail?metadataId=2956&searchlist=True`

Joshi G (2011) Digital Elevation Model of Hindu Kush Himalayan (HKH) Region. URL http://rds.icimod.org/Home/DataDetail?metadataId=8744&searchlist=True

Kääb A, Berthier E, Nuth C, Gardelle J, Arnaud Y (2012) Contrasting patterns of early twenty-first-century glacier mass change in the Himalayas. Nature 488(7412):495 – 498, DOI 10.1038/nature11324

Kehrwald NM, Thompson LG, Tandong Y, Mosley-Thompson E, Schotterer U, Alfimov V, Beer J, Eikenberg J, Davis ME (2008) Mass loss on Himalayan glacier endangers water resources. Geophysical Research Letters 35(22):L22,503, DOI 10.1029/2008GL035556

Kizza M, Guerrero JL, Rodhe A, Xu CY, Ntale HK (2013) Modelling catchment inflows into Lake Victoria: regionalisation of the parameters of a conceptual water balance model. Hydrology Research 44(5):789 – 808, DOI 10.2166/nh.2012.152

Li H (2015) Bias Correction with Trend Conserving. URL http://folk.uio.no/hongli/Pub/QmapTrendBiasCorrection.r

Li H, Beldring S, Xu CY, Huss M, Melvold K, Jain S (2015) Integrating a glacier retreat model into a hydrological model—results for three glacierised catchments. Journal of Hydrology DOI 10.1016/j.jhydrol.2015.05.017

Nash J, Sutcliffe J (1970) River flow forecasting through conceptual models part I—A discussion of principles. Journal of Hydrology 10(3):282 – 290, DOI 10.1016/0022-1694(70)90255-6

Pastor AV, Ludwig F, Biemans H, Hoff H, Kabat P (2014) Accounting for environmental flow requirements in global water assessments. Hydrology and Earth System Sciences 18(12):5041 – 5059, DOI 10.5194/hess-18-5041-2014

Pfeffer WT, Arendt AA, Bliss A, Bolch T, Cogley JG, Gardner AS, Hagen JO, Hock R, Kaser G, Kienholz C, Miles ES, Moholdt G, Mölg N, Paul F, Radić V, Rastner P, Raup BH, Rich J, Sharp MJ (2014) The Randolph Glacier Inventory: a globally complete inventory of glaciers. Journal of Glaciology 60(221):537, DOI 10.3189/2014JoG13J176

Rogelj J, Meinshausen M, Knutti R (2012) Global warming under old and new scenarios using IPCC climate sensitivity range estimates. Nature Climate Change 2(4):248 – 253, DOI 10.1038/nclimate1385

Rupper S, Schaefer JM, Burgener LK, Koenig LS, Tsering K, Cook ER (2012) Sensitivity and response of Bhutanese glaciers to atmospheric warming. Geophysical Research Letters 39(19),

DOI 10.1029/2012GL053010

Samuelsson P, Jones CG, Willén U, Ullerstig A, Gollvik S, Hansson U, Jansson C, Kjellstrom E, Nikulin G, Wyser K (2011) The Rossby Centre Regional Climate model RCA3: model description and performance. Tellus A 63(1):4 – 23, DOI 10.1111/j.1600-0870.2010.00478.x

SANDRP (2015) Hydro Electric Projects in Beas River Basin. URL http://sandrp.in/basin_maps/Hydropower_Projects_in_Beas_Basin.pdf

Schewe J, Heinke J, Gerten D, Haddeland I, Arnell NW, Clark DB, Dankers R, Eisner S, Fekete BM, Colón-González FJ, Gosling SN, Kimk H, Liu X, Masakim Y, Portmann FT, Satoh Y, Stacke T, Tang Q, Wada Y, Wisser D, Albrecht T, Frieler K, Piontek F, Warszawski L, Kabat P (2014) Multimodel assessment of water scarcity under climate change. Proceedings of the National Academy of Sciences 111(9):3245 – 3250, DOI 10.1073/pnas.1222460110

Singh P, Kumar N (1997a) Effect of orography on precipitation in the western Himalayan region. Journal of Hydrology 199(1-2):183 – 206, DOI 10.1016/S0022-1694(96)03222-2

Singh P, Kumar N (1997b) Impact assessment of climate change on the hydrological response of a snow and glacier melt runoff dominated Himalayan river. Journal of Hydrology 193(1-4):316 – 350, DOI 10.1016/S0022-1694(96)03142-3

Smakhtin V, Revenga C, Döll P (2004) A Pilot Global Assessment of Environmental Water Requirements and Scarcity. Water International 29(3):307 – 317, DOI 10.1080/02508060408691785

SMHI (2015) Rossby Centre regional atmospheric model, RCA4. URL http://www.smhi.se/en/research/research-departments/climate-research-rossby-centre2-552/rossby-centre-regional-atmospheric-model-rca4-1.16562

Stahl K, Moore RD, Shea JM, Hutchinson D, Cannon AJ (2008) Coupled modelling of glacier and streamflow response to future climate scenarios. Water Resources Research 44(2):W02,422, DOI 10.1029/2007WR005956

Teichmann C, Eggert B, Elizalde A, Haensler A, Jacob D, Kumar P, Moseley C, Pfeifer S, Rechid D, Remedio AR, Ries H, Petersen J, Preuschmann S, Raub T, Saeed F, Sieck K, Weber T (2013) How Does a Regional Climate Model Modify the Projected Climate Change Signal of the Driving GCM: A Study over Different CORDEX Regions Using REMO. Atmosphere 4(2):214 – 236, DOI 10.3390/atmos4020214

Wikipedia (2015) MannWhitney U test. URL http://en.wikipedia.org/wiki/Mann%E2%80%93Whitney_U_test

World Bank (2014) Health Nutrition and Population Statistics: Population estimates and projections. URL http://databank.worldbank.org/data/views/variableselection/selectvariables.aspx?source=health-nutrition-and-population-statistics:-population-estimates-and-projections

Xu CY (1999) From GCMs to river flow: a review of downscaling methods and hydrologic modelling approaches. Progress in Physical Geography 23(2):229 – 249, DOI 10.1177/030913339902300204

Xu CY, Widén E, Halldin S (2005) Modelling hydrological consequences of climate change—Progress and challenges. Advances in Atmospheric Sciences 22(6):789 – 797, DOI 10.1007/BF02918679

Figures

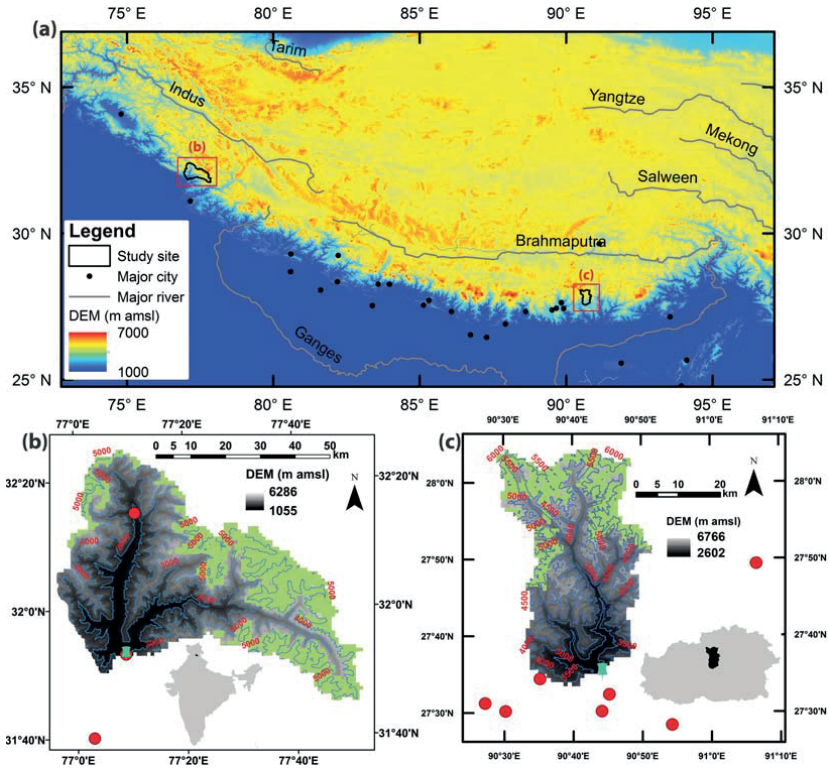

Fig. 1: (a) Map of the Himalaya showing the elevations (DEM), major rivers and major cities (Joshi, 2007, 2008, 2011) and the locations of the study sites. (b) The Beas basin at the Bhuntar station. (c) The Chamkhar Chhu basin at the Kurjey station. The range of DEM in (a) is assigned to give a better presentation rather than the minimum and maximum for the displaying area. In (b) and (c), the light green indicates glacier covered area. The contours are elevations (m amsl). The red dots denote meteorological stations measuring precipitation and temperature and the cyan pins mark the locations of the discharge gauging stations.

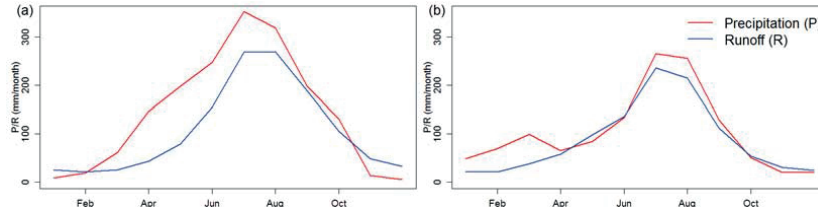

Fig. 2: Monthly mean precipitation and runoff of (a) the Chamkhar Chhu basin and (b) the Beas basin during their respective historical periods.

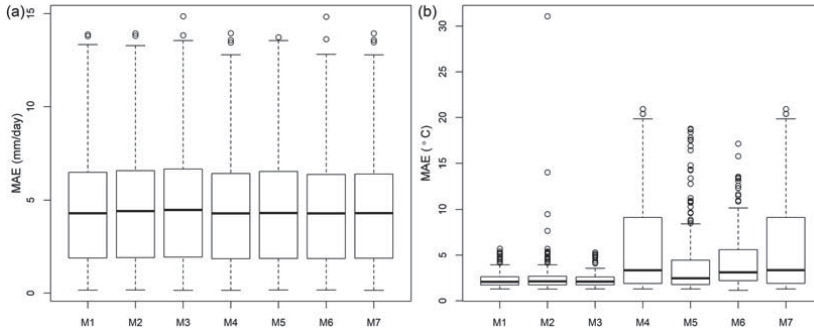

Fig. 3: Comparison of the bias correction methods for (a) precipitation and (b) temperature. A plotted value is MAE between all observations of an individual station and a corrected RCM series for each month.

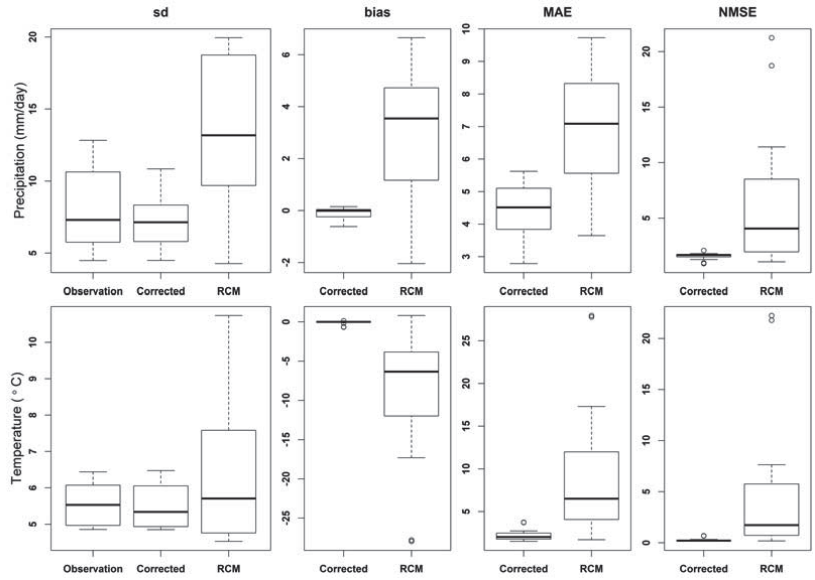

Fig. 4: Comparison of the original RCM series and the corrected series for precipitation and temperature. A plotted *sd* value is computed from a series of observations, the RCM grid or the corrected RCM series for an individual station. A value of the remaining criteria is calculated according to its corresponding equation in Table 2 between the observation series and the RCM series or the corrected series of an individual station.

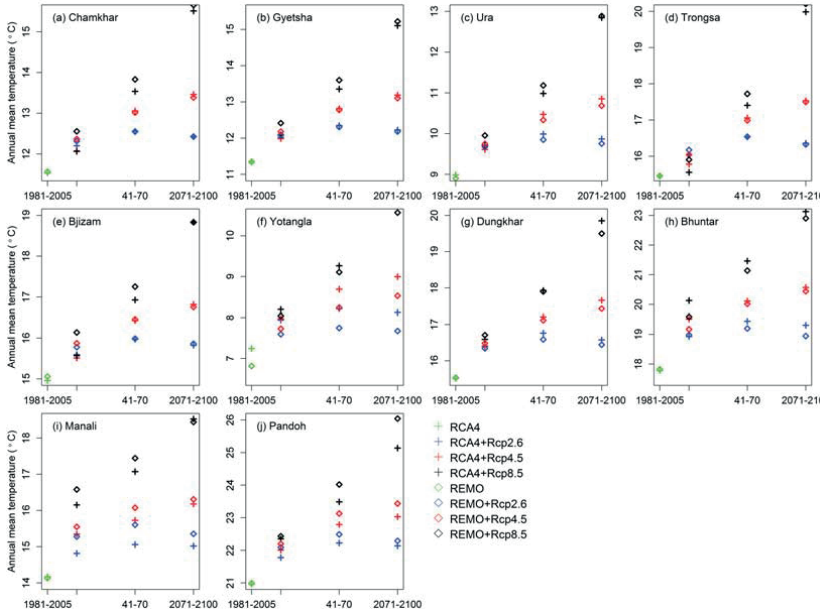

Fig. 5: Changes of annual mean temperature. All changes except at the Trongsa station in the period 2011–2040 under Rcp8.5 and Rcp4.5 by RCA4 are significant by the Mann-Whitney test at the 0.05 significant level.

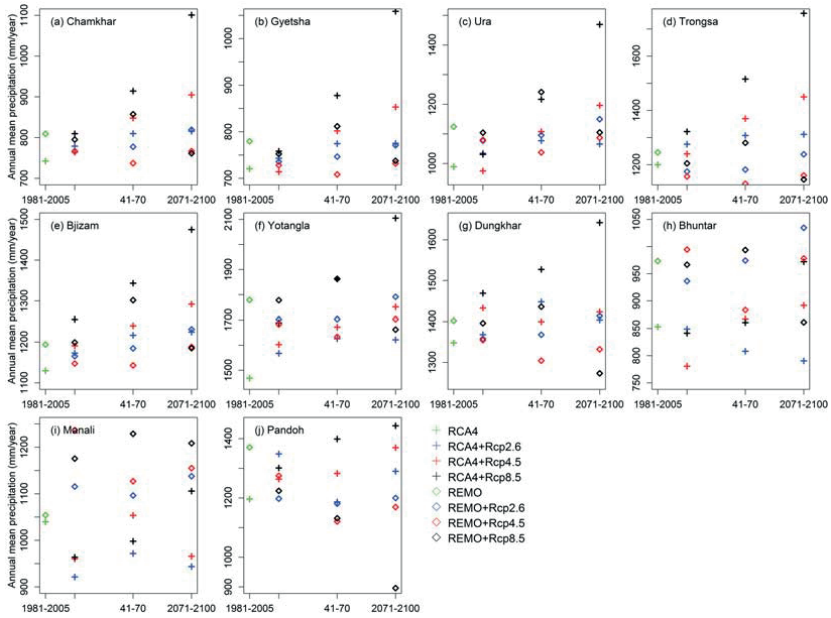

Fig. 6: Changes of annual mean precipitation. Among the 180 test, 49 of the changes are not significant by the Mann-Whitney test at the 0.05 significant level.

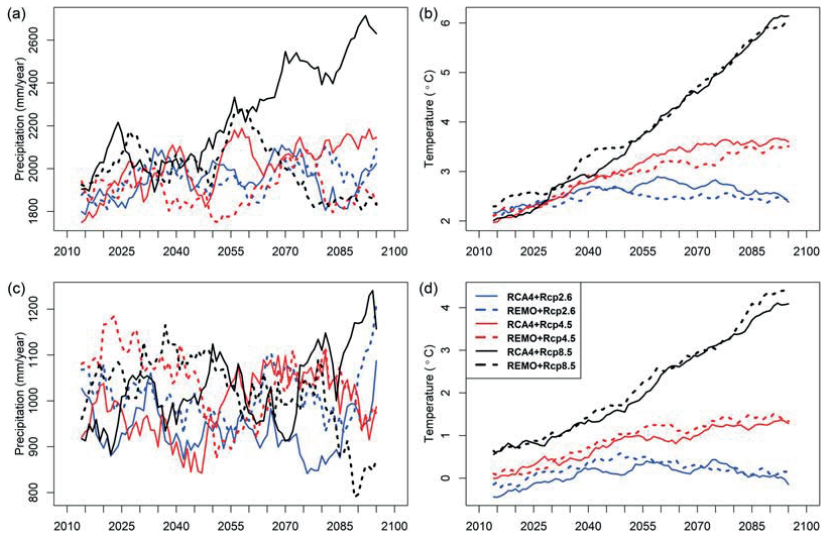

Fig. 7: Ten-year moving average of annual precipitation and temperature. (a) Precipitation of the Chamkhar Chhu basin; (b) Temperature of the Chamkhar Chhu basin; (c) Precipitation of the Beas basin; (d) Temperature of the Beas basin.

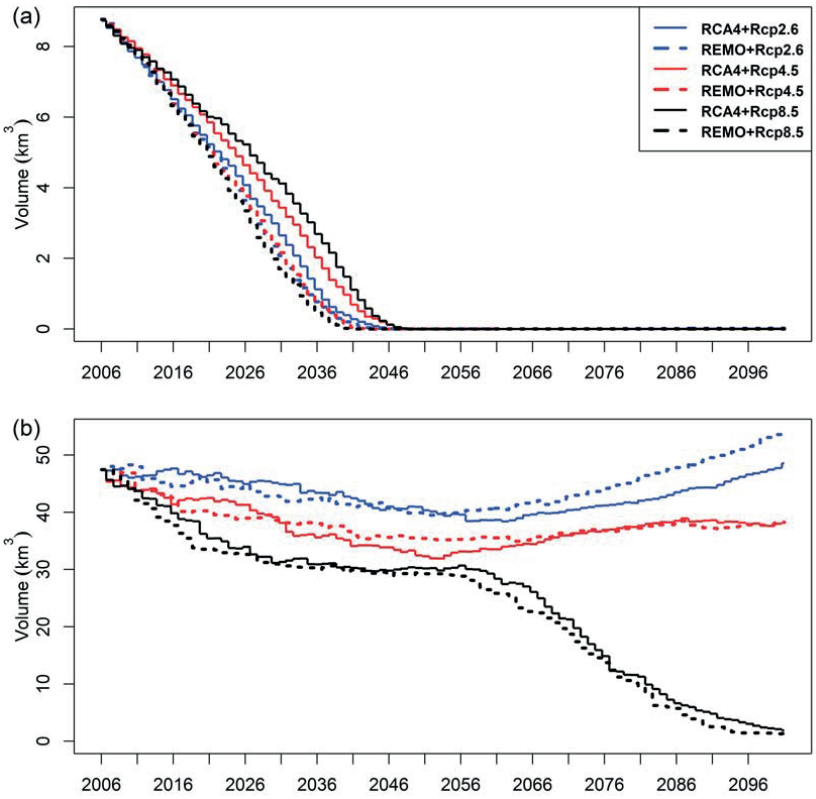

Fig. 8: Simulated Changes of glacier volumes in (a) the Chamkhar Chhu basin and (b) the Beas basin.

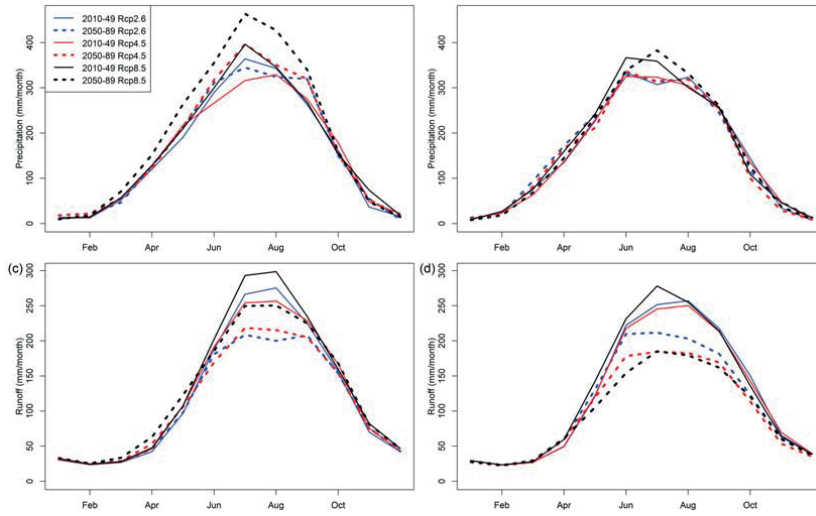

Fig. 9: Monthly mean precipitation and runoff of the Chamkhar Chhu basin in the periods 2010–2049 and 2050–2089. (a) Precipitation by RCA4 (b) Precipitation by REMO (c) Runoff by RCA4 (d) Runoff by REMO.

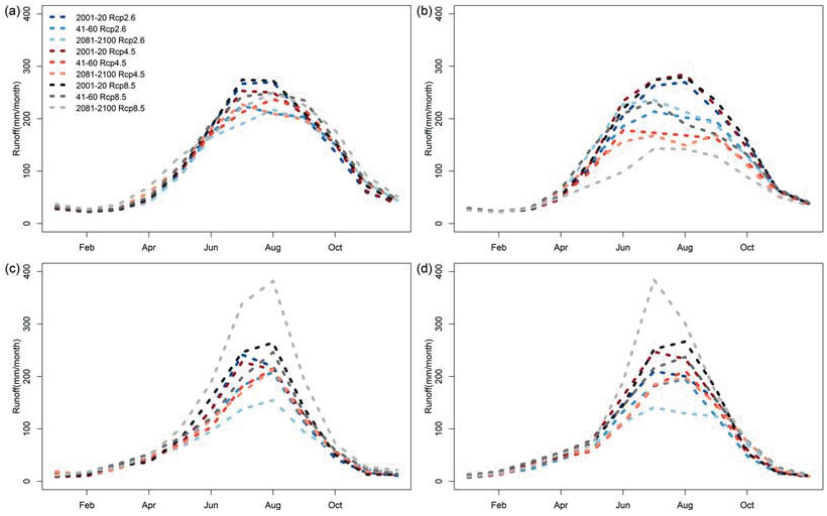

Fig. 10: Monthly mean runoff for the selected two-decades of (a) the Chamkhar Chhu basin by RCA4, (b) the Chamkhar Chhu basin by REMO, (c) the Beas basin by RCA4 and (d) the Beas basin by REMO.

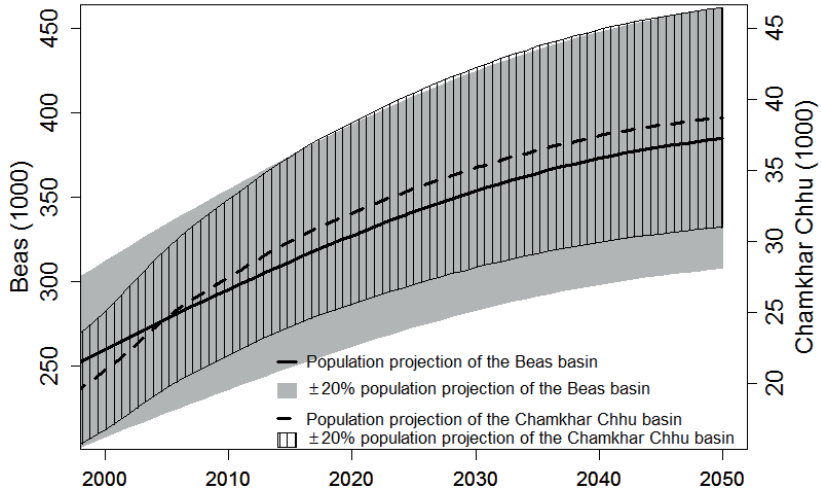

Fig. 11: Population projections for the Chamkhar Chhu basin and the Beas basin for the period from 2000 to 2050.

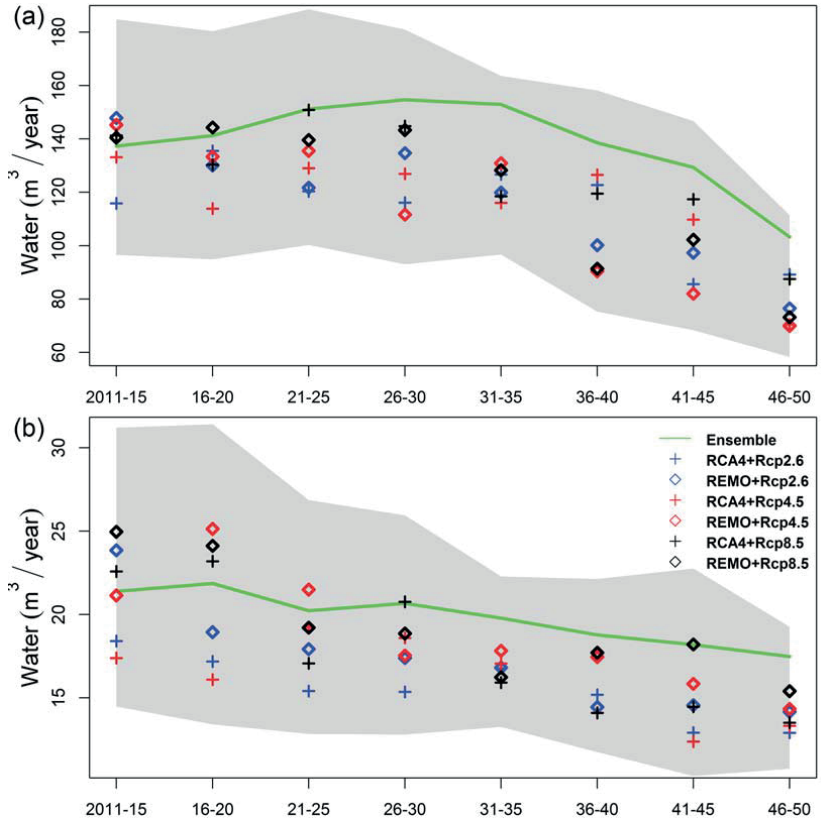

Fig. 12: Water resources per capita of (a) the Chamkhar Chhu basin and (b) the Beas basin. The shaded area represents the ranges consider ±20% of the population projections. The top boundary is calculated by using the maximum projected available water resources and 80% of the population and the bottom boundary is calculated by using the minimum projected available water resources and 120% of the population. The ensemble is computed by using the mean of six runoff projections and assuming the population does not increase after the period 2011–2015.

Tables

Table 1: Formulas of seven statistical bias correction methods. $\widehat{P_{\mathrm{o}}}$ is the calculated value at a observation site. P_{m} is the RCM modelled value. a, b, c, x and τ are free parameters that are estimated from series of observation period.

Method (short)	Formula
M1 (empirical)	Empirical quantiles
M2 (splines)	Smoothing splines
M3 (linear)	$\widehat{P_{\mathrm{o}}} = a + bP_{\mathrm{m}}$
M4 (power.x)	$\widehat{P_{\mathrm{o}}} = b(P_{\mathrm{m}} - x)^c$
M5 (exponential)	$\widehat{P_{\mathrm{o}}} = (a + bP_{\mathrm{m}}) \times (1 - e^{-(P_{\mathrm{m}}-x)/\tau})$
M6 (scale)	$\widehat{P_{\mathrm{o}}} = bP_{\mathrm{m}}$
M7 (power)	$\widehat{P_{\mathrm{o}}} = bP_{\mathrm{m}}^c$

Table 2: Formulas of the numerical criteria. O_i is the observed series; S_i is the simulated series; n is the length of the series; $\bar{O}$ and $\bar{S}$ are respectively the mean of observed series and simulated series. The series are abbreviated in the column of Series: Precipitation (P, mm/day), Temperature (T, ^{o}C), Discharge (Q, m^3/s), Human population (H). In the column Unit, — indicates dimensionless and the remaining criteria are in the unit of their used series.

Criteria	Formula	Perfect value	Range	Series	Unit
bias	$\frac{\sum_{i=1}^{n}(S_i-O_i)}{n}$	0	$(-\infty, +\infty)$	P, T, H	
RME	$\frac{\sum_{i=1}^{n}(S_i-O_i)}{\sum_{i=1}^{n}O_i} \times 100$	0	$(-\infty, +\infty)$	Q, H	—
MAE	$\frac{\sum_{i=1}^{n}\lvert S_i-O_i\rvert}{n}$	0	$[0, +\infty)$	P, T	
sd	$\sqrt[2]{\frac{(S_i-\bar{S})^2}{n}}$	$\sqrt[2]{\frac{(O_i-\bar{O})^2}{n}}$	$[0, +\infty)$	P, T	
NMSE	$\frac{\sum_{i=1}^{n}(O_i-S_i)^2}{N \times sd^2}$	0	$[0, +\infty)$	P, T	—
NSE	$1-\frac{\sum_{i=1}^{n}(O_i-S_i)^2}{\sum_{i=1}^{n}(O_i-\bar{O})^2}$	1	$(-\infty, 1]$	Q	—

Table 3: A summary information of the two basins. Note: The area is in km^2. ME is median elevation in m amsl. GF is glacier fraction (%). P is annual precipitation in mm/year. T is annual air temperature in °C. The values are calculated from the observation period (the calibration and validation periods).

Basin	Location (E, N)	Area	ME	GF	P	T	Calibration	Validation
Chamkhar Chhu	(90.74, 27.59)	1,353	4,479	15.0	1,786	1.75	1998–2004	2005–2008
Beas	(77.15, 31.88)	3,202	4,213	32.7	1,116	-1.04	1997–2002	2003–2005

Table 4: Summary of meteorological stations. Height is in m amsl and the column Period is the observed period.

Basin	Name	(Lon(E),Lat(N))	Height	Period
Chamkhar Chhu	Bjizam	(90.45, 27.52)	1,840	1994–2008
	Trongsa	(90.50, 27.50)	2,120	1990–2008
	Yotangla	(90.59, 27.57)	3,530	2003–2008
	Gyetsha	(90.74, 27.50)	2,630	1993–2008
	Chamkhar	(90.75, 27.54)	2,470	1994–2008
	Ura	(90.90, 27.47)	3,090	1990–2008
	Dungkhar	(91.11, 27.82)	2,010	1990–2008
Beas	Pandoh	(77.05, 31.67)	899	1985–2005
	Bhuntar	(77.15, 31.88)	1,080	1985–2005
	Manali	(77.18, 32.25)	1,926	1985–2005

Table 5: Numerical criteria of model calibration and validation.

Basin	Criteria	Calibration	Validation
Chamkhar Chhu	NSE	0.87	0.85
	RME	-0.02	10.32
Beas	NSE	0.65	0.73
	RME	2.07	-22.38

Table 6: Population error of the linear function used in basin population projection.

Chamkhar Chhu	1990	1995	2000	sum
bias	1,439	-745	-694	0
RME	7.9	-3.9	-3.2	0.3
Beas	1990	1995	2000	sum
bias	134	-269	135	0
RME	0.1	-0.1	0.1	0.0

Table 7: Statics of ranges (R) of Wp caused by RCMs, Rcps and ±20 inaccuracy in population estimations (Pop). For the period i, $Wp_{(\mathrm{i,j})}$ is the available water resources per capita estimated by the projection j ($1 \leq j \leq 6$). In the first row, R_i is $\frac{\max\limits_{1\leq j\leq 6} Wp_{(\mathrm{i,j})} - \min\limits_{1\leq j\leq 6} Wp_{(\mathrm{i,j})}}{\sum_{j=1}^{j=6} Wp_{(\mathrm{i,j})}/6} \times 100$ and in the second row, R_i is $\frac{\max\limits_{1\leq j\leq 6} Wp_{(\mathrm{i,j})}/0.8 - \min\limits_{1\leq j\leq 6} Wp_{(\mathrm{i,j})}/1.2}{\sum_{j=1}^{j=6} Wp_{(\mathrm{i,j})}/6} \times 100$. Mean, Min and Max are the mean, minimum and maximum of the series of R.

	Chamkhar Chhu			Beas		
	Mean	Min	Max	Mean	Min	Max
RCMs;Rcps	25.1	12.0	35.7	29.2	11.4	43.5
RCMs;Rcps;±20%Pop	67.6	54.2	79.1	72.5	53.8	86.6